# The Versatility of Metal Nanoparticle-Decorated Titanium Dioxide for Catalysis Including Hydrogen Generation, Solvent Radical Initiation, and Calcium Carbide Chemistry

**Andrew Hainer**

Thesis submitted to the University of Ottawa
in partial fulfillment of the requirements for the degree of

Doctorate of Philosophy
In
Chemistry

Department of Chemistry and Biomolecular Sciences
Faculty of Science
University of Ottawa

Supervisor: Juan (Tito) Scaiano

In dedication to

My wife, Kenzie, and my cat, Sir. Isaac Newton.

They both gave me the love and support I needed over these years of hard work.

&

My parents, who instilled a love for science in me throughout my life,

and always supported me in all I have done.

"You see, technically, chemistry is the study of matter, but I prefer to see it as the study of change. Electrons change their energy levels. Molecules change their bonds. Elements combined and change into compounds. But that's all of life, right? It's the constant, it's the cycle. It's solution, dissolution. Just over and over and over. It is growth, then decay, then transformation. It's fascinating really. It's a shame so many of us never take time to consider it's implications."

-Walter Hartwell White Sr.

# Abstract

Metal nanoparticle-decorated titanium dioxide (M@$TiO_2$) materials are an increasingly popular class of heterogeneous catalyst, useful in both photochemical and thermal systems. Heterogenous catalysts offer the advantage of reusability and ease of catalyst separation, when compared to similar homogeneous systems. M@$TiO_2$ catalysts also have the benefit of water/air environment stability, strong photoactivity for oxidation and reduction reactions, as well as easy and low cost synthesis of the catalyst. Other heterogeneous catalysts can offer better activity for certain reactions; however, M@$TiO_2$ materials are extremely versatile in a variety of different reactions and applications, and often are cheaper than other alternatives. In this dissertation, M@$TiO_2$ catalysts will be evaluated in hydrogen generation, solvent radical chemistry, and organic synthesis utilizing calcium carbide.

Firstly, M@$TiO_2$ were evaluated for photocatalytic hydrogen generation from pure water splitting, and with the presence of sacrificial electron donors (SEDs) such as methanol. Efficient pure water splitting is of great interest for fuel production as it offers a perfect cycle with hydrogen gas burning to reform water as the only product. However, quite often SEDs are utilized to boost hydrogen gas generation due to poor conversion from pure water. It is often assumed that a photocatalyst effective with a SED will also be effective with water splitting. This assumption was tested, by comparing a variety of different M@$TiO_2$ photocatalysts for both water splitting, and SED-based hydrogen generation. Interestingly, it was found that the trends of hydrogen generation between photocatalysts are not the same in pure water splitting, as when SEDs are present. For example, Pd@$TiO_2$ shows great activity with a 1% methanol solution; however, no considerable $H_2$ generation for pure water splitting. This shows that the mechanisms of hydrogen generation with water splitting, and when SEDs are present, are very different and not directly comparable. It was also found that M@$TiO_2$ materials offer decent hydrogen generation rates, especially when considering the overall cost of the material.

M@$TiO_2$ materials were then tested for their ability to photocatalytically form usable free-radicals from ethers. This was evaluated with scavenging of generated radicals by TEMPO,

as well as monitoring the resulting $H_2$ production during the reduction portion of the system. Overall, it was found that M@$TiO_2$ photocatalysts are exceptional at forming radicals from ethers. All the ethers tested are able to undergo proton-coupled electron transfer (PCET) with the hole of $TiO_2$, as seen by the $H_2$ generation observed. The main considerations are instead for the ether-radical, and if the radical will fragment or primarily undergo other reactions. This led to only some of the ethers being able to form TEMPO-ether adducts. The photogenerated hole of $TiO_2$ is also strong enough to form benzylic radicals from toluene, highlighting the further versatility of the catalyst.

To further explore $TiO_2$-generated radicals, heterogeneous laser flash photolysis techniques were then developed. Laser flash photolysis of $TiO_2$ suspensions is an uncommon, and underdeveloped technique in the research field. It was considered if low concentration suspensions of $TiO_2$ could allow for lowered impact from the absorbance and scattering from the $TiO_2$ particles. This allowed for monitoring the transient absorbance of a benzylic radical from the reaction between 1,1-diphenylethylene and 1,3-dioxolane solvent radicals formed by the photogenerated hole of $TiO_2$. The strength of this transient signal also showed dependence on the solvent, with 1,4-dioxane showing lower signal as expected from it's reactivity. This technique, with further development, should prove useful in expanding the kinetic evaluation of radicals generated by $TiO_2$ suspensions.

Finally, Pd@$TiO_2$ was evaluated as a thermal catalyst for a Sonogashira-like reaction between calcium carbide and bromobenzene in DMSO under low water conditions. This palladium catalyst was effective in catalyzing the reaction; however, the more interesting aspect was in the chemistry of the calcium carbide itself. Calcium carbide is typically used for the in-situ formation of acetylene gas through the addition of water. However, it was found that in DMSO with low amounts of water, the formation of a soluble ethynyl calcium hydroxide intermediate could be selected for. This allowed for a more controlled and effective coupling with bromobenzene in solution. Further expansion on the use of this intermediate may be invaluable in expanding calcium carbide chemistry beyond the formation of acetylene gas.

# Acknowledgements

I would first like to give my appreciation for all of the support from my Ph.D. supervisor, Prof. Scaiano. You gave me a chance, coming from a bachelor's degree in Biomedical science, to prove myself as a chemist. You have truly been an inspiration, and I would not be the chemist I am now without you. Everything from your exciting and interesting stories from your life, or your unique out of the box ideas that I initially think have no possibility of working but somehow worked every time. I always grew to regret putting off an experiment you said I should try, as when I finally tried I would often be surprised. Without you supervising me, I would not be considering a career in Academia as much as I am. Even if I find myself exploring other career avenues, I have a feeling I will be drawn back by the call of Academia. I hope to one day pass on the skills you have given me.

I would also like to thank Dr. Anabel Lanterna. You were a true inspiration in our group, and I strive to be as committed of a researcher as you are. You were constantly in or around the lab to help out anyone who had a quick question, or needed help. You also were a great person to talk to about anything else in our lives outside of just chemistry. I wish you the best of luck as a Professor at the University of Nottingham. If I ever end up in the UK, I will be sure to reach out!

I also want to personally thank Bowen Wang, and Ayda Elhage in our group. As senior members in the group you both were extremely helpful in developing my chemistry skills, and I knew I could always count on your help in any problem I may have had. I also would like to thank the rest of the Scaiano group, both current and previous members. You all have been an extremely welcoming group, and I wish you all the best of luck in your future careers! I know you all will do great things.

I also give my thanks to my parents, Steven and Penny. You both have always been there to help me achieve my dreams. To think from being a scientist for career day (by your recommendation) all those years ago, I would now be completing my Ph.D. in chemistry. You have always pushed me to reach for my full potential, even if you would have loved me no matter what.

I also thank the rest of my friends and family. Specifically I will mention my brothers Jeffrey and Ben, and of course my closest friend Shea. I always have been able to count on you all for support whenever I need it, and I appreciate being able to hangout out like we are kids again playing video games whenever I need a break from research.

My biggest thanks however goes out to my wife, Kenzie. You have always been there to help me through, and push me when I am at my lowest. I don't know if I could have done this without your constant support. You make a great teacher, as you have taught me so much about myself, and I would not be the person I am now without you. I also, of course, must thank my cat Sir. Isaac Newton, who was always by my side as my co-writer offering his emotional support.

# Contribution Statement

The dissertation presented is based upon 3 peer-reviewed publications, and 1 publication currently undergoing the submission process. I was the first contributing author for all of these presented works, thus the majority of the experimental work was completed by me. However, as they include many other listed authors, I have had the fortunate opportunity to collaborate with a variety of different colleagues in this scientific research. I also was directly involved in research that lead to publications in which I was not the first author, which are listed in the 'List of Publications' section. Firstly, I aided in the $H_2$ generation analysis of $TiO_2$ fibers synthesized by Sivuyisiwe Mapukata for the listed publication. I also gave guidance on the further modification of the material with metal nanoparticles. Also, through collaboration with the Universidad Nacional de Córdoba in Argentina, I learned much about electrochemical $H_2$ generation techniques, while also contributing to the experimental work in the two listed electrochemical publications. This work also involved a work trip to Argentina where I learned various techniques. Much of my collaboration was directly with Dr. Esteban Franceschini, along with directly working with Melisa Gomez and Victoria Benavente-Llorente. Melisa was also kind enough to host me during my trip to Argentina. These publications where I am not first author are not discussed further in this dissertation, due to the main contributor to the research not being myself. However, they still acted as an important part of my research journey.

Throughout my graduate studies I received great help from both Prof. Scaiano and Dr. Lanterna. Prof. Tito Scaiano, as my supervisor, aided in giving feedback and ideas throughout in frequent meetings. I especially appreciated his particularly out of the box thinking, which often lead to some unique solutions to problems that I faced. I hope I can continue to think in the same unique ways that he has taught me. Dr. Anabel Lanterna, as a research associate in the group, also was directly involved in helping me and other graduate students up until she left the group in 2020. She was invaluable in giving direction, and often helped in the more day to day aspects of the lab. The senior researchers Ayda Elhage and Bowen Wang also gave everyday guidance in the lab. I always knew that if I was lost, or didn't know how to do something, they could help put me in the right direction.

Before starting my graduate studies, I worked as a volunteer in the Scaiano group under the guidance of Nancy Marina. She helped with much of my initial training in the procedures conducted in our group. This included the methods of synthesizing M@$TiO_2$ catalysts by photo-deposition, as well as performing organic reactions with these materials. This included the analytical procedures using gas-chromatography with flame ionization detection (GC-FID).

The $H_2$ generation research presented in chapter 2 was primarily conducted by me personally; however, initial experiments were conducted by other researchers before I took over the project. Firstly, Victoria Sandre had conducted the initial explorations into evaluating hydrogen generation with M@$TiO_2$ photocatalysts. This was done as part of a summer exchange with the RISE program that Prof. Scaiano runs. After this, Justin Hodgins began working on the project for his honours thesis. He continued to develop the methodologies from Victoria further, and set a strong groundwork for how to conduct $H_2$ generation experiments in the group. When I joined the group, I worked directly with Justin for 1 month, learning how he had been conducting these experiments. During this time, I also began to experiment with how to better calibrate our gas-chromatography with thermal conductivity detector (GC-TCD) for $H_2$ gas formation. $H_2$ generation rates found by Justin and Victoria appeared much higher than expected when comparing to other published materials. I then developed a consistent method of injecting known amounts of $H_2$ gas into our sample vials to accurately simulate a known formation of $H_2$ gas. Due to this, none of the work done by Justin or Victoria is directly presented in the publication; however, their preliminary work was important for the initial development of the project. While conducting these experiments, I began to train an undergraduate student, Morgan Vallieres, in the lab before she began working on her own research honours project. While being trained, she conducted some of the experiments presented in this work under my guidance. The writing of this publication also involved great collaboration with both Prof. Scaiano and Dr. Lanterna.

The work on radical generation from ethers in Chapter 3 also involved collaboration. Initial findings of THF radicals being involved in organic reactions was found by Nancy Marina in her prior work in the group. As such, she was involved during the beginning stages of this project, and helped teach me some of the basics of the concepts. However, most of the experiments

presented were still conducted by me personally. Stefanie Rincon, a visiting student from Colombia, also helped perform some of the experiments under my guidance. This, similar to Morgan, acted as training on the techniques within our group. Her aid was especially useful for some of the kinetic evaluations with measurements at multiple time points. During the writing stages of the project, Paolo Costa became involved to aid in the DFT calculations to further evaluate the surface interactions. The writing of this publication also involved great collaboration with both Prof. Scaiano and Dr. Lanterna.

Chapter 4 describes a research project almost entirely led by me. The concept of looking into heterogeneous laser-flash photolysis (LFP) of these radical processes was brought forward by me to Prof. Scaiano, who then gave me insight on how I should initially approach the project. Interestingly he was skeptical on if it would work at all, and was excited when it ended up working! There was also guidance from Neeraj Joshi on the laser techniques. Neeraj is a laser technician who works with our group, and was invaluable in helping to fine-tune the laser setup. He also aided in brainstorming many of the solutions to problems that came along the way. Other than occasional help with fixing the laser setup, I performed all the experimental work myself. The writing of the manuscript was primarily conducted by myself, with guidance in edits and additions from Prof. Scaiano

The calcium carbide research in chapter 5 was also led almost entirely by myself. The concept of using calcium carbide was brought up by Prof. Scaiano after I mentioned an interest in looking at acetylene chemistry as a direction for these M@$TiO_2$ catalysts. The findings and realizations about the ethynyl calcium hydroxide intermediate were done by me through my own literature review on the topic. The writing of the manuscript was also primarily done by myself, with edits and additions from Prof. Scaiano and Dr. Lanterna.

# Table of Contents

**A. Appendix**

# List of Publications

## Publications Presented in this Thesis

Andrew S. Hainer, Justin S. Hodgins, Victoria Sandre, Morgan Vallieres, Anabel E. Lanterna*, and Juan C. Scaiano*; Photocatalytic Hydrogen Generation Using Metal-Decorated $TiO_2$: Sacrificial Donors vs True Water Splitting. ACS Energy Letters. **2018**, 3(3), 542-545.

Andrew Hainer, Nancy Marina, Stefanie Rincon, Paolo Costa, Anabel E. Lanterna*, and Juan C. Scaiano*; Highly electrophilic titania hole as a versatile and efficient photochemical free radical source. J. Am. Chem. Soc. **2019**, 141(11), 4531-4535.

Andrew Hainer, Neeraj Joshi, and Juan C. Scaiano*; Laser flash photolysis of titanium dioxide suspensions for the evaluation of solvent-mediated radical reactions. Phys. Chem. Chem. Phys. **2023**, 25(4), 2747-2751.

Andrew S. Hainer, Anabel E. Lanterna, and Juan C. Scaiano*; Beyond acetylene: Solvent stabilisation of calcium carbide derived acetylide intermediates for small organic molecule synthesis. ***(Submitted)***

## Co-Authored Publications Not Discussed in this Thesis

Esteban A. Franceschini, **Andrew Hainer**, and Anabel E. Lanterna*; Niobium-based semiconductor electrodes for hydrogen evolution reaction. Int. J. Hydrog. Energy. **2019,** 44(60), 31940-31948.

Sivuyisiwe Mapukata, **Andrew S. Hainer**, Anabel E. Lanterna, and Juan C. Scaiano*, and Tebello Nyokong*; Decorated titania fibers as photocatalysts for hydrogen generation and organic matter degradation. J. Photochem. Photobiol. A. **2020**, 388, 112185.

Melisa J. Gomez, Victoria Benavente-Llorente, **Andrew Hainer**, Gabriela I. Lacconi*, and Juan C. Scaiano*; Evaluation of different Ni-semiconductor composites as electrodes for enhanced hydrogen evolution reaction. Sustain. **2020**, 4(8), 3963-3970.

# List of Figures

# List of Schemes

# List of Tables

# List of Abbreviations

| | |
|---|---|
| [ ] | Concentration |
| A | Electron acceptor |
| ACN | Acetonitrile |
| $Bu^tO^\bullet$ | *tert*-butoxy radical |
| CB | Conduction band |
| D | Electron donor |
| DCM | Dichloromethane |
| DEE | Diethyl ether |
| DFT | Density functional theory |
| DMF | N,N-Dimethylformamide |
| DMM | Dimethoxymethane |
| DMPO | 5,5-Dimethyl-1-pyrroline-N-oxide |
| DMSO | Dimethyl sulfoxide |
| DOL | 1,3-Dioxolane |
| DOX | Dioxane |
| DPE | 1,1-Diphenylethylene |
| DR | Diffuse Reflectance |
| DTBP | Di-*tert*-butyl peroxide |
| $e^-$ | Electron |
| EPR | Electron paramagnetic resonance |
| ESI | Electrospray ionization |

| | |
|---|---|
| FID | Flame ionization detector |
| GC | Gas chromatography |
| $H^+$ | Proton |
| $h^+$ | Hole |
| HAT | Hydrogen atom transfer |
| hv | Light |
| I-2959 | Irgacure 2959 |
| ICP | Inductively coupled plasma |
| LED | Light emitting diode |
| LFP | Laser flash photolysis |
| LSPR | Localized surface plasmon resonance |
| M | Metal |
| M@$TiO_2$ | Metal nanoparticle-decorated titanium dioxide |
| MDOL | 2-Methyl-1,3-dioxolane |
| MeOH | Methanol |
| MOP | 1-Methoxypropane |
| MS | Mass spectrometry |
| NMR | Nuclear magnetic resonance |
| ND | Not detected |
| Nd-YAG | Neodymium-doped yttrium aluminum garnet |
| NP | Nanoparticle |
| OES | Optical emission spectroscopy |

| | |
|---|---|
| PCET | Proton-coupled electron transfer |
| Ph | Phenyl |
| SED | Sacrificial electron donor |
| SEM | Scanning electron microscopy |
| STEM | Scanning transmission electron microscopy |
| TEMPO | 2,2,6,6-Tetramethyl-1-piperidinyloxyl |
| $TiO_2$ | Titanium dioxide |
| TEM | Transmission electron microscopy |
| TCD | Thermal conductivity detector |
| THF | Tetrahydrofuran |
| THP | Tetrahydropyran |
| UV | Ultraviolet |
| UVA | Ultraviolet A (315-400 nm) |
| VB | Valence band |
| Vis | Visible |
| XPS | X-ray photoelectron spectroscopy |
| $\lambda_{ex}$ | Excitation wavelength |
| ΔOD | Change in optical density |

# 1. Introduction

## 1.1 Opening Remarks

This dissertation is focused on the heterogeneous catalysis of metal nanoparticle-decorated titanium dioxide materials (M@$TiO_2$). The focus is primarily on photocatalysis, with hydrogen generation and solvent radical chemistry being the highlighted areas of research. However, some chemistry is also done with thermal catalysis for organic synthesis using these catalytic materials in conjunction with solubilized calcium carbide intermediates. This doctoral thesis has been composed from 3 peer-reviewed publications[1-3] (chapters 2-4), and 1 publication currently undergoing the peer-review process (chapter 5). This includes the manuscripts and supporting information, as well as additional commentary and alterations to allow for further insights and to highlight the overarching story through the chapters. This introductory chapter will aid the reader in gaining the background knowledge required to understand the proceeding chapters, as well as highlight relevant research in the fields of hydrogen generation, radical chemistry, and laser flash photolysis.

The photochemically synthesized M@$TiO_2$ materials developed by our research group are easy and cheap to synthesize, while also being extremely versatile in a variety of different chemical applications. This includes hydrogen generation, water purification, radical chemistry, and other organic synthesis. When directly photoexciting the $TiO_2$ itself, this chemistry is dependent on the careful balance and control of both the reduction and the oxidation reactions that are initiated by the photocatalyst. Careful analysis of the chemistry occurring in these heterogeneous systems is important to allow informed decisions for future catalyst development. For instance, it is very important to understand the differences between hydrogen generation from water splitting, and from sacrificial electron donors, as will be discussed in chapter 2. The overall goals and outline of the dissertation will be discussed further at the end of this chapter.

## 1.2 Photoactive Semiconductors

Semiconductors, by definition, are materials that fall between conductors and insulators in their electronic properties. They are defined by a gap in energy between the valence band (VB), which is the highest occupied collection of energy levels, and the conduction band (CB). This gap in energy, or void region, is most commonly referred to as the band gap of the semiconductor.[4] (Figure 1.2.1) Typically, this structure allows the semiconductor to have photoactive properties as they can absorb light to excite an electron ($e^-$) from the valence band to the conduction band. This in turn leaves a 'hole' ($h^+$) in the valence band where the electron once was. For simplicity in discussion, both the electron and hole will be considered as separate charge carriers, even if the hole is simply the absence of an electron.

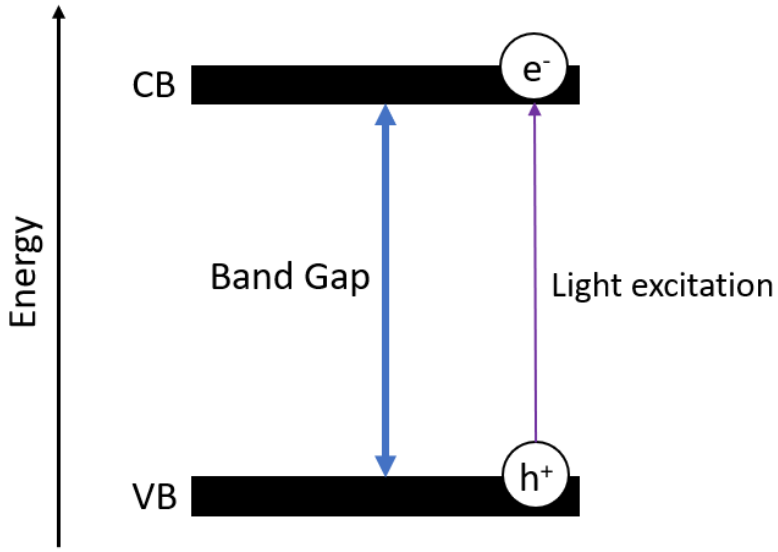


**Figure 1.2.1.** Electronic structure of a semiconductor, showing the band gap between the valence band (VB) and conduction band (CB). Light excitation is shown exciting an electron ($e^-$) to the conduction band leaving a 'hole' ($h^+$) in the valence band.

After photoexcitation of a semiconductor, the two charge carriers ($e^-$ and $h^+$) can have a variety of different fates. The fate of these carriers will be discussed using $TiO_2$ as an example, as it will be the focus of this dissertation; however, similar rules apply with most semiconductors. Most simply the charge carriers can recombine, either emitting light or releasing heat as the

electron returns to the energy of the valence band. However, the charge carriers can also migrate to the surface to be trapped in surface sites, or sites within the bulk of the material. These trap sites tend to involve defects in the crystal lattice of the material, and are most common on the surface. However, lattice mismatches can also be present in the bulk of the material creating charge traps. Trapped charge carriers recombine at a slower rate, within the nanosecond range rather than picosecond. If the charge carriers are trapped on the surface, the carriers can undergo redox reactions with compounds in the surrounding solution, with trapped holes being strong electron acceptors, and the trapped electrons electron donors.[5-6] Migration to trapped states occurs under fast time scales; however, are limited by the amount of usable defect sites present. This means initial charge recombination is still typically the process with the highest quantum yield in unmodified titanium dioxide. (Figure 1.2.2)

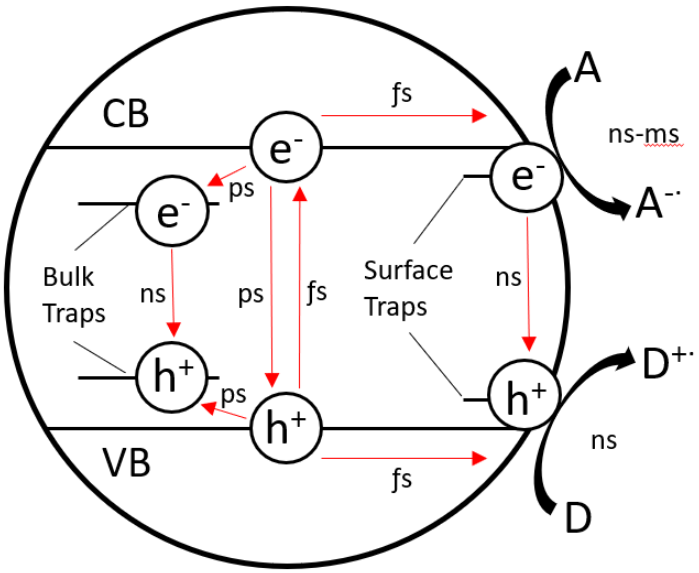


**Figure 1.2.2.** The fate of charge carriers ($e^-$ and $h^+$) in $TiO_2$ particles in solution after light excitation. Approximate time scales are shown for the various recombination events, as well as migrations to trapped states in the bulk or surface. Electron acceptors (A) and donors (D) from surrounding solution can also react with charge carriers on surface trap sites.[5-7]

For electrons to be excited from the VB into the CB, light with energy equal to or greater than the band-gap of the semiconductor must be absorbed. However, the actual energies of the

VB and CB must also be considered when evaluating possible reactions that may occur with electron acceptors or donors on the surface. The energy of the conduction band must be more negative than the reduction potential of an electron acceptor, and the energy of the valence band must be more positive than the oxidation potential of an electron donor.[4] (Figure 1.2.3) With this in mind, anatase $TiO_2$ is a very common and useful photocatalyst for both oxidation and reduction reactions. $TiO_2$ has three different main possible crystal structures, including rutile, anatase, and brookite.[8] Of the three, rutile and anatase are the most common. Rutile and anatase have very similar band levels; however, the conduction band of rutile is slightly lower compared to anatase. This means that rutile has lower reductive potential compared to anatase, and specifically cannot adequately reduce $H^+$ ions into $H_2$ gas. However, one of the most popular commercial powder $TiO_2$ types is P25, which is a 3:1 mixture of anatase (25 nm size) and rutile (85 nm size) particles. Interestingly this mixed $TiO_2$ powder is better performing in photocatalysis in comparison to pure anatase $TiO_2$ powder.[9] This can be partially explained by the presence of phase-junctions, which allow for separation of the charge carriers between crystal phases. Charge transfer between anatase and rutile by the phase-junction interfaces is one aspect that drives the higher reactivity of this mixed material, as there is more separation between charge carriers.[10]

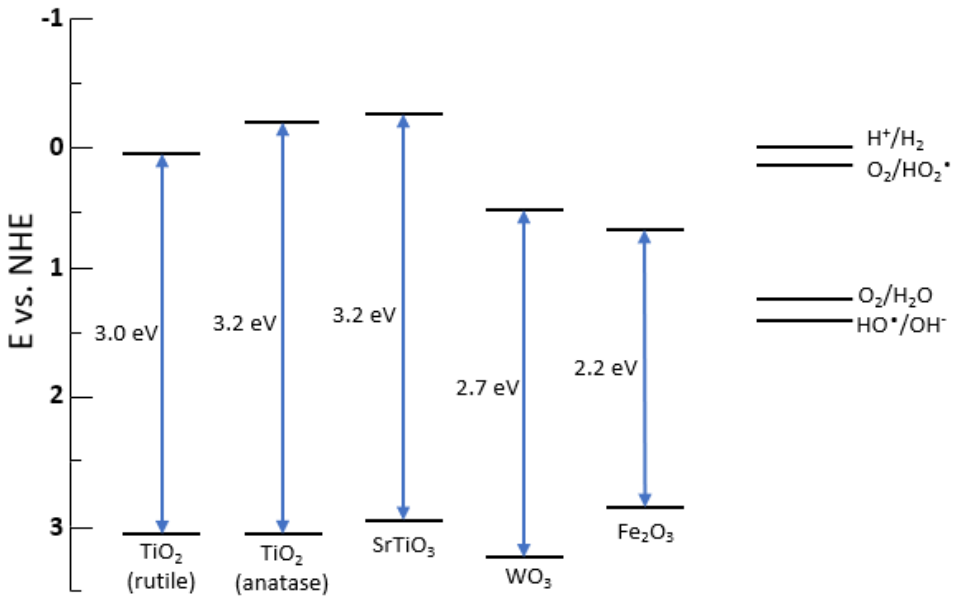


**Figure 1.2.3.** Band-energy diagrams of various semiconductors showing bandgap energies of each. Relevant common reduction/oxidation potentials are shown on the right.[4]

## 1.3 Heterogeneous Metal-Nanoparticle Decorated Titanium Dioxide

Heterogeneous photocatalysis is the process of using a material that is suspended in a reaction solution instead of being dissolved homogeneously. Heterogeneous photocatalysis classically involves a photoactive semiconductor that absorbs light to induce oxidation and reduction reactions on its surface.[11] One of the main advantages over homogeneous systems is that heterogeneous catalysts can be more easily removed from solution post reaction, and possibly reused. However, it also comes with disadvantages as heterogeneous systems can be more difficult to control and understand in comparison to their homogeneous counterparts. Heterogeneous catalysts are not typically perfectly uniform, and thus can have poor control of the active site.[4, 11-12] They also typically have a poor ratio of active catalytic sites per volume of catalyst, and it can be difficult to evaluate the actual number of catalytic sites.[13] Nonetheless, the advantages of reusability still make heterogeneous catalysts a current interest in chemistry, as many researchers attempt to overcome the issues given by the heterogeneous approach to catalysis.

One currently popular heterogeneous photocatalyst is metal nanoparticle-decorated $TiO_2$ (M@$TiO_2$). $TiO_2$ by itself has two big limitations as a photocatalyst, the rates of electron-hole recombination are high, and the catalyst has a limit of only absorbing light up to 400 nm, meaning it cannot use visible light. One method of improving the reactivity of titanium dioxide is to decorate the surface with metal nanoparticles. Decoration is chosen to describe this modification since doping, the other way of adding a new element to $TiO_2$, involves direct addition of the element into the crystal structure of the material. Decoration can greatly improve the photocatalyst through a few different mechanisms. Firstly the metal acts as an electron trap to greatly decrease the rate of charge recombination, as electrons excited into the conduction band are transferred into the metal nanoparticle.[14] The specific metal nanoparticle surface can also directly alter the chemical interactions that occur with substrates of reactions. These two mechanisms are the main methods of improving catalytic efficiency when directly exciting the titanium dioxide. (Figure 1.3.1(A))

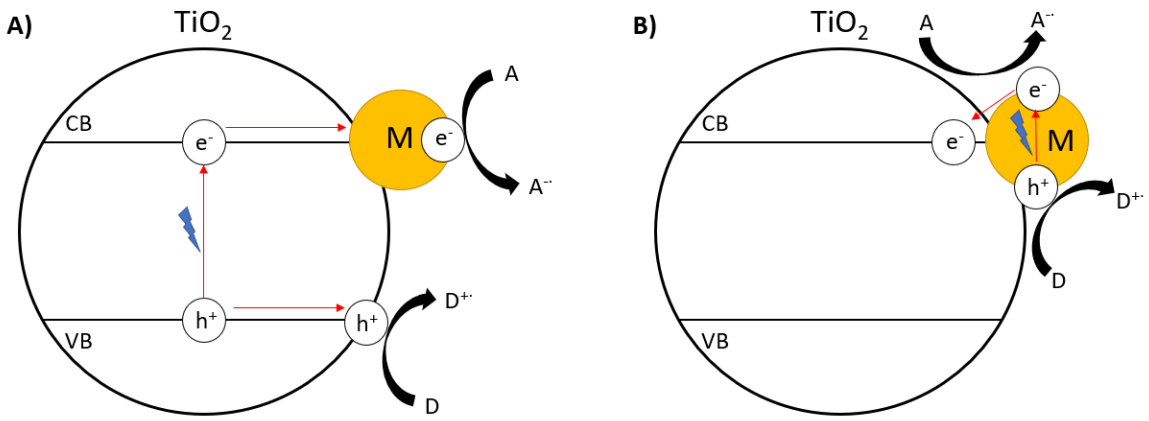


**Figure 1.3.1.** Fate of charge carriers in photoexcited metal nanoparticle-decorated titanium dioxide during **(A)** absorbance by $TiO_2$ causing electron ($e^-$) excitation from the valence band (VB) to the conduction band (CB), before charge transfer to the metal nanoparticle (M). The electron in the metal nanoparticle can then react with an electron acceptor (A), and the hole ($h^+$) in the valence band moves to the surface to react with electron donors. Or **(B)** absorbance by the metal nanoparticle, where excited electrons can either directly react with an electron acceptor (A) or react after transfer to the conduction band of $TiO_2$. The hole in the metal can then react with electron donors, with transfer to the valence band of $TiO_2$ being typically not possible.

Metal decoration can also improve the catalyst by increasing its absorbance in the visible range. These nanoparticles can either absorb light through their free-electrons, inducing localized surface plasmon resonance (LSPR) with high visible absorbance, or can have inter-band transitions of bound electrons into higher energy levels which can also often extend into the visible region.[15] In both cases, light excited electrons are induced in the metal which can either directly catalyze reactions with substrates without influence from the $TiO_2$ support, or can be inserted into the conduction band of $TiO_2$ acting as a photosensitizer for visible light.[16] (Figure 1.3.1(B)) It should be noted however that under most situations, the metal nanoparticles can only inject excited electrons into the conduction band, and cannot create a hole in the valence band of $TiO_2$ by accepting electrons. This is due to the energy levels of the metal typically being much higher than the energy level of the valence band. This behaviour means that metal decoration can increase the photoactivity of the catalyst into longer visible wavelengths, which overcomes the limitations of $TiO_2$ only absorbing UV light. However, this metal decoration is better at photosensitizing for reduction reactions, while photosensitization for oxidation reactions is limited due to the higher energy levels of the metal preventing transfer of an electron

from the valence band of $TiO_2$. Absorbance of light by the nanoparticle can also induce a form of high localized heating around the particle, which has been shown in our group for Pd@$TiO_2$ particles catalyzing Sonogashira C-C coupling.[17]

Another change to the semiconductor induced by a metal nanoparticle is the introduction of a Schottky barrier at the metal-semiconductor interface.[18-19] A Schottky barrier is a form of band bending of the conduction and valence bands of the semiconductor as it approaches the interface of the metal. This typically leads to bending to higher energies at the junction, as titanium dioxide is typically an n-type semiconductor due to the presence of oxygen vacancies in the bulk of the material. This interaction also increases charge separation, pulling holes towards the junction and pushing electrons into the bulk. However, electrons can still transfer into the metal itself due to the process being thermodynamically favorable, though somewhat affected by the reduced rate of movement of the electron to the surface.[6] The Schottky model can be somewhat simplistic when considering metal nanoparticles on titanium dioxide powders, especially mixed ones like P25, however is still worth considering when evaluating charge carrier dynamics.

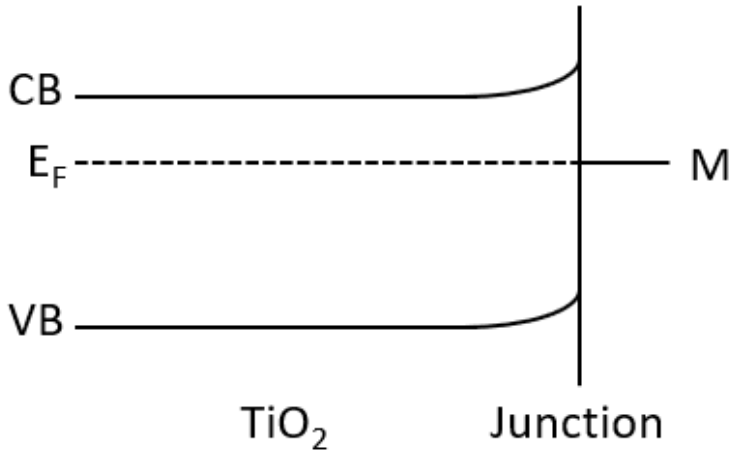


**Figure 1.3.2.** Representation of the band bending of the conduction band (CB) and valence band (VB) of $TiO_2$ as it approached the junction with a metal (M). The Fermi level ($E_F$) is also shown.

In many cases, metal nanoparticles deposited on $TiO_2$ particles are not truly metallic. They can instead be a metal oxide, either fully or partially. This is typically due to initial nanoparticle

deposition, before fast partial, or full oxidation under ambient air conditions. Since the aim of these materials is reuse and stability, they are typically not handled under fully inert glove-box conditions, so partial to full surface oxidation of more oxidizable metals is common.[20] This complicates evaluation of the interaction between the nanoparticle and the $TiO_2$ support. This is due to the fact that a metal oxide does not have light induced LSPR, and cannot act as a metal. The metal oxide nanoparticles, such as CuO, are instead typically semiconductors, which means they will possess a bandgap with a VB and CB. Bandgaps are typically smaller compared to the $TiO_2$ support, and have energies closer to the CB of $TiO_2$. This means that they can often behave similarly to metal nanoparticles, but with a wider spread for the relative energy levels. This is further complicated by the fact that the nanoparticles are often only partially oxidized, meaning there is a mixture of true metal and metal-oxide in the particle. This leads to charge transfer interactions that can be difficult to fully predict, especially since it is often not consistent between nanoparticles either. Metal oxide particles also often display changes in oxidation state over time from certain reactions, sometimes playing an integral role in the chemistry occurring. This has been shown in our research group with our $CuO_x@TiO_2$ photocatalysts in copper click-chemistry, in which air conditions are required for regeneration of the active sites on the nanoparticle surface.[20] The active state of copper is most likely Cu(I) with interconversion between Cu(0), Cu(I), and Cu(II). The titanium dioxide helps to reduce it when it is too oxidized, and the oxygen helps to oxidize it when it is too reduced. $Pd@TiO_2$ has also been shown in our group to change it's oxidation state over time with certain reactions, and must be reactivated by either an activation cycle or through use of 'catalytic farming' of different reactions to allow reactivation after detrimental reactions.[21] However, changes in nanoparticle state over time are dependent on the specific reaction that is occurring, with Sonogashira coupling showing more deactivation and Ullman homo-coupling being more stable. For the remainder of this dissertation, all of these nanoparticles will often be described as metal-nanoparticles, even if they contain a percentage of metal oxide. This will be done for ease of discussion when comparing all of the different metal nanoparticles, and to simplify the overall name of the materials to $M@TiO_2$.

Overall, metal decoration is a widely used method to create exceptional photocatalysts from titanium dioxide, as well as other semiconductor materials. Because of this, $M@TiO_2$

photocatalysts have been well documented, with Au@$TiO_2$ being commonly researched and commercially available. Applications of these M@$TiO_2$ photocatalysts include hydrogen generation[22-23], water purification[24], nitrogen oxidation[25], C-C cross coupling[17, 26], click chemistry[20], phenol photodecomposition[27], and hydrogenation[28]. M@$TiO_2$ catalysts can also be active thermally, for instance with Suzuki-Miyaura coupling reactions[29] and other organic reactions. This list of applications is by no means comprehensive, as M@$TiO_2$ catalysts are quite widespread, and truly are versatile.

The method of M@$TiO_2$ synthesis utilized in this dissertation is photochemical, as $TiO_2$ can directly reduce the metal through photoexcitation with ultraviolet light. Direct photoreduction by the $TiO_2$ can be used with more easily reduced metals; however, with metals such as copper or cobalt a photo initiator (such as Irgacure-2959) can be used to more readily reduce the metal. Reduction of the metals leads to the formation of nanoparticle seeds on the surface of the $TiO_2$ that then grow into nanoparticles. Altering the concentrations, irradiation time and intensity can alter the metal loading and nanoparticle size. This method of synthesis is easy to perform, scalable, and cost effective, making these M@$TiO_2$ catalysts desirable.

## 1.4 Photocatalytic Hydrogen Generation

Photocatalytic hydrogen generation is any catalytic process that generates hydrogen gas after excitation with light. The most popular process that is discussed is 'water splitting' in which water is oxidized into $O_2$ gas, and the resulting $H^+$ ions in solution are reduced into $H_2$ gas.[30] This process, if made efficient, would be extremely useful for fuel production as it presents a perfectly 'green' fuel cycle. This is because when $H_2$ gas is burned for fuel, it then forms $H_2O$ as the only product, which could be used to make more $H_2$ gas. Water splitting can be conducted both electrocatalytically[30] and photocatalytically; however, the later is typically much more inefficient of a process.[31] Electrocatalytic water splitting is currently a much more effective and common method; however, it is somewhat energy intensive as it requires passing a large current through the water. Currently, steps to improve the efficiency of electrodes for this process are underway to improve the energy efficiency of the process, and such research was also the subject of some of my collaborative publications that are not discussed in detail in this dissertation.[32-33]

Photocatalytic water splitting, especially if solar light active, has the potential of using light energy to initiate the reaction as a more green approach to hydrogen generation. However, photocatalytic water splitting is not currently viable for practical applications.[34] Photocatalytic water splitting efficiency is held back by two problems. Firstly the process of oxidizing water in the oxidation half of the reaction is quite inefficient, as water is an extremely stable molecule. Also, the process will generate $O_2$ and $H_2$ in solution together, and unseparated $O_2$ gas can negatively impact the overall reaction. This is an issue due to the backwards reaction of $O_2$ being re-reduced into water in the reduction half of the process instead of forming $H_2$ gas.[35] This competition of processes makes the overall splitting of water into $H_2$ and $O_2$ gas with a photocatalyst in solution extremely inefficient. This is further exacerbated by the fact that $O_2$ gas also tends to be slow to leave the surface of the catalyst, making it quite likely to be reduced back into water. Similarly, generated $HO^{\bullet}$ radicals can react back into water with $H^+$ ions, typically aided through reduction by the reducing portion of the catalyst.[36]

In contrast, photocatalytic hydrogen generation from other compounds is much more efficient. This is typically conducted with compounds known as sacrificial electron donors (SEDs), which act in the oxidation half of the reaction to be converted into oxidation products and forming the $H^+$ ions to be used in the reduction half of the reaction. Examples of common SEDs include methanol, glycerol, triethanolamine, and formate.[37] However, any easily oxidizable compound can be used as a SED. $H_2$ generation with SEDs is more efficient as the oxidation step is more favorable, and the products are less likely to recombine with the generated $H^+$ ions. The main limitation of this approach for energy production is that SEDs, as they are sacrificial, are used up in the reaction. Unlike with water, these SEDs are not reformed when burning $H_2$ gas, thus it is not a renewable cycle. $H_2$ production by SEDs may still be useful for uses outside of fuel production, as $H_2$ gas is useful in other chemical processes. Fuel production from SEDs may also be useful in cases where the SED is converted into other useful compounds in the process, or when the SED is an organic contaminant being degraded. For instance, methanol would be a bad choice for $H_2$ fuel production as it can eventually (after conversion to formaldehyde) form carbon monoxide and carbon dioxide as products, thus burning it would be just as ‘green’ as if you

generated $H_2$ gas from it. However, methanol is still useful as a SED for hydrogenation of alkenes as a source of hydrogen.[38]

One problem within the scientific community, although less in more recent years, is the accidental habit of equating overall water splitting to hydrogen generation with SEDs present. This can either involve claiming that water splitting is occurring when a SED is present[39], or conducting experiments to design an efficient water splitting catalyst by using SEDs due to poor or undetectable yields with just water. Directly claiming water splitting with SEDs present is less common currently. However, using SEDs when designing a catalyst for water splitting has been quite common practice in the research space for many years. For example, a popular review (over 1800 citations) from *Ran et al.*[40] about earth abundant co-catalysts for photocatalytic water splitting is a good example to highlight. For all the listed semiconductors with co-catalysts for the reduction half-reaction, sacrificial electron donors are used for the hydrogen gas yields given. This issue is accented when a $CuO/TiO_2$ photocatalyst, with high efficiencies in a glycerol-water mixture, is discussed as showing a bright future for water splitting. This habit is making the assumption that the oxidation half-reaction (oxidation of the electron donor, either $H_2O$ or SED), and reduction half reaction (conversion of $H^+$ ions into $H_2$ gas) are adequately separate processes. If this assumption is true, improving the reduction half-reaction should improve hydrogen generation no matter the electron donor during the oxidation half-reaction. This however is quite often not the case with SEDs. SEDs will form radical products after oxidation, which can then go on to directly interact with the reduction half of the reaction.[41-42] These radicals can even directly inject electrons into the conduction band of the semiconductor, further effecting the reduction step. The generated $O_2$, which is not generated with SEDs, also competes with the formation of $H_2$ gas to reform $H_2O$ in water splitting. A catalyst efficient with SEDs may be ineffective with pure water splitting due to this $O_2$ effect. This habit is also seen in another popular review (over 5000 citations) by *Ong et al.*[43] which is evaluating the effectiveness of various graphitic carbon nitride catalysts. This review has a chart listing improved graphitic carbon nitride catalysts for 'water splitting'; however, most of the listed materials show activities with SEDs present. The quality of these reviews should not be fully disparaged, since they are still quite comprehensive and useful, and the issue is more indicative of an overall systemic issue within the scientific community.

However, within recent years this issue of equating SED oxidation to water splitting appears to be less common, with most publications avoiding stating 'water splitting' unless it truly is without any SEDs. I hope that the research conducted in chapter 2 of this dissertation played a small role in this shift, but it nonetheless is a positive change in the research field of photocatalytic hydrogen generation.

There are many different heterogeneous photocatalysts that have been evaluated for hydrogen generation activity. However, standards of comparing hydrogen generation rates are poor, outside of accounting for the mass of catalyst used in the units (i.e. μmol $h^{-1}$ $g^{-1}$). Lack of standards include different setups for evaluating $H_2$ generation (inline flow, batch reaction, etc..), different types of light sources (wavelengths and intensity), and different SEDs being used. With these caveats in mind, some strong examples of effective photocatalysts may be discussed. Common photocatalysts include perovskites, metal organic frameworks (MOFs), carbon nitride ($C_3N_4$) based catalysts, and the previously discussed M@$TiO_2$ catalysts. For cheap visibly absorbing photocatalysts for hydrogen generation, $C_3N_4$ catalysts show great potential. Some examples of various hydrogen generation photocatalysts can be found in the table below (Table 1.4.1)

**Table 1.4.1.** Comparison of various photocatalysts with reported hydrogen generation yields

| Catalyst | Sacrificial Electron Donor | Light Source | $H_2$ production ($\mu mol\ g^{-1}\ h^{-1}$) | Ref |
|---|---|---|---|---|
| Al-ATA-Ni MOF | None | Xe Lamp (300 W) | 62 | [44] |
| $La_2Ti_2O_7$:Ba(8%) | None | Hg Lamp (450 W) | 900 | [45] |
| Pt-Co/g-$C_3N_4$ | None | >300 nm (Xe Lamp, 300 W)<br>>420 nm (Xe Lamp, 300 W) | 61<br>6 | [46] |
| $C_3N_4$/C-dots | None | >420 nm (Xe Lamp, 300 W) | 575 | [47] |
| Ag-AgMOM | Triethanolamine | >420 nm (Xe Lamp, 300 W) | 1025 | [48] |
| Au/$TiO_2$ | Methanol | Hg Lamp | 1800 | [49] |
| CuO/$TiO_2$ | Methanol | Hg Lamp | 2785 | [49] |
| $Cd_{0.5}Zn_{0.5}S$-8%$CuInS_2$ | $Na_2SO_3$ | >420 nm (Xe Lamp, 300 W) | 7732.6 | [50] |
| Am-$CuO_x$/$TiO_2$ | Methanol | Solar Simulation | 400 | [51] |
| 5%C-$MoS_2$@g-$C_3N_4$ | Triethanolamine | Solar Simulation | 157.14 | [52] |
| $SrTiO_3$:Al – 0.1%Rh/ 0.05%$Cr_2O_3$/0.05%C oOOH | None | Xe Lamp (300 W)<br>Solar Simulation | 3900*<br>105* | [53] |
| 1%Pt/$TiO_2$-NP | None | Hg Lamp (500 W) | 7410 | [54] |

*Reported as $\mu mol\ h^{-1}$ with no listed mass of catalyst
ATA = 3-amino-1,2,4-triazole, MOF = metal organic framework, MOM = metal organic matrix, Am = amorphous, C-Dots = carbon quantum dots.

## 1.5 Activation of the C-H bond by radical chemistry

Activation of the C-H bond to initiate chemical processes, such as coupling reactions, is of great interest in chemistry today. This is because the C-H bond is often quite stable, and typically additional steps are required to replace the bond with a more reactive one. Direct activation of a C-H bond is desirable to allow for better step economy in synthetic procedures, as well as avoiding the requirement of more costly compounds. One interesting method of activating the

C-H bond is through the formation of a carbon-centered radical, usually coupled with some form of hydrogen atom transfer (HAT).

One method of activating C-H bonds is with the use of a radical initiator. One of the most common radical initiators is di-tert-butyl peroxide (DTBP). DTBP can decompose, either photochemically or thermally, into tert-butoxyl radicals. These *tert*-butoxyl radicals may then initiate the formation of other radicals through hydrogen abstraction by HAT from a compound (Scheme 1.5.1). If the abstracted hydrogen is attached to carbon, this is an efficient method of activating this C-H bond to form a carbon centred radical.[55]

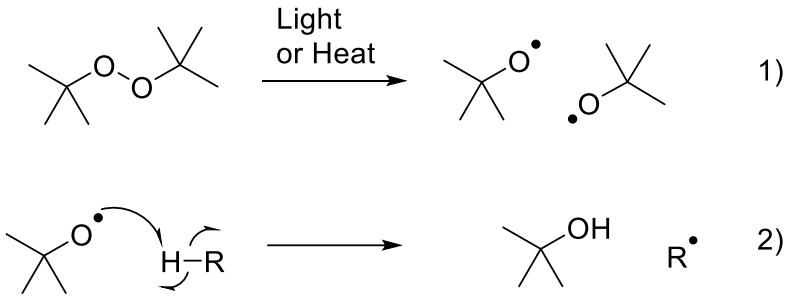


**Scheme 1.5.1.** *tert*-Butoxyl radical formation from di-*tert*-butyl peroxide (DTBP) with subsequent hydrogen abstraction from HR (R is any compound susceptible to H abstraction) to form an R• radical by hydrogen atom transfer (HAT)

Other radical initiators such as benzoyl peroxide, with added aromatic groups, can also be used for increased range of absorbance for photochemical activation. After activation of the C-H bond to form a carbon centered radical, this activated species may then go on to react. Such possible reactions include homo or cross-coupling with other radical species[56-57], additions to alkenes[58], carbonyl addition[59], and halogenation[60]. This list is by no means comprehensive, as radicals are extremely reactive species (Scheme 1.5.2). Other radical chemistry with C-H bond activation can include amination, esterification, and alkynylation[61-62]

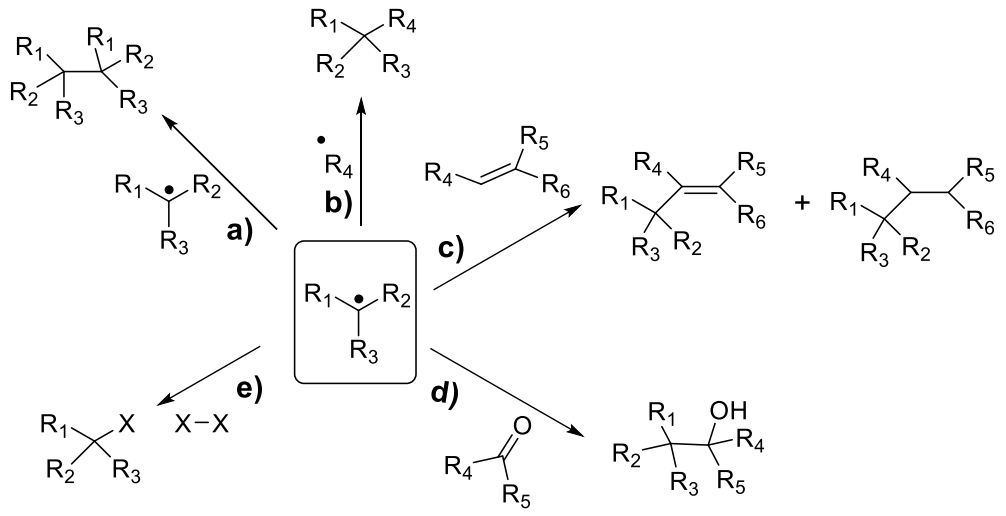


**Scheme 1.5.2.** Various reactions with a carbon centered radical (with various R groups), including **a)** homo-coupling with identical species, **b)** cross-coupling with another radical species, **c)** alkene addition, **d)** carbonyl addition, **e)** and halogenation (halide = X). The products of c) and c) are shown as the final expected radical-quenched products.

The formation of carbon-centered radicals also opens up interesting chemistry through direct formation of radicals from the solvent itself. The C-H bond of a solvent could be activated to allow for reactions either with itself, or with other compounds in solution. This can be very effective with electron-rich solvents such as ethers, and solvent-radical formation through HAT from radical initiators such as DTBP has been well documented. However, there are also many issues that appear when attempting to conduct chemistry such as this. Firstly, radicals from the radical initiator itself can directly participate with the reaction intended for the solvent-radicals. Also, radical initiators will form other chemical products in solution that will need to be removed, and the radical initiators often form 2 radicals which can recombine.

Another form of C-H bond activation to form a carbon centered radical is proton-coupled electron transfer (PCET).[63] This process, in contrast to typical HAT using a radical initiator, has separate movement of the electron and proton. This is often conducted with transition metal complexes, for example $[Ru^{IV}O(bpy)_2py]^{2+}$, in which the metal centre accepts an electron from the C-H bond-containing molecule, and a ligand of the metal accepts the proton. This forms the

expected carbon-centered radical for hydrogen abstraction (Scheme 1.5.3 equation 3). PCET with transition metal complexes often is a process involving one kinetic step, with both the electron and proton moving at the same time. However, two-step processes are also possible, and the proton does not require movement to the oxidizer compound. The electron can be first transferred to the oxidizer, forming a radical cation in the oxidized molecule. Loss of the proton may then follow to form the final carbon-centered radical (Scheme 1.5.3 equation 4). These two processes are still typically coupled, hence it is still considered as PCET.

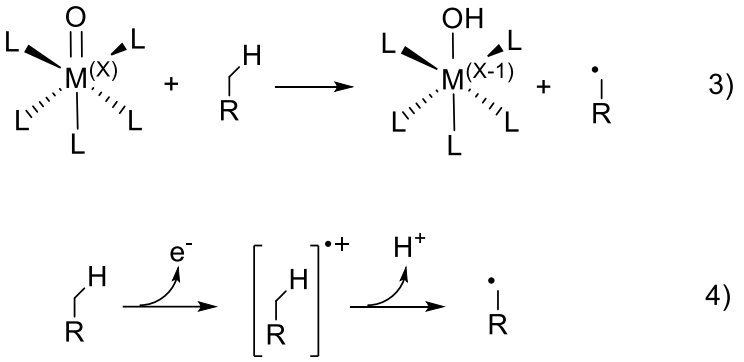


**Scheme 1.5.3.** Proton-coupled electron transfer (PCET) mechanisms for carbon-centered radical formation. Equation 3 shows the one-step PCET mechanism using a transition metal complex (initial oxidation state = X). Equation 4 shows the two step mechanism with initial removal of an electron by an oxidizer to form a radical cation. Loss of $H^+$ then forms the final carbon-centered radical.

As mentioned previously, semiconductors such as $TiO_2$ can perform oxidation reactions upon excitation, due to the photogenerated 'hole' in the valence band of the semiconductor. $TiO_2$ is well established to form reactive oxygen species, such as $HO^{\bullet}$, and this process typically involves a two step PCET mechanism with initial formation of a radical cation. Pd@$TiO_2$ was also shown in our group to create some tetrahydrofuran (THF) carbon-centered radicals in solution, as a side effect during Ullman-coupling reactions. This prompted interested in the investigation of the power of $TiO_2$-based photocatalysts to form carbon-centered radicals by PCET from other ethers. This research will be the focus of chapter 3 of this dissertation, and highlights the true

oxidative strength of M@$TiO_2$ photocatalysts for the activation of C-H bonds. It also has benefits over typical radical initiators, as the M@$TiO_2$ does not leave initiator-derived debris, and it only forms one radical at a time.

## 1.6 Laser Flash Photolysis

Laser flash photolysis (LFP) is an approach for evaluating chemical reaction kinetics under short time scales. The invention of the laser in the 1960s allowed for the use of the fast and consistent pulses that they can induce to provide the groundwork for developing this field of research.[64] The first report of LFP, with a final system similar to the current day, is from Lindqvist in 1966 which showed the detection of the triplet excited state of acridine using excitation from a nitrogen laser (337 nm)[65]. This typical setup involves exciting a sample with a short laser pulse, and measuring the change in absorbance over time using a probe beam. The probe beam passes through the sample perpendicular to the direction of the laser pulse, and then passes through a monochromator which selects for a desired detection wavelength. This then enters a photomultiplier tube which amplifies the signal into an electrical current for detection. By measuring the absorbance signal before the laser pulse, then evaluating the absorbance signal over time after excitation, a change in absorbance over time can be plotted. This change in absorbance is from transient species created in the sample from the laser excitation, and the formation and decay of these species can be monitored with this time-resolved technique (Figure 1.6.1). Transient absorbance spectra can also be taken at different time-points for showing the full absorbance spectra of a transient species, which can allow for conclusions on the structure of the species.

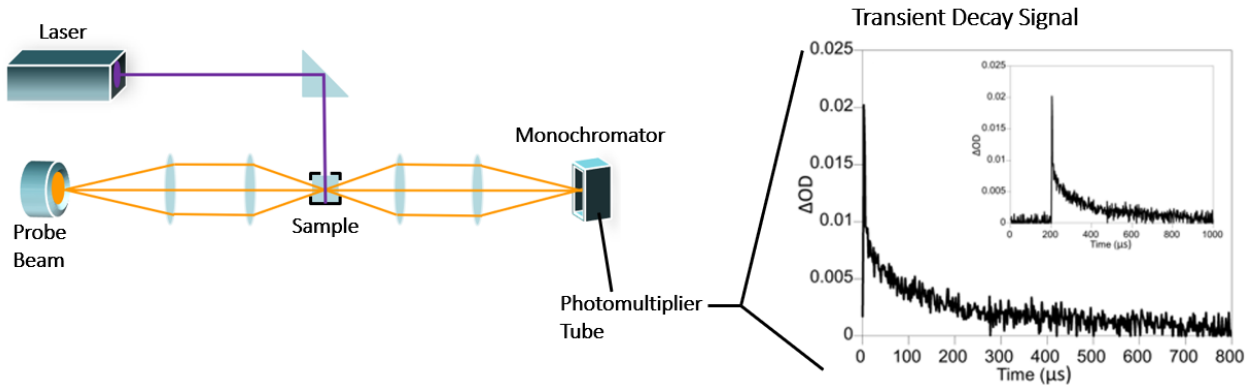


**Figure 1.6.1.** Typical optical setup for laser flash photolysis.

The duration of the laser pulse limits the timescales that can be evaluated with laser-flash photolysis. The length of the pulse has to be significantly shorter than the timescales being evaluated. For instance, timescales of 20 ns – 1 μs are the lower limit for a laser with a nanosecond pulse. Nanosecond LFP was the first developed, with nitrogen lasers commonly used. However, excimer, neodymium-doped yttrium aluminum garnet (Nd/YAG), and pumped optical parametric oscillator (OPO) are more commonly used today due to being more convenient. The Nd/YAG laser, used in this dissertation, produces a 1064 nm pulse; however, this can be converted into higher harmonics by frequency doubling into 532 nm, or frequency tripling into 355 nm.[64] This gives a nice range of useful excitation wavelengths to be used, with the 355 nm harmonic being utilized in this dissertation. Femto- and picosecond LFP techniques are becoming increasingly popular; however, nanosecond LFP is still adequate for evaluating many photochemical systems.

LFP of $TiO_2$ systems typically uses diffuse reflectance instead of absorbance for measurements. This setup is very similar to absorbance; however, it is instead measuring the reflected light off of a surface. $TiO_2$ by itself has induced transient signals after excitation with 355 nm light, due to formation of the photogenerated charge carriers. The presence of these charge carriers induces a variety of changes in the $TiO_2$ that induce transient signals over the whole spectral range (300-900 nm). Much of the nature of these transient signals is still disputed; however, general trends and theories have been established. Transient signals below 500 nm are typically considered to be due to the presence of photogenerated holes. Much of this signal is

due to signals from trapped hole sites, often coupled with lattice deformations or surface interactions. For instance, some of the signal may also be due to interactions between trapped holes on the surface, and the surrounding solvent. Transient signals at higher wavelengths can typically be attributed to trapped electrons, again often inducing lattice deformations in these trapping sites.

## 1.7 Calcium Carbide

Calcium carbide ($CaC_2$) is a highly reactive solid which rapidly forms acetylene gas when exposed to water, forming $Ca(OH)_2$ in the process. This allows for a convenient way for the *in situ* formation of acetylene gas for various chemical transformations. This is preferable to storing large quantities of explosive acetylene gas. Figure 1.7.1 shows some examples of common reactions that can utilize $CaC_2$ as a precursor. Reactions A-C show products that maintain the alkyne moiety. This includes the addition of iodo or silyl groups (A), aryl acetylene synthesis (B), and Favorskii alkynylations (C). The use of transition metal catalysis can also allow for the formation of highly functionalized alkenes (D), and nucleophilic additions can form O-, S-, and N-vinyl derivatives (E). Alternatively, ring structures can be formed with Diels-Alder reactions (F), or other cycloadditions (H+G).[66-67] Typically these reactions simply involve the formation of acetylene gas, which is then used in the reaction. However, in rare cases solubilized intermediates of calcium carbide have been proposed.[68-69] The formation of these solubilized intermediates will be further investigated in chapter 5 of this dissertation.

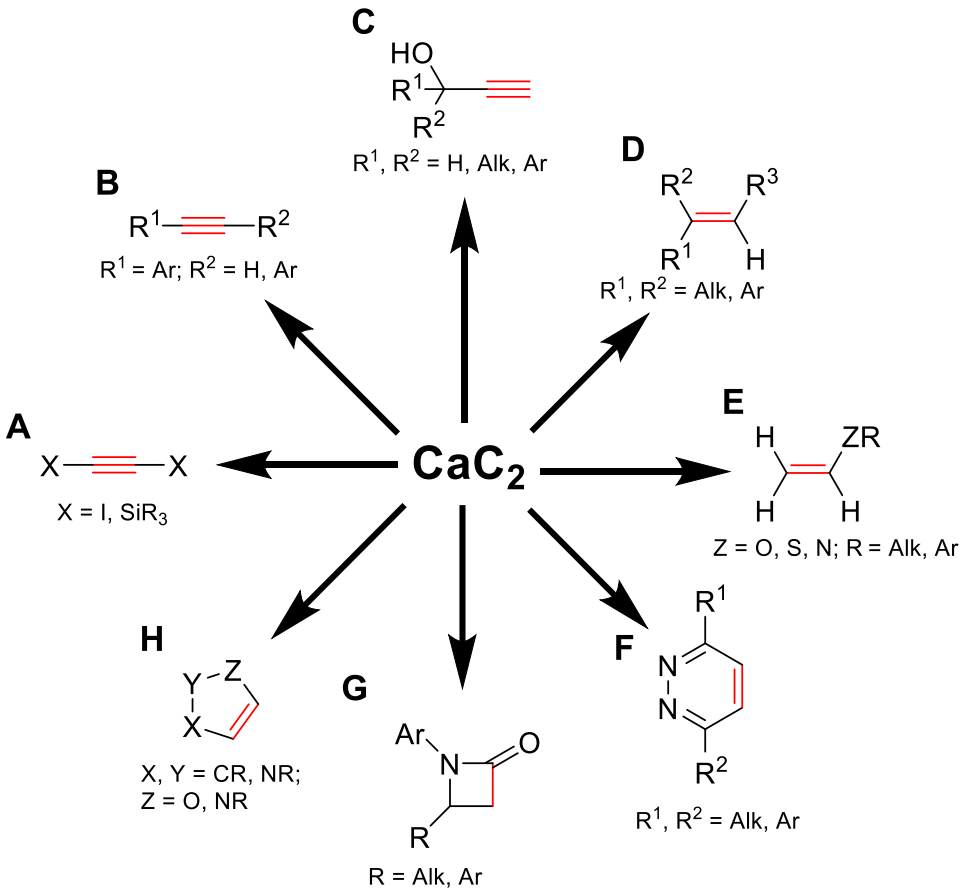


**Figure 1.7.1.** Example reaction products involving $CaC_2$ as a source of acetylene. The red bonds indicate the carbons coming from the $CaC_2$.

## 1.8 Outline of Thesis

The overarching goal of this dissertation is to show the versatility of $TiO_2$-based materials in a variety of different chemical applications, overall testing the limits of this cheap and easily synthesized heterogeneous photocatalyst. This will start with the evaluation of various M@$TiO_2$ photocatalysts for hydrogen generation both for pure 'water splitting', and with SEDs (Chapter 2). All of these materials were synthesized by the photochemical methods developed by our group, and are also compared to a commercial Au@$TiO_2$ photocatalyst (Table 2.2.1). Under pure water splitting conditions, Au, Cu, Pt, and Co were the best performing metals in M@$TiO_2$ photocatalysts in decreasing order, with $H_2$ generation rates in the range of 0.1-0.175 mmol $g^{-1}$ $h^{-1}$. Ru, Pd, and bare $TiO_2$ had no significant detectable hydrogen production from pure water

(Figure 2.2.4(A)). However, once a SED such as methanol or formic acid is used, hydrogen generation rates increase up to a max of 22 mmol $g^{-1}$ $h^{-1}$. Interestingly, the relative reactivity order of the catalysts also changes (Figure 2.2.4(B-C)). If the oxidation and reduction half-reactions are truly separate, it would be expected that the relative order of reactivities should be the same no matter the SED (or lack of). This is due to the fact that if they are separate, the SED is not involved with the reaction occurring at the metal. One notable difference is Pd@$TiO_2$ which is ineffective in water splitting, but has one of the better activities with methanol or formic acid. Also, Pt@$TiO_2$ has almost double the activity compared to commercial Au@$TiO_2$ with methanol; however, Au@$TiO_2$ is better than Pt@$TiO_2$ with formic acid. All of this implies strong interactions between the oxidation and reduction half reactions, meaning that the interactions between the metal nanoparticle are not as simple as just forming the $H_2$ gas. This is strong confirmation of the possibility of radicals from SEDs interacting further in the reaction, as has been proposed previously.[41] Overall, this chapter confirms the problems with extrapolating $H_2$ generation efficiencies for 'water splitting' from results with SEDs present. Overall, the only way to accurately design a catalyst for water splitting is to conduct testing in pure water conditions. Also, the various M@$TiO_2$ catalysts behave well when compared to published $H_2$ generation photocatalysts, especially when considering the overall price and ease of synthesis for the M@$TiO_2$ catalysts.

Chapter 3 is focused on evaluating the efficiency of M@$TiO_2$ photocatalysts for generating radical species directly from organic solvents, with a focus on radical generation from ethers. Our group had noticed previously that some organic solvents were not inert with M@$TiO_2$ catalysts, specifically seeing the formation of products from THF-derived radicals when it was used as a solvent.[26] It was proposed that, as with most SEDs, THF and other ethers could undergo PCET to form a radical through hydrogen atom abstraction. Firstly, various M@$TiO_2$ catalysts were tested for their ability to form THF solvent radicals, and if these radicals are 'free' enough in solution to react. This was done by using TEMPO (a radical scavenger) to trap the THF radicals in solution, and then evaluating formation of the TEMPO-THF adduct. Also, $H_2$ generation rates were measured as an indirect method of evaluating the chemistry occurring, as the $H_2$ being generated is from any abstracted hydrogens from the solvent. Overall, it was found that Pd@$TiO_2$ was the

most effective photocatalyst for forming a usable THF radical with a ~90% yield of TEMPO-THF adduct after 4 hours of 368 nm LED irradiation with 4 mg/ml of catalyst (Figure 3.2.2). This catalyst also gave the highest rate of $H_2$ generation, with the differences being larger in $H_2$ generation (Figure 3.2.3). Overall, most metals performed decently in TEMPO-THF adduct formation, with some metals performing much worse with $H_2$ generation. This makes sense as the metals should all trap electrons well, increasing the lifetime of the oxidizing photogenerated holes; however, the specific metal would alter the $H_2$ production side of the reaction more. Since Pd@$TiO_2$ was the most effective catalyst overall, it was then tested with a variety of different ethers. Overall, best yields were observed with THF and diethyl ether (DEE), with dioxane (DOX) and tetrahydropyran (THP) having less but still considerable TEMPO-Ether adduct yield. Dimethoxymethane (DMM), 1-methoxypropane (MOP), 1,3-dioxolane (DOL), and 2-methyl-1,3-dioxolane (MDOL) all had no detectable formation of the TEMPO-ether adduct. However, these all still showed formation of $H_2$ gas, implying that H abstraction is still occurring (Table 3.2.2). Instead, these ether radicals are forming, but then fragment in the case of DMM and MOP. The lack of DOL and MDOL adduct formation is less clear, and may be due to the specific conditions increasing formation of TEMPO side products, especially as DOL is shown to have usable radicals in the research in chapter 4. Relative activities of DOX and DEE in competition with THF are also shown to be different than activities shown with abstraction by *tert*-butoxyl radicals (Table 3.2.3). DEE is more oxidizable by *tert*-butoxyl radicals, while DOX is more oxidizable by the $TiO_2$ hole. This is due to surface affinity being a larger factor in competition in heterogeneous systems, and DOX has high surface affinity on the $TiO_2$ surface. DFT calculations were also used to evaluate the interaction between the surface of $TiO_2$ and ether during the PCET process (Figure 3.2.5), and the adsorption is shown to be especially favorable when the surface has a positive charge from a trapped hole. Interestingly, solvent-radical generated species were also observed from toluene, and small amounts from acetonitrile as well. Overall, this chapter will show the true strength of the photogenerated hole of M@$TiO_2$ photocatalysts, and the possible usability of generated solvent radicals from the PCET process.

Chapter 4 will further explore the chemistry of the photogenerated hole of $TiO_2$ for solvent radical reactions. This will be done through developing new nanosecond LFP procedures

for evaluating the chemistry of low concentration suspensions of $TiO_2$. This research was conducted with simple P25 $TiO_2$, to allow for a more simple system to understand; however, similar methods may be implemented with M@$TiO_2$ catalysts, and the conclusions presented may also give insight into the activities of the M@$TiO_2$ catalysts. The goal was to evaluate transient species in solution over the full spectral range, even from 300-400 nm where $TiO_2$ absorbs. Firstly, background transients of the $TiO_2$ itself were to be evaluated. It was found that low concentration suspensions of 10 mg/L $TiO_2$ In 1,3-dioxolane show very long stretched exponentials for the hole and electron transients of $TiO_2$, up to the 1 ms range (Figure 4.2.2). This was consistent with fractal models proposed with diffuse reflectance LPF, due to the many different pathways the hole and electron may take for recombination (Figure 4.2.3). With an understanding of the dynamics of background transients for $TiO_2$, the chemistry of generated solvent radicals of 1,3-dioxolane (DOL) was evaluated. This was done by treating generated DOL radicals with 1,1-diphenylethylene (DPE), a reactive alkene that forms a radical with a characteristic transient peak at 330 nm. It was found that when DPE is present, a signal with longer lifetime is introduced at 330 nm, implying formation of DOL radicals that react with DPE (Figure 4.2.6-7). This is interesting as DOL did not show TEMPO-DOL formation in chapter 3, which shows this is a more sensitive and accurate technique for evaluating the formation and usability of generated solvent radicals. The strength of the 330 nm signal from the solvent-DPE adduct is also strongly dependent on the solvent, with 1,3-dioxolane giving greater signal than 1,4-dioxane, and acetonitrile showing no signal (Figure 4.2.11). This follows the expected trend of reactivity of these solvents for PCET. Overall, this chapter will highlight this new technique of evaluating $TiO_2$ suspensions, and shows the overall possibilities present for evaluating heterogeneous mixtures by nanosecond LFP. This chapter also will conclude one of the largest themes of this dissertation, which is the chemistry of solvent-generated radicals from $TiO_2$ catalysts.

In chapter 5, this dissertation will explore a somewhat different topic, tangentially related to the rest of the work presented. The work started with the hope of conducting photocatalysis with Pd@$TiO_2$; however, the chemistry instead worked thermally. This chemistry is still using the same type of catalyst, and helps to highlight the versatility of it for other chemical systems even outside of photochemistry. With this in mind, the more interesting aspect of the chapter is the

unique chemistry of calcium carbide ($CaC_2$) in dimethyl sulfoxide (DMSO) under low water conditions. As discussed above, $CaC_2$ is an interesting precursor for organic transformations, and is especially interesting for use in Sonogashira-like reactions for the formation of symmetrical diarylethynes.[67] The investigation started with testing if our Pd@$TiO_2$ catalyst can form 1,2-diphenylacetylene from bromobenzene using $CaC_2$ as the source of acetylene. Initial investigations found that this was possible with DMSO as a solvent; however, only under thermal conditions, with a yield of 48.3% for the desired 1,2-diphenylacetylene product with the best conditions (Table 5.2.1). Interestingly, no additional water was required, and additional water also would start to decrease yields with more than 10 µL added (Table 5.2.2). This implied that the chemistry occurring was not a simple in-situ formation of acetylene gas, as additional water should instead improve the reaction due to more acetylene formation. Through investigations with a two-step reaction, it was found that initial heating of $CaC_2$ in DMSO (with 10 µL of added water) forms a solubilized species identified as ethynyl calcium hydroxide. The filtrate solution containing this intermediate was somewhat stable, and the mixture could then be used with bromobenzene and Pd@$TiO_2$ as a catalyst to form 1,3-diphenylacetylene (Table 5.2.3). Overall, this chapter shows that low water conditions in DMSO can be used to select for a solubilized ethynyl calcium hydroxide instead of acetylene gas. This intermediate allows for safe conditions, with the reduced presence of explosive acetylene gas, while also having more reactive species in solution. This intermediate also is reactive with Pd@$TiO_2$ catalyst for the Sonogashira-like generation of symmetrical diarylethynes.

## 1.8 References

1. Hainer, A. S.; Hodgins, J. S.; Sandre, V.; Vallieres, M.; Lanterna, A. E.; Scaiano, J. C., Photocatalytic hydrogen generation using metal-decorated $TiO_2$: sacrificial donors vs true water splitting. *ACS Energy Lett.* **2018,** *3* (3), 542-545.
2. Hainer, A.; Marina, N.; Rincon, S.; Costa, P.; Lanterna, A. E.; Scaiano, J. C., Highly electrophilic titania hole as a versatile and efficient photochemical free radical source. *J. Am. Chem. Soc.* **2019,** *141* (11), 4531-4535.
3. Hainer, A.; Joshi, N.; Scaiano, J. C., Laser flash photolysis of titanium dioxide suspensions for the evaluation of solvent-mediated radical reactions. *Phys. Chem. Chem. Phys.* **2023,** *25* (4), 2747-2751.

4. Mills, A.; Le Hunte, S., An overview of semiconductor photocatalysis. *J. Photochem. Photobiol. A.* **1997,** *108* (1), 1-35.
5. Martin, S. T.; Herrmann, H.; Choi, W.; Hoffmann, M. R., Time-resolved microwave conductivity. Part 1.—$TiO_2$ photoreactivity and size quantization. *J. Chem. Soc., Faraday Trans.* **1994,** *90* (21), 3315-3322.
6. Schneider, J.; Matsuoka, M.; Takeuchi, M.; Zhang, J.; Horiuchi, Y.; Anpo, M.; Bahnemann, D. W., Understanding $TiO_2$ Photocatalysis: Mechanisms and Materials. *Chem. Rev.* **2014,** *114* (19), 9919-9986.
7. Pitre, S. P.; Yoon, T. P.; Scaiano, J. C., Titanium dioxide visible light photocatalysis: surface association enables photocatalysis with visible light irradiation. *Chem. Commun.* **2017,** *53* (31), 4335-4338.
8. Fujishima, A.; Zhang, X.; Tryk, D. A., $TiO_2$ photocatalysis and related surface phenomena. *Surf. Sci. Rep.* **2008,** *63* (12), 515-582.
9. Ohno, T.; Sarukawa, K.; Tokieda, K.; Matsumura, M., Morphology of a $TiO_2$ Photocatalyst (Degussa, P-25) Consisting of Anatase and Rutile Crystalline Phases. *J. Catal.* **2001,** *203* (1), 82-86.
10. Li, R.; Li, C., Photocatalytic water splitting on semiconductor-based photocatalysts. *Adv. Catal.* **2017,** *60*, 1-57.
11. Fox, M. A.; Dulay, M. T., Heterogeneous photocatalysis. *Chem. Rev.* **1993,** *93* (1), 341-357.
12. Fujishima, A.; Rao, T. N.; Tryk, D. A., Titanium dioxide photocatalysis. *J. Photochem. Photobiol. C* **2000,** *1* (1), 1-21.
13. Kisch, H., On the problem of comparing rates or apparent quantum yields in heterogeneous photocatalysis. *Angew. Chem. Int. Ed.* **2010,** *49* (50), 9588-9589.
14. Subramanian, V.; Wolf, E. E.; Kamat, P. V., Catalysis with $TiO_2$/gold nanocomposites. Effect of metal particle size on the Fermi level equilibration. *J. Am. Chem. Soc.* **2004,** *126* (15), 4943-4950.
15. Wu, X.; Jaatinen, E.; Sarina, S.; Zhu, H. Y., Direct photocatalysis of supported metal nanostructures for organic synthesis. *J. Phys. D* **2017,** *50* (28), 283001.
16. Kowalska, E.; Mahaney, O. O. P.; Abe, R.; Ohtani, B., Visible-light-induced photocatalysis through surface plasmon excitation of gold on titania surfaces. *Phys. Chem. Chem. Phys.* **2010,** *12* (10), 2344-2355.
17. Elhage, A.; Lanterna, A. E.; Scaiano, J. C., Light-induced Sonogashira C-C coupling under mild conditions using supported palladium nanoparticles. *ACS Sustain. Chem. Eng.* **2018,** *6* (2), 1717-1722.
18. Wang, H.; Li, X.; Zhao, X.; Li, C.; Song, X.; Zhang, P.; Huo, P., A review on heterogeneous photocatalysis for environmental remediation: From semiconductors to modification strategies. *Chin. J. Catal.* **2022,** *43* (2), 178-214.
19. Chen, X.; Shen, S.; Guo, L.; Mao, S. S., Semiconductor-based photocatalytic hydrogen generation. *Chem. Rev.* **2010,** *110* (11), 6503-6570.
20. Wang, B.; Durantini, J.; Nie, J.; Lanterna, A. E.; Scaiano, J. C., Heterogeneous photocatalytic click chemistry. *J. Am. Chem. Soc.* **2016,** *138* (40), 13127-13130.
21. Elhage, A.; Lanterna, A. E.; Scaiano, J. C., Catalytic farming: reaction rotation extends catalyst performance. *Chem. Sci.* **2019,** *10* (5), 1419-1425.
22. Murdoch, M.; Waterhouse, G. I. N.; Nadeem, M. A.; Metson, J. B.; Keane, M. A.; Howe, R. F.; Llorca, J.; Idriss, H., The effect of gold loading and particle size on photocatalytic hydrogen production from ethanol over Au/$TiO_2$ nanoparticles. *Nat. Chem.* **2011,** *3* (6), 489-492.
23. Seh, Z. W.; Liu, S.; Low, M.; Zhang, S.-Y.; Liu, Z.; Mlayah, A.; Han, M.-Y., Janus Au-$TiO_2$ photocatalysts with strong localization of plasmonic near-fields for efficient visible-light hydrogen generation. *Adv. Mater.* **2012,** *24* (17), 2310-2314.
24. Pelaez, M.; Nolan, N. T.; Pillai, S. C.; Seery, M. K.; Falaras, P.; Kontos, A. G.; Dunlop, P. S. M.; Hamilton, J. W. J.; Byrne, J. A.; O'Shea, K.; Entezari, M. H.; Dionysiou, D. D., A review on the visible light active titanium dioxide photocatalysts for environmental applications. *Appl. Catal. B.* **2012,** *125*, 331-349.

25. Zhang, X.; Shi, R.; Li, Z.; Zhao, J.; Huang, H.; Zhou, C.; Zhang, T., Photothermal-assisted photocatalytic nitrogen oxidation to nitric acid on palladium-decorated titanium oxide. *Adv. Energy Mater.* **2022,** *12* (13), 2103740.
26. Marina, N.; Lanterna, A. E.; Scaiano, J. C., Expanding the color space in the two-color heterogeneous photocatalysis of Ullmann C-C coupling reactions. *ACS Catal.* **2018,** *8* (8), 7593.
27. Su, R.; Tiruvalam, R.; He, Q.; Dimitratos, N.; Kesavan, L.; Hammond, C.; Lopez-Sanchez, J. A.; Bechstein, R.; Kiely, C. J.; Hutchings, G. J.; Besenbacher, F., Promotion of phenol photodecomposition over $TiO_2$ using Au, Pd, and Au–Pd nanoparticles. *ACS Nano* **2012,** *6* (7), 6284-6292.
28. Corma, A.; Serna, P., Chemoselective hydrogenation of nitro compounds with supported gold catalysts. *Science* **2006,** *313* (5785), 332-334.
29. Han, D.; Zhang, Z.; Bao, Z.; Xing, H.; Ren, Q., Pd-Ni nanoparticles supported on titanium oxide as effective catalysts for Suzuki-Miyaura coupling reactions. *Front. Chem. Sci. Eng.* **2018,** *12* (1), 24-31.
30. Fujishima, A.; Honda, K., Electrochemical photolysis of water at a semiconductor electrode. *Nature* **1972,** *238* (5358), 37.
31. Pan, H., Principles on design and fabrication of nanomaterials as photocatalysts for water-splitting. *Renew. Sust. Energ. Rev.* **2016,** *57*, 584-601.
32. Franceschini, E. A.; Hainer, A.; Lanterna, A. E., Niobium-based semiconductor electrodes for hydrogen evolution reaction. *Int. J. Hydrogen Energy* **2019,** *44* (60), 31940-31948.
33. Gomez, M. J.; Benavente-Llorente, V.; Hainer, A.; Lacconi, G. I.; Scaiano, J. C.; Franceschini, E. A.; Lanterna, A. E., Evaluation of different Ni-semiconductor composites as electrodes for enhanced hydrogen evolution reaction. *Sustainable Energy Fuels* **2020,** *4* (8), 3963-3970.
34. Yuan, L.; Han, C.; Yang, M.-Q.; Xu, Y.-J., Photocatalytic water splitting for solar hydrogen generation: fundamentals and recent advancements. *Int. Rev. Phys. Chem.* **2016,** *35* (1), 1-36.
35. Ni, M.; Leung, M. K. H.; Leung, D. Y. C.; Sumathy, K., A review and recent developments in photocatalytic water-splitting using $TiO_2$ for hydrogen production. *Renew. Sust. Energ. Rev.* **2007,** *11* (3), 401-425.
36. Bie, C.; Wang, L.; Yu, J., Challenges for photocatalytic overall water splitting. *Chem* **2022,** *8* (6), 1567-1574.
37. Pellegrin, Y.; Odobel, F., Sacrificial electron donor reagents for solar fuel production. *C. R. Chim.* **2017,** *20* (3), 283-295.
38. Elhage, A.; Lanterna, A. E.; Scaiano, J. C., Tunable photocatalytic activity of palladium-decorated $TiO_2$: non-hydrogen-mediated hydrogenation or isomerization of benzyl-substituted alkenes. *ACS Catal.* **2017,** *7* (1), 250-255.
39. Liu, H.; Yuan, J.; Shangguan, W., Photochemical reduction and oxidation of water including sacrificial reagents and $Pt/TiO_2$ catalyst. *Energy Fuels* **2006,** *20* (6), 2289-2292.
40. Ran, J.; Zhang, J.; Yu, J.; Jaroniec, M.; Qiao, S. Z., Earth-abundant cocatalysts for semiconductor-based photocatalytic water splitting. *Chem. Soc. Rev.* **2014,** *43* (22), 7787-7812.
41. Schneider, J.; Bahnemann, D. W., Undesired role of sacrificial reagents in photocatalysis. *J. Phys. Chem. Lett.* **2013,** *4* (20), 3479-3483.
42. Schneider, J. T.; Firak, D. S.; Ribeiro, R. R.; Peralta-Zamora, P., Use of scavenger agents in heterogeneous photocatalysis: truths, half-truths, and misinterpretations. *Phys. Chem. Chem. Phys.* **2020,** *22* (27), 15723-15733.
43. Ong, W.-J.; Tan, L.-L.; Ng, Y. H.; Yong, S.-T.; Chai, S.-P., Graphitic carbon nitride ($g\text{-}C_3N_4$)-based photocatalysts for artificial photosynthesis and environmental remediation: Are we a step closer to achieving sustainability? *Chem. Rev.* **2016,** *116* (12), 7159-7329.
44. An, Y.; Liu, Y.; An, P.; Dong, J.; Xu, B.; Dai, Y.; Qin, X.; Zhang, X.; Whangbo, M. H.; Huang, B., Ni(II) Coordination to an Al-based metal-organic framework made from 2-aminoterephthalate for photocatalytic overall water splitting. *Angew. Chem. Int. Ed.* **2017,** *56* (11), 3036-3040.

45. Kim, J.; Hwang, D. W.; Kim, H. G.; Bae, S. W.; Lee, J. S.; Li, W.; Oh, S. H., Highly efficient overall water splitting through optimization of preparation and operation conditions of layered perovskite photocatalysts. *Top. Catal.* **2005,** *35* (3), 295-303.
46. Zhang, G.; Lan, Z.-A.; Lin, L.; Lin, S.; Wang, X., Overall water splitting by Pt/g-C3N4 photocatalysts without using sacrificial agents. *Chem. Sci.* **2016,** *7* (5), 3062-3066.
47. Liu, J.; Liu, Y.; Liu, N.; Han, Y.; Zhang, X.; Huang, H.; Lifshitz, Y.; Lee, S.-T.; Zhong, J.; Kang, Z., Metal-free efficient photocatalyst for stable visible water splitting via a two-electron pathway. *Science* **2015,** *347* (6225), 970-974.
48. Liu, Y.; Liu, C.-H.; Debnath, T.; Wang, Y.; Pohl, D.; Besteiro, L. V.; Meira, D. M.; Huang, S.; Yang, F.; Rellinghaus, B.; Chaker, M.; Perepichka, D. F.; Ma, D., Silver nanoparticle enhanced metal-organic matrix with interface-engineering for efficient photocatalytic hydrogen evolution. *Nat. Commun.* **2023,** *14* (1), 541.
49. Sreethawong, T.; Yoshikawa, S., Comparative investigation on photocatalytic hydrogen evolution over Cu-, Pd-, and Au-loaded mesoporous $TiO_2$ photocatalysts. *Catal. Commun.* **2005,** *6* (10), 661-668.
50. Chen, F.; Liao, J.; Lu, X.; Xu, Y.; Jiang, X.; Tian, M., Constructing an S-scheme heterojunction of 2D/2D Cd0.5Zn0.5S/CuInS2 nanosheet with vacancies for photocatalytic hydrogen generation under visible light. *Appl. Surf. Sci.* **2023,** *621*, 156721.
51. Guo, S.; Ji, Y.; Li, Y.; Li, H.; An, P.; Zhang, J.; Yan, J.; Liu, S.; Ma, T., Amorphous quantum dots co-catalyst: Defect level induced solar-to-hydrogen production. *Appl. Catal., B* **2023,** *330*, 122583.
52. Wei, X.; Zhang, X.; Ali, S.; Wang, J.; Zhou, Y.; Chen, H.; Zhang, G.; Qi, J.; He, D., Carbon intercalated $MoS_2$ cocatalyst on g-$C_3N_4$ photo-absorber for enhanced photocatalytic $H_2$ evolution under the simulated solar light. *Int. J. Hydrogen Energy* **2023,** *48* (37), 13827-13842.
53. Takata, T.; Jiang, J.; Sakata, Y.; Nakabayashi, M.; Shibata, N.; Nandal, V.; Seki, K.; Hisatomi, T.; Domen, K., Photocatalytic water splitting with a quantum efficiency of almost unity. *Nature* **2020,** *581* (7809), 411-414.
54. Wang, L.; Cao, S.; Guo, K.; Wu, Z.; Ma, Z.; Piao, L., Simultaneous hydrogen and peroxide production by photocatalytic water splitting. *Chin. J. Catal.* **2019,** *40* (3), 470-475.
55. Malatesta, V.; Scaiano, J. C., Absolute rate constants for the reactions of tert-butoxyl with ethers - importance of the stereoelectronic effect. *J. Org. Chem.* **1982,** *47* (8), 1455.
56. Li, M.; Berritt, S.; Matuszewski, L.; Deng, G.; Pascual-Escudero, A.; Panetti, G. B.; Poznik, M.; Yang, X.; Chruma, J. J.; Walsh, P. J., Transition-metal-free radical C($sp^3$)-C($sp^2$) and C($sp^3$)-C($sp^3$) coupling enabled by 2-azaallyls as super-electron-donors and coupling-partners. *J. Am. Chem. Soc.* **2017,** *139* (45), 16327-16333.
57. Masuda, K.; Nagatomo, M.; Inoue, M., Direct assembly of multiply oxygenated carbon chains by decarbonylative radical-radical coupling reactions. *Nat. Chem.* **2017,** *9* (3), 207-212.
58. Minisci, F., Free-radical additions to olefins in the presence of redox systems. *Acc. Chem. Res.* **1975,** *8* (5), 165.
59. Zhang, S. Y.; Zhang, F. M.; Tu, Y. Q., Direct $Sp^3$ alpha-C-H activation and functionalization of alcohol and ether. *Chem. Soc. Rev.* **2011,** *40* (4), 1937.
60. Masterson, D. S.; Porter, N. A., Diastereoselective free radical halogenation, azidation, and rearrangement of β-silyl Barton esters. *Org. Lett.* **2002,** *4* (24), 4253-4256.
61. Zhang, T.; Wu, Y.-H.; Wang, N.-X.; Xing, Y., Advances in C($sp^3$)-H bond functionalization via radical processes. *Synthesis* **2019,** *51* (24), 4531-4548.
62. Yi, H.; Zhang, G. T.; Wang, H. M.; Huang, Z. Y.; Wang, J.; Singh, A. K.; Lei, A. W., Recent advances in radical C-H activation/radical cross-coupling. *Chem. Rev.* **2017,** *117* (13), 9016.
63. Mayer, J. M., Understanding hydrogen atom transfer: from bond strengths to Marcus theory. *Acc. Chem. Res.* **2011,** *44* (1), 36.

64. Scaiano, J. C., Nanosecond Laser Flash Photolysis: A Tool for Physical Organic Chemistry. In *Reactive Intermediate Chemistry*, John Wiley & Sons: 2003; pp 847-871.
65. Lindqvist, L., Utilization of a laser with pulsed ultraviolet emission in flash photolysis. Triplet state of acridine. *C. R. Hebd. Seances Acad. Sci., Ser. C* **1966,** *263* (15), 852.
66. Rodygin, K. S.; Werner, G.; Kucherov, F. A.; Ananikov, V. P., Calcium carbide: A unique reagent for organic synthesis and nanotechnology. *Chem Asian J.* **2016,** *11* (7), 965-976.
67. Rodygin, K. S.; Ledovskaya, M. S.; Voronin, V. V.; Lotsman, K. A.; Ananikov, V. P., Calcium carbide: versatile synthetic applications, green methodology and sustainability. *Eur. J. Org. Chem.* **2021,** *2021* (1), 43-52.
68. Gao, L.; Liu, Z.; Ma, X.; Li, Z., Direct synthesis of propen-2-yl sulfones through cascade reactions using calcium carbide as an alkyne source. *Org. Lett.* **2020,** *22* (13), 5246-5250.
69. Polynski, M. V.; Sapova, M. D.; Ananikov, V. P., Understanding the solubilization of Ca acetylide with a new computational model for ionic pairs. *Chem. Sci.* **2020,** *11* (48), 13102-13112.

# 2. Photocatalytic Hydrogen Generation Using Metal-Decorated $TiO_2$: Sacrificial Donors vs. True Water Splitting

This chapter has been adapted from ACS Energy Lett. **2018**, 3, 542-545 with permission from the American Chemical Society. To allow for consistent formatting and clarity, some changes have been made.

## 2.1 Preamble to chapter 2

The following chapter compares a variety of different metal-decorated $TiO_2$ photocatalysts for their differing efficiencies for hydrogen generation using pure water or water with sacrificial electron donors (SEDs). This was done to evaluate the effectiveness of the various metal decorations, while also evaluating the assumption, wide-spread in literature at the time, that hydrogen generation with SEDs can give accurate predictions of expected activity for 'water splitting' efficiency. To conduct this comparison, standardized analytical procedures for the detection of hydrogen gas were developed, which are still used as the standard within our group.

This project started as an investigation of the photocatalysts used by our group for hydrogen generation, as a way of comparing the differences between the various metal nanoparticle decorations. However, the focus of this project shifted as it became clear that many publications in our literature review appeared to falsely attribute hydrogen generation utilizing SEDs as 'water splitting'. It was common practice to add SEDs during initial tests of a catalyst's performance, with the assumption that a catalyst with improved activity with SEDs would also have improvement with water splitting. This was done as hydrogen generation from water gives low hydrogen yields that are often difficult to detect. This project aimed to test the accuracy of this assumption by showing the catalytic efficiency for both processes with various catalysts. It quickly became apparent that this assumption was false, with a different relative trend of activity of our catalysts when comparing SED hydrogen generation to water splitting. Most notably, $Pd@TiO_2$ which is a very efficient photocatalyst for hydrogen generation with SEDs showed no hydrogen generation under pure water conditions. These findings are interesting as they also imply that the mechanisms of the two processes are quite different. Due to the implications of this project, the impact of the publication was strong leading to ~100 citations by the time of writing this dissertation.

## 2.2 Post-print Version of Manuscript

First published in: ACS Energy Lett. 2018, 3, 542-545

The ubiquitous use of the term "water splitting" has made it virtually a synonym for hydrogen generation from water, even when sacrificial electron donors (SEDs) are used. Yet, the only true water splitting corresponds to the chemistry and stoichiometry of eq. 1 (Scheme 2.2.1).[1]

$$2H_2O \rightarrow 2H_2 + O_2 \qquad (1)$$

**Scheme 2.2.1.** Stoichiometric equation of hydrogen generation from 'true water splitting'.

Given that hydrogen is truly a zero greenhouse gas (GHG) emissions fuel, a lot of effort has been devoted to solar water splitting mediated by a variety of photocatalysts, notably, modified $TiO_2$.[2] Unfortunately, true water splitting in the absence of sacrificial donors (that act as hole traps) and with catalysts that are not oxidized in the process is very inefficient.[3] Photocatalytic hydrogen generation assisted by SED has been widely used as a surrogate for true water splitting as hydrogen yields are much higher under these conditions. The use of SED for $H_2$ generation cannot be considered as water splitting, and its efficiency depends on both the catalyst and SED used. Thus, when comparing several $TiO_2$-based catalysts in true water splitting and in SED-assisted $H_2$ photogeneration, the overriding conclusion is that the knowledge acquired in one is not transferable to the other, thus putting to rest any expectation that sacrificial donors can be used to learn about true water splitting. Criticism of the SED approach[4] becomes less important if water contaminants fulfill this role.[5] For such strategies, the knowledge acquired through the SED approach with a diversity of substrates is important, illustrated here with methanol and formic acid, both leading to excellent $H_2$ generation performance. While many forms of metal-decorated $TiO_2$ can be evaluated as catalysts, the discovery and eventual optimization of catalysts that perform well with earth-abundant materials[6] will open the path to practical applications in this field.

The use of methanol and formate as SEDs has been commonly explored;[7-8] in both cases, the radicals produced following hole trapping ($^{\bullet}CH_2OH$ and $^{\bullet}CO_2^-$) are themselves excellent electron donors. This leads to enhanced yields, sometimes described as a "doubling" effect.[4, 9] It

has been frequently assumed that $H_2$ generation, half of the water splitting reaction, is much the same whether just water or SEDs are used, as illustrated graphically in Figure 2.2.1(A). Unfortunately, this is not quite true as the cycle for $H_2$ generation involves trapping of the photogenerated hole and subsequent reactions of the SED-derived radicals formed, and therefore, the efficiency of hydrogen generation with SEDs such as methanol simply reflects methanol splitting, Figure 2.2.1(B). Indeed, experiments suggest hole lifetimes are strongly influenced by SEDs[10] and that $H_2$ is generated by the reduction of two protons originating from both water and the SEDs.[11] This has led to severe criticism of the use of SEDs to study water splitting as the value of the information acquired and its significance in the understanding of water splitting become questionable.[4]

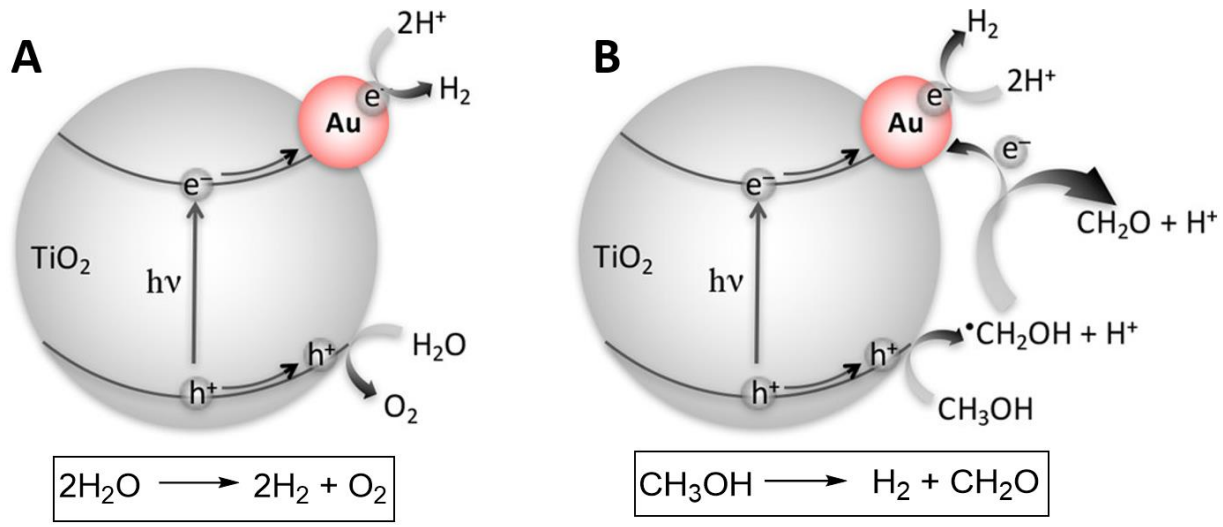


**Figure 2.2.1. (A)** Water splitting and **(B)** methanol splitting upon UV excitation, illustrated for Au@$TiO_2$

While we agree with the questionable value of sacrificial donor strategies that result in the consumption of valuable chemicals, we have proposed that if common water contaminants, such as organic matter in river water, can be the SED then photocatalytic solar exposure could generate hydrogen while destroying pollutants, including bacterial water contaminants.[5] While hoping that reported data on water splitting catalysts will be useful, several questions should be

addressed: Is the knowledge acquired in true water splitting and in SED-mediated hydrogen production interchangeable? In other words, is catalyst performance in both processes correlated? Is the best catalyst for hydrogen generation from water splitting also the best when SEDs are used? Finding an answer to these questions is the central subject of this Viewpoint. Direct solar $H_2$ generation may pose major engineering challenges, and while we acknowledge this issue, it is not an aspect discussed in this Viewpoint.[12-13]

In order to compare $H_2$ generation in the presence and absence of SEDs, seven $TiO_2$-based catalysts (Table 2.2.1) were examined under conditions of solar simulation (AM 1.5) or under 368 nm LED irradiation. Some of these catalysts were already described by our group as photocatalysts for different organic transformations.[14-16] Further details on synthesis and characterization can be found in the appendix.

**Table 2.2.1.** General description of the catalytic materials utilized in this work

| Entry | Material[a] | General description | Source |
|---|---|---|---|
| i | $TiO_2$ | P25, predominantly anatase, particle size ~50 nm | Univar Canada |
| ii | Cu@$TiO_2$ | 2.5% Cu[b], particle size 1.1 nm | Ref[15] |
| iii | Pt@$TiO_2$ | 2% Pt[b], particle size < 1 nm | Ref[14] |
| iv | Co@$TiO_2$ | 2% Co[b], particle size <1 nm | This Work |
| v | Ru@$TiO_2$ | 2% Ru[b], particle size <1 nm | This work |
| vi | Pd@$TiO_2$ | 2% Pd[b], particle size ~1.6 nm | Ref[16] |
| vii | Au@$TiO_2$ | 1% Au, particle size ~2.5 nm | Strem |

[a] The $TiO_2$ in entry 1 was the base material for samples in entries 2-6. [b] Nominal concentrations, not representative of actual % metal loading. See appendix for accurate loadings.

We established unequivocally that with all catalysts the rate of production of hydrogen using SEDs exceeded that under conditions of true water splitting. In order to establish to what extent we could distinguish the efficiency of SED and non-SED systems, we first tested one of the catalysts, Cu@$TiO_2$, in the presence of variable concentrations of the two selected SEDs, formic acid and methanol. We noted that for this particular catalyst formic acid is more efficient for $H_2$ generation than methanol, as expected.[17] In order to rule out a pH effect on this, a series of

experiments were performed using HCl to adjust the pH and Cu@$TiO_2$ as the catalyst. The results are illustrated in Table 2.2.2 and confirm that the $H_2$ generation enhancement by formic acid is not due to a simple pH change. Indeed, the presence of HCl not only lowers the pH of the system but also decreases the performance of the $H_2$ generation in the presence and the absence of SED (cf. entries i-iii and vi-vii). Additional experiments in the presence of KCl rule out counter ion ($Cl^-$) interference (entry iv).

**Table 2.2.2.** SED and pH nature effect on the production of $H_2$ upon UV light irradiation of Cu@$TiO_2$

| Entry | SED[a] | Others | pH | $H_2$ Production (mmol $g^{-1}h^{-1}$) |
|---|---|---|---|---|
| i | None | -- | 6-7 | 0.15 |
| ii | None | 0.1 mM HCl | 4 | 0.10 |
| iii | None | 6.9 mM HCl | 2 | 0.03 |
| iv | None | 6.9 mM KCl | 6-7 | 0.17 |
| v | Formic Acid | -- | 2 | 9.78 |
| vi | Methanol | -- | -- | 3.67 |
| vii | Methanol | 6.9 mM HCl | ~2 | 1.22 |

Reaction conditions: 5 mg of Cu@$TiO_2$ in 4 mL of water under Argon atmosphere irradiated for 4 hours with 368 nm LED working at 0.33 W $cm^{-2}$.

[a] Reactions using 1% SED performed under same conditions during 1 hour of irradiation

The use of a 368 nm LED as the irradiation source can help to establish the relative performance under SED vs. non-SED conditions. The rationale behind this choice includes the fact that all catalysts have a single dominant absorber in the UV region, i.e., $TiO_2$, thus ensuring that the data for various systems are readily comparable. Notice that the presence of formic acid in the solution does not change the optical properties of the $TiO_2$ suspension (Figure 2.2.2). Thus, no charge-transfer complexes are formed between the SED selected and the semiconductor (many molecules do),[18] and the mechanism under study can be considered to reflect the true photocatalytic activity of $TiO_2$.[19] We note that in our nomenclature we always refer to metal@$TiO_2$; however, in many of these systems, the nanostructure can easily be oxidized (see XPS analysis in the SI for further details).

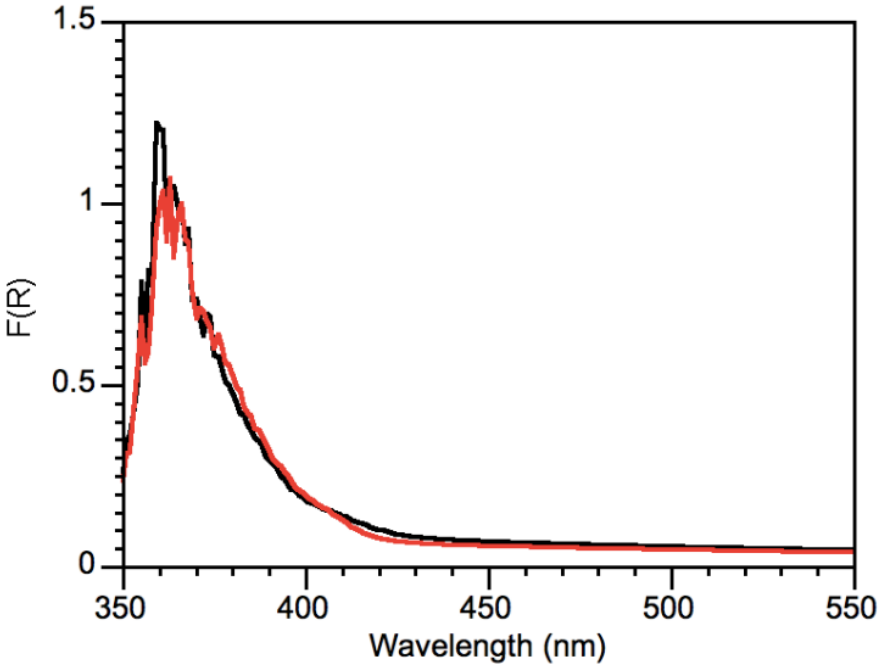


**Figure 2.2.2.** Diffuse reflectance spectra of a suspension of $TiO_2$ in pure water (black) and 1% formic acid added (red).

Additionally, at relatively high SED concentration, the $H_2$ generation is linear with time, showing that at least in this time scale the photocatalyst performance does not deteriorate (Figure 2.2.3); in contrast, at very low SED, the plot shows that this curvature does not reflect catalyst deterioration but rather a dramatic reduction in SED concentration, a desirable feature for applications in water decontamination.

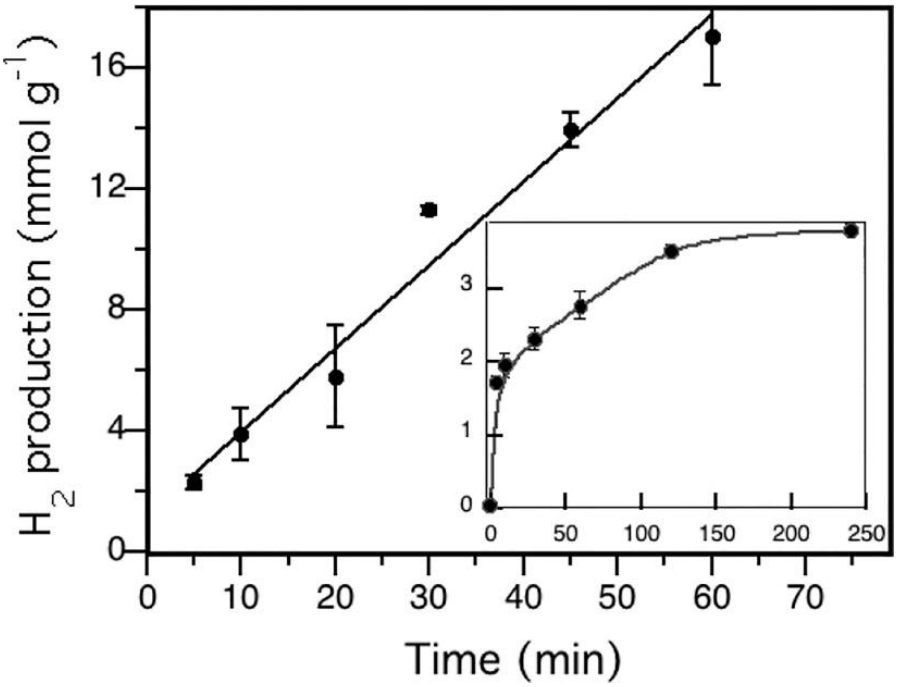


**Figure 2.2.3.** Kinetic plot for the generation of $H_2$ under 368 nm irradiation for 1% (main plot) and 0.01% (insert) formic acid SEDs using as catalysts Pd@$TiO_2$ (main plot) and Pt@$TiO_2$ (insert).

Figure 2.2.4 shows the rates of $H_2$ generation for the seven systems examined. Similar experiments in the absence (Figure 2.2.4(A)) or presence of SEDs (Figure 2.2.4(B,C)) show about 2 orders of magnitude larger efficiencies than true water splitting conditions, as expected. The values in Figure 2.2.4(A) are significantly lower than the rates of $H_2$ generation in this spectral region (300−400 nm) found for gold nanoplate on multilayer graphene, to date, one of the most efficient photocatalysts for "true water splitting" with rates up to 1.2 mol $H_2$/g h.[20]

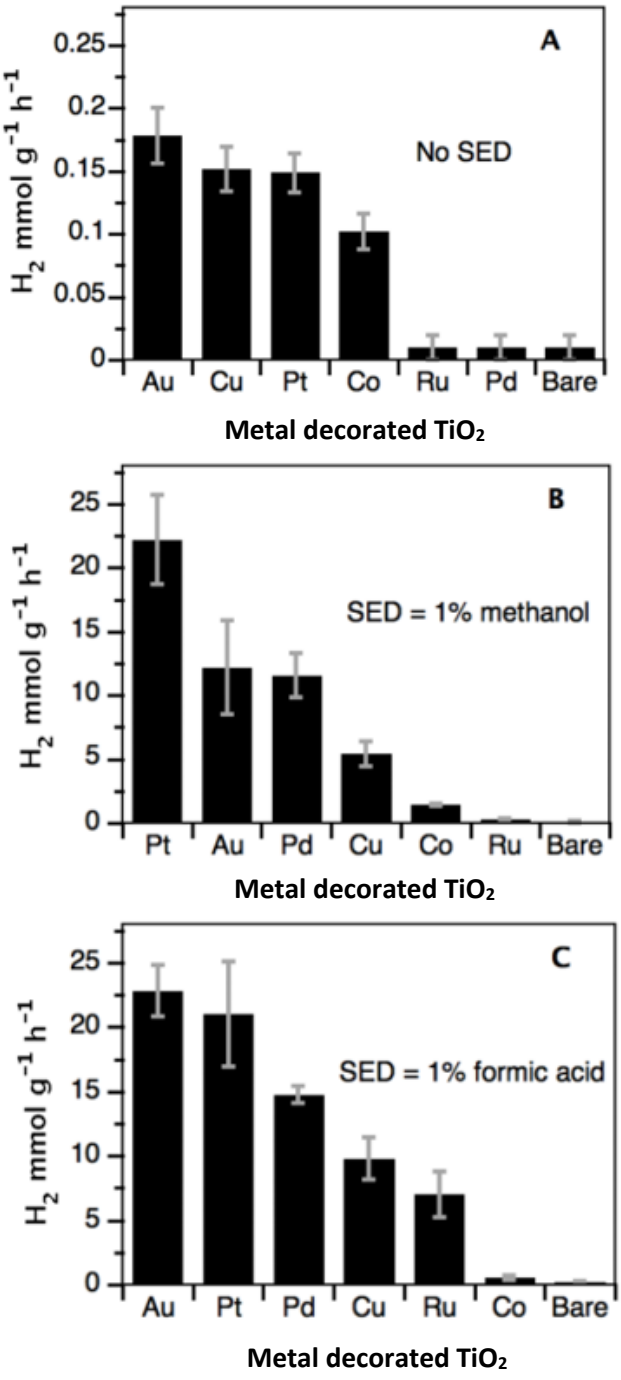


**Figure 2.2.4.** $H_2$ generation rates by different catalysts tested using 368 nm irradiation (0.33 W $cm^{-2}$) for **(A)** true water splitting conditions (rates for Ru@$TiO_2$, Pd@$TiO_2$, and pure $TiO_2$ are zero within experimental error), **(B)** in the presence of 1% methanol, and **(C)** in the presence of 1% formic acid (pH ≈ 2.2). Note that the scale for panel (A) is expanded x100 relative to panels (B) and (C).

Notice in Figure 2.2.4 that the catalysts are arranged in their order of performance, and while the order in panels (B) and (C) is not identical, they bear a strong resemblance. In contrast, the order for true water splitting (Figure 2.2.4(A)) is quite different. In other words, using Figure 3B,C, it would be impossible to predict the catalytic performance in true water splitting shown in Figure 2.2.4(A). Additionally, the relative increases in $H_2$ production rates are illustrated in Figure 2.2.6 and range from 5 to 130; thus, while SEDs bring a major increase in $H_2$ generation, it is clear that these increases are extremely different depending on the catalyst used. Note that Ru@$TiO_2$ is such a poor performer that the ratio has large uncertainty and the errors are hard to estimate (see also Figure 2.2.4). For the top performers, Au, Pd, and Pt, the effect of 1% SED is almost the same for methanol and formic acid, suggesting that at least for the examples examined SED-assisted performance may be rather insensitive to the specific donor used, a desirable characteristic for applications in water treatment. Naturally, this may not apply to electron-poor contaminants or to molecules (such as indoles) that associate with the $TiO_2$ surface.[18] Thus, knowledge about catalytic performance in true water splitting and SED-assisted systems is simply not transferable.

Notably, results using solar illumination show basically the same tendency described above (Figure 2.2.5).

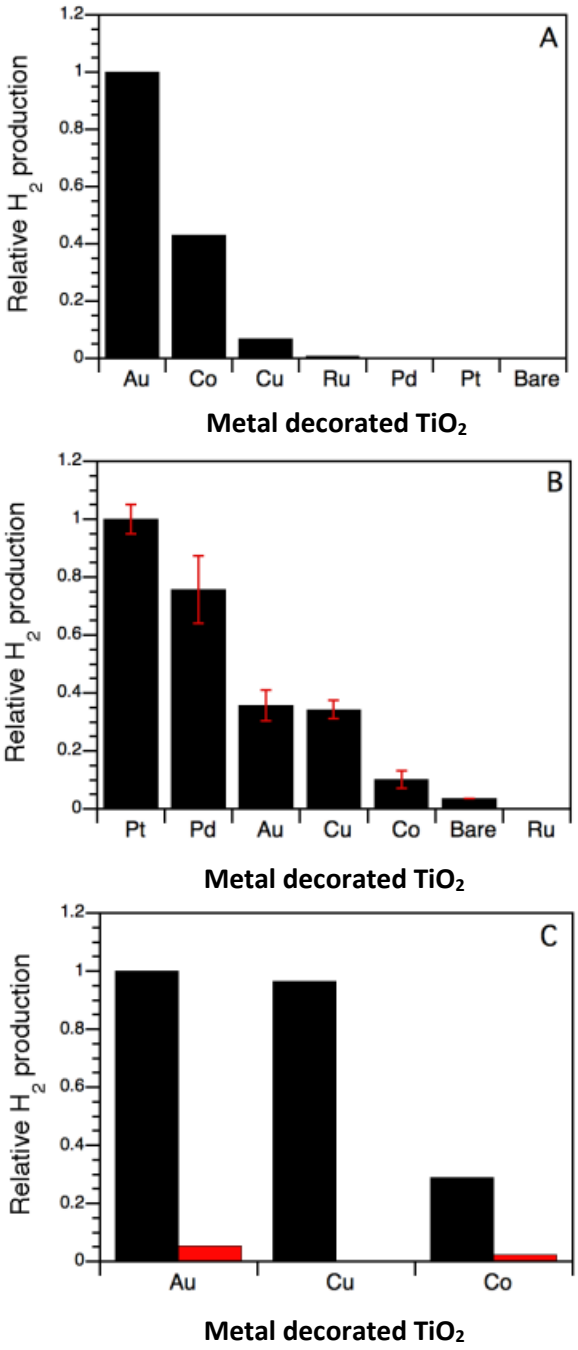


**Figure 2.2.5.** Relative values of $H_2$ generation for **(A)** pure water splitting and (**B)** 10% methanol upon solar simulated irradiation (AM 1.5) of $TiO_2$-based photocatalysts. (**C)** Comparison of the $H_2$ generation in the presence of 10% methanol (black bars) and in the absence (red bars) of any sacrificial electron donor (pure water splitting).

The fact that SED-assisted hydrogen generation does not track true water splitting is perhaps a simple reflection that electron and hole behavior are not independent, and thus, trying to influence one-half of the water splitting reaction provides limited information. On the other hand, hydrogen generation using SEDs can be 2 orders of magnitude more efficient than true water splitting. Rather than dismiss SED use as irrelevant, perhaps the key resides in finding SEDs with zero value; in the case of water contaminants, one could argue that in fact they have a negative value as their destruction enhances the uses and value of the waters that contain them. If contaminant-assisted $H_2$ generation has a future, then catalysts must be optimized, be robust (i.e., durable), make use of the visible spectral region, and ideally be able to perform in flow systems. These are clearly challenging but not insurmountable problems.

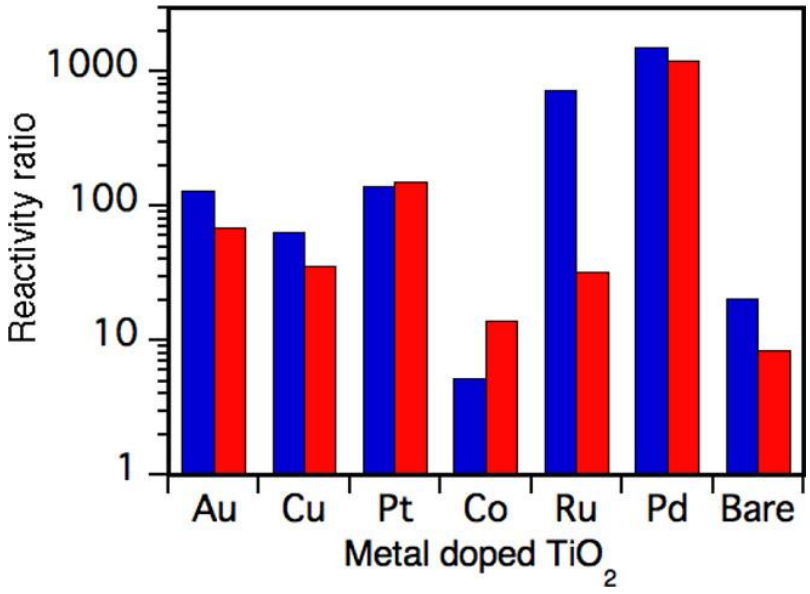


**Figure 2.2.6.** Relative rate for $H_2$ production ($H_2$ generation when a SED is used, relative to the data for true water splitting (i.e., Figure 2.2.4.a)) in the presence and absence of 1% SED for formic acid (blue) and methanol (red). The semilogarithmic scale used facilitates the comparison of extremely different systems such as Co and Pd.

In conclusion, this Viewpoint demonstrates the validity of SED utilization for the parallel objectives of water purification and hydrogen fuel formation, with results that concentrate on the latter. Although catalysts are not optimized, it is nice to see that an earth-abundant element

such as Cu@$TiO_2$ shows competitive performance with other catalysts that utilize some of the scarce elements in the earth's crust.[6, 21] Implementation of these technologies would require catalyst optimization, including good performance in the visible region, where solar light is about 10 times more abundant than that in the UV region. Our results establish unequivocally that knowledge about performance in true water splitting and in SED-assisted systems is simply not transferable. At the same time, the fact that the performances with formic acid and methanol are similar (Figure 2.2.6) gives us hope that one will be able to build a generalized paradigm for a diversity of SED molecules, hopefully including those that are common water contaminants.

Developing SED-assisted processes requires a good understanding of the free radical chemistry that evolves from hole trapping that can lead to "doubling" processes as they relate to hydrogen formation or electrochemical performance.[4, 9, 11]

Further, while a batch approach may be useful for hydrogen generation, it would be desirable to develop fixed-bed catalysts, more suited to solar flow photochemistry, as will be required in water purification applications. Performance, durability, cost, and toxicity all will need to be considered in the development of catalysts that can truly make a difference in both the energy and potable water fields.

## 2.3 Post-print Version of Supporting Information

**EXPERIMENTAL METHODS**

**Materials and instruments**

Unless otherwise stated all chemicals were purchased from Sigma-Aldrich and used without further modifications. The P25 $TiO_2$ was purchased from Univar Canada and 1% Au@$TiO_2$ from Strem Chemicals (AUROlite™ Au/TiO2). X-ray photoelectron spectroscopy (XPS) was recorded using Kratos analytical model Axis Ultra DLD, using monochromatic aluminum Ka X-rays at 140 W. XPS data was analyzed using CasaXPS software, Version 2.3.15 and all fittings obtained using a Gaussian 30% Laurentian and a Shirley baseline. Transmission electron microscopy (TEM) images were collected on a JEM2100F FETEM (JEOL) operating at 200 kV. Diffuse reflectance (DR) measurements were carried out in VARIAN Cary 7000 UV-VIS Spectrophotometer coupled with

Agilent praying Mantis accessory or in the VARIAN Cary 100 UV-VIS Spectrophotometer coupled to an integrating sphere accessory. Photo-induced hydrogen generation was performed upon irradiation utilizing Light-emitting diodes (LEDs) of 10 W from LedEngin centered at 368 nm and a Luzchem's SolSim providing solar simulated radiation based on a 300W ceramic Xe lamp with a circular irradiation area of approximately 6.0" (15.2 cm) in diameter matching spectrally and approximately in intensity the AM1.5 solar spectrum. Hydrogen detection was carried out in a Perkin Elmer, Claurus Gas Chromatograph coupled to Thermal Conductivity Detector (TCD) using Argon as a carrier gas and a 5A Zeolite molecular sieve column.

**Photocatalyst Synthesis**

Synthesis of metal-decorated $TiO_2$ The syntheses of the metal-decorated $TiO_2$ catalysts were performed following the protocols previously described by our group in earlier publications[14-16, 22]. A summary of the properties of these materials is presented in Table 2.2.1. Further details on the synthesis of these materials can be found in the appendix.

**Photo-induced hydrogen generation**

5 mg of the catalyst are suspended in 4 mL of milliQ water (or the correspondent solution of sacrificial electron donor) under Argon atmosphere and sealed in a crimp vial. Irradiation is performed under vigorous stirring for one hour unless otherwise stated. Samples of the headspace are taken with a sample lock syringe and immediately injected in the GC-TCD. Signal of $H_2$ was detected at ~ 4.0 min.

**Hydrogen detection**

The quantification of $H_2$ was performed by running a calibration curve of the gas detection in the GC-TCD instrument. For that, a separatory funnel was filled up with distilled water ensuring no air bubbles inside. The funnel was then secured in a glass container one third full with water and pure $H_2$ gas was then injected through a septum at the top of the funnel, allowing for equilibration with atmospheric pressure. Then 6 mL vials were filled with 4 mL of distilled water under Argon atmosphere. A known amount of $H_2$ gas was then added to each vial in order to run a calibration curve that contains from 0.02 to 2 mL of $H_2$. After giving time for equilibration of

gases within the headspace of the vials, 1 mL of gas sample from each vial was analyzed using GC-TCD.

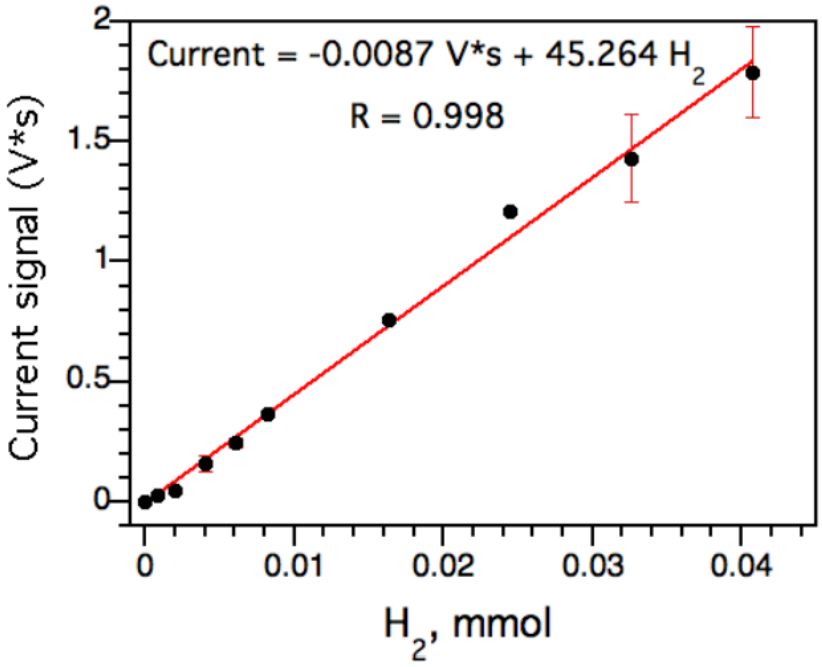


**Figure 2.3.1.** Calibration curve obtained from the protocol described above.

## 2.4 Accompaniment to Chapter 2

This manuscript acted as my first peer-reviewed publication with me as the primary contributing author. Upon starting my career as a graduate student, I took over this project after preliminary experiments conducted by the contributors J. Hodgins and V. Sandre. I then developed new standard procedures for the calibration and analysis of $H_2$ gas production, as the values obtained by prior contributors were not in-line with expected yields when comparing to prior publications. This was at no fault of their own, as creating an accurate $H_2$ calibration curve for headspace analysis of products proved to be more difficult than initially assumed. The development of these procedures acted as the first challenge of my graduate career, and ultimately lead to creating standards still utilized in our laboratory to this day.

The utilization of these catalysts for water purification, with contaminants as the SEDs, was alluded to within this chapter. Our group has continued to explore this concept, and is still exploring it to this day. This included a joint IDRC grant with groups from Kenya and South Africa which I was directly involved in one publication as a contributing author[23] utilizing my skills at $H_2$ gas analysis for initial testing of metal-nanoparticle decorated electro-spun $TiO_2$ fibers. Overall, this research has continued into the development of materials with greater compatibility in flow systems. The $H_2$ analysis standards I developed are still a useful method of quickly probing the efficiency of catalysts at oxidizing organic matter. However, this method of probing does require that the reduction half ($H_2$ production) of the reaction is not rate limiting. With this limitation in mind, probing for $H_2$ production will not typically give false positives for organic oxidation (as the $H_2$ gas synthesis requires oxidation of a SED); however, false negatives are possible if the catalyst does not efficiently catalyze the reduction ($H_2$ production) step.

However, the main focus of my research moving forward was instead in the further analysis of organic radicals being generated by $TiO_2$-based photocatalysts. This began with evaluating the formation of TEMPO-radical adducts from solvent generated radicals, which will be the focus of the following chapter (Chapter 3). The solvent radicals are formed by the same method as the SEDs are oxidized in this chapter. The solvent radicals, as well as the $H_2$ gas formed, can both be evaluated to better understand the chemistry occurring.

## 2.5 References


1. Fujishima, A.; Honda, K., Electrochemical photolysis of water at a semiconductor electrode. *Nature* **1972,** *238* (5358), 37.
2. Tee, S. Y.; Win, K. Y.; Teo, W. S.; Koh, L.-D.; Liu, S.; Teng, C. P.; Han, M.-Y., Recent progress in energy-driven water splitting. *Adv. Sci.* **2017,** *4* (5), n/a.
3. Pan, H., Principles on design and fabrication of nanomaterials as photocatalysts for water-splitting. *Renew. Sust. Energ. Rev.* **2016,** *57*, 584-601.
4. Schneider, J.; Bahnemann, D. W., Undesired role of sacrificial reagents in photocatalysis. *J. Phys. Chem. Lett.* **2013,** *4* (20), 3479-3483.
5. Lanterna, A. E.; Scaiano, J. C., Photoinduced hydrogen fuel production and water decontamination Technologies. Orthogonal Strategies with a Parallel Future? *ACS Energy Lett.* **2017,** *2* (8), 1909-1910.
6. Fukuzumi, S.; Hong, D.; Yamada, Y., Bioinspired photocatalytic water reduction and oxidation with earth-abundant metal catalysts. *J. Phys. Chem. Lett.* **2013,** *4* (20), 3458-3467.
7. Liu, H.; Yuan, J.; Shangguan, W., Photochemical reduction and oxidation of water including sacrificial reagents and Pt/$TiO_2$ Catalyst. *Energy Fuels* **2006,** *20* (6), 2289-2292.
8. Chen, W.-T.; Chan, A.; Al-Azri, Z. H. N.; Dosado, A. G.; Nadeem, M. A.; Sun-Waterhouse, D.; Idriss, H.; Waterhouse, G. I. N., Effect of $TiO_2$ polymorph and alcohol sacrificial agent on the activity of Au/$TiO_2$ photocatalysts for H2 production in alcohol-water mixtures. *J. Catal.* **2015,** *329*, 499-513.
9. Schneider, J.; Matsuoka, M.; Takeuchi, M.; Zhang, J.; Horiuchi, Y.; Anpo, M.; Bahnemann, D. W., Understanding $TiO_2$ Photocatalysis: Mechanisms and Materials. *Chem. Rev.* **2014,** *114* (19), 9919-9986.
10. Tang, J.; Durrant, J. R.; Klug, D. R., Mechanism of photocatalytic water splitting in $TiO_2$. Reaction of water with photoholes, importance of charge carrier dynamics, and evidence for four-hole Chemistry. *J. Am. Chem. Soc.* **2008,** *130* (42), 13885-13891.
11. Belhadj, H.; Hamid, S.; Robertson, P. K. J.; Bahnemann, D. W., Mechanisms of simultaneous hydrogen production and formaldehyde oxidation in $H_2O$ and $D_2O$ over platinized $TiO_2$. *ACS Catal.* **2017,** *7* (7), 4753-4758.
12. Jing, D.-W.; Guo, L.-j.; Zhao, L.; Zhang, X.-M.; Liu, H.; Li, M.-T.; Shen, S.-H.; Liu, G.-J.; Hu, X.-W.; Zhang, X.-H.; Zhang, K.; Ma, L.-J.; Guo, P.-H., Efficient solar hydrogen production by photocatalytic water splitting: From fundamental study to pilot demonstration. *Int. J. Hydrogen Energy* **2010,** *35* (13), 7087-7097.
13. Chandross, E. A., Shining a light on solar water splitting. *Science* **2014,** *344* (6183), 469.
14. McTiernan, C. D.; Pitre, S. P.; Ismaili, H.; Scaiano, J. C., Heterogeneous light-mediated reductive dehalogenations and cyclizations utilizing platinum nanoparticles on titania (PtNP@$TiO_2$). *Adv. Synth. Catal.* **2014,** *356* (13), 2819-2824.
15. Wang, B.; Durantini, J.; Nie, J.; Lanterna, A. E.; Scaiano, J. C., Heterogeneous photocatalytic click chemistry. *J. Am. Chem. Soc.* **2016,** *138* (40), 13127-13130.
16. Elhage, A.; Lanterna, A. E.; Scaiano, J. C., Tunable photocatalytic activity of palladium-decorated $TiO_2$: non-hydrogen-mediated hydrogenation or isomerization of benzyl-substituted alkenes. *ACS Catal.* **2017,** *7* (1), 250-255.
17. Liao, H.; Qiu, Z.; Wan, Q.; Wang, Z.; Liu, Y.; Yang, N., Universal electrode interface for electrocatalytic oxidation of liquid fuels. *ACS Appl. Mater. Interfaces* **2014,** *6* (20), 18055-18062.
18. Pitre, S. P.; Yoon, T. P.; Scaiano, J. C., Titanium dioxide visible light photocatalysis: surface association enables photocatalysis with visible light irradiation. *Chem. Commun.* **2017,** *53* (31), 4335-4338.
19. Barbero, N.; Vione, D., Why dyes should not be used to test the photocatalytic activity of semiconductor oxides. *Environ. Sci. Technol.* **2016,** *50* (5), 2130-2131.

20. Mateo, D.; Esteve-Adell, I.; Albero, J.; Royo, J. F. S.; Primo, A.; Garcia, H., 111 oriented gold nanoplatelets on multilayer graphene as visible light photocatalyst for overall water splitting. *Nat. Commun.* **2016,** *7*, 11819.
21. Lim, X., The new breed of cutting-edge catalysts. *Nature* **2016,** *537* (7619), 156-158.
22. Lanterna, A. E.; Elhage, A.; Scaiano, J. C., Heterogeneous photocatalytic C–C coupling: mechanism of plasmon-mediated reductive dimerization of benzyl bromides by supported gold nanoparticles. *Catal. Sci. Technol.* **2015,** *5* (9), 4336-4340.
23. Mapukata, S.; Hainer, A. S.; Lanterna, A. E.; Scaiano, J. C.; Nyokong, T., Decorated titania fibers as photocatalysts for hydrogen generation and organic matter degradation. *J. Photochem. Photobiol. A.* **2020,** *388*, 112185.

# 3. Highly electrophilic titania hole as a versatile and efficient photochemical free radical source

This chapter has been adapted from J. Am. Chem. Soc. **2019**, 141, 4531-4535 with permission from the American Chemical Society. To allow for consistent formatting and clarity, some changes have been made.

## 3.1 Preamble to Chapter 3

The following chapter evaluates the efficiency of metal nanoparticle decorated $TiO_2$ photocatalysts for the generation of solvent radicals for uses in organic synthesis. As discussed in the previous chapter, M@$TiO_2$ photocatalysts can be quite adept at oxidizing organic compounds such as methanol or other SEDs. Other solvents such as ethers are similarly electron rich, and thus should be easily oxidized by M@$TiO_2$ catalysts. The scope of this activity was thus evaluated with a variety of ethers, and the usability of the radicals tested with TEMPO as a radical scavenger by detection of the TEMPO-ether adduct. Detection of $H_2$ gas production, using the same methods developed in chapter 2, was also used to evaluate the reactions occurring.

This investigation started with evaluating a variety of different M@$TiO_2$ photocatalysts with tetrahydrofuran (THF) as the solvent of interest. It quickly became apparent that these catalysts showed great activity at generating ether radicals, showing much improved activity when comparing against P25 $TiO_2$ alone. Pd@$TiO_2$ was then chosen as a model catalyst to compare a variety of different ethers. Overall, activity of M@$TiO_2$ for solvent radical formation was quite comparable to that of tert-butoxyl radicals, showing similar trends in reactivity, with some differences due to interactions on the surface of the $TiO_2$. Interestingly benzylic radicals could also be formed from toluene as a solvent, which was further explored in a publication by another researcher in our group, Teresa Gawargy.[1] Small amounts of acetonitrile radical products were also observed, which was surprising as it is typically considered to be a relatively 'inert' solvent.

Overall, this research shows the true strength and versatility of M@$TiO_2$ based photocatalysts for the generation of solvent radicals that are truly free and usable in organic reactions. It also acted as the groundwork for my continued research in chapter 4.

## 3.2 Post-print Version of Manuscript

First published in: J. Am. Chem. Soc. **2019**, 141, 4531-4535

**Abstract**

Photogenerated holes in nanometric semiconductors, such as $TiO_2$, constitute remarkably powerful electrophilic centers, capable of capturing an electron from numerous donors such as ethers, or nonactivated substrates like toluene or acetonitrile, and constitute an exceptionally clean and efficient source of free radicals. In contrast with typical free radical precursors, semiconductors generate single radicals (rather than pairs), in which the precursors can be readily removed by filtration or centrifugation after use, thus providing a convenient tool in organic chemistry. The process can be described as an example of dystonic proton coupled electron transfer.

**Manuscript**

C−H bond activation has gained much interest due to its atom and step-economy in the synthesis of functional molecules;[2] many of which are of importance in drug development. Among these, the sp3 α-C−H reactions of heteroatomic compounds (e.g., alcohols, ethers, or amines) have particular synthetic value as they can directly introduce active groups.[3] For example, the THF motif ranks 11 among the 100 most frequently used ring systems from small molecule drugs listed by FDA,[4] and is part of eribulin and afatinib, two commercial cancer treatment drugs.[5] Thus, the study of different methodologies to couple this and other structures to organic molecules has gained much attention.[6-7] Two mechanisms proposed for radical C−H activation, involve the cleavage of a C−H bond by hydrogen atom transfer (HAT) or a single-electron transfer, usually coupled to proton loss, described as proton coupled electron transfer (PCET),[8] Scheme 3.2.1.

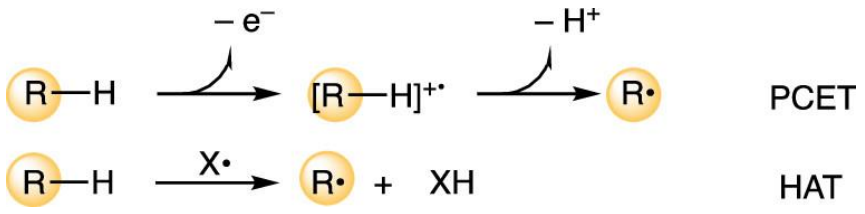


**Scheme 3.2.1.** C-H Activation via HAT and PCET

These mechanisms normally require the presence of a free radical initiator that generates two radicals, leaving initiator-derived debris in the solution along with residual initiator, which can be difficult to remove. Here, we demonstrate that photoactivated $TiO_2$ can be used as a clean free radical initiator, circumventing some of the disadvantages mentioned.

Many of the studies involving $TiO_2$ radical formation deal with the generation of reactive oxygen species (ROS), whose involvement ranges from applications in environmental remediation[9] to potential concerns when ROS are formed in sunscreens.[10-12] In contrast, our report is focused on the clean formation of free carbon-centered radicals for applications in organic chemistry. Two recent examples show that semiconductor-based photocatalysts can activate THF, ultimately leading to C−C coupling reactions.[13-14] Here, we explore in detail the initiation reaction with various substrates. While ethers are not very good electron donors (for example, they show a broad electrochemical window),[15] it is remarkable that the photogenerated $TiO_2$-hole is so electrophilic that it readily oxidizes ethers. Indeed, it can also oxidize nonactivated substrates such as toluene and acetonitrile. While most initiators generate a pair of free radicals, $TiO_2$ makes a single radical−therefore, cage recombination is not an issue. Further, residual $TiO_2$ and any $H_2$ produced are readily removed. While the key reaction occurs at the hole (Scheme 3.2.2), the electron-hole recombination can be slowed down by decorating $TiO_2$ with metal nanoparticles, one of the strategies explored here.

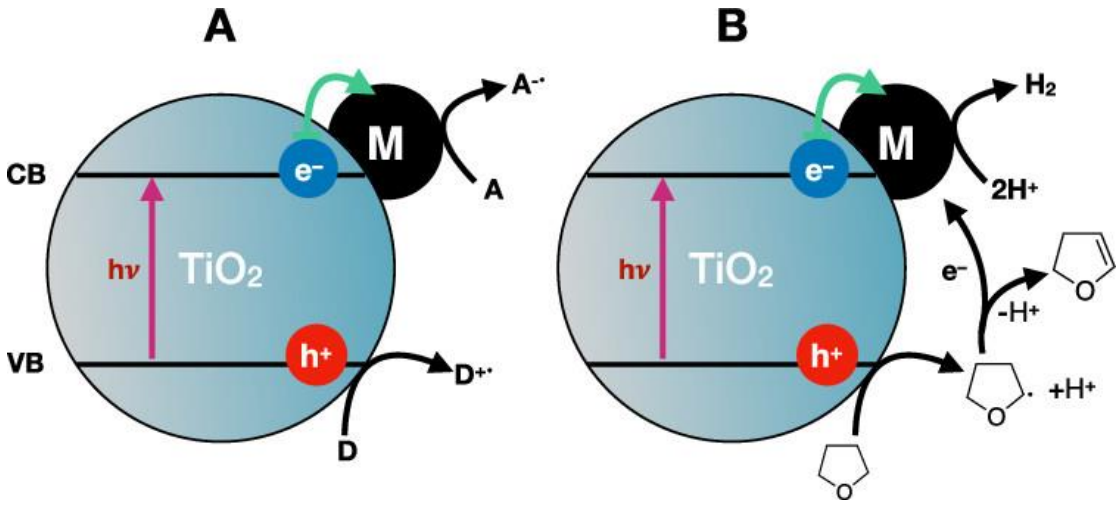


**Scheme 3.2.2. (A)** Metal nanoparticles improve charge separation in $TiO_2$ semiconductors facilitating both reduction and oxidation pathways; **(B)** Proposed mechanism for ethers (illustrated for THF)

Our experiments use 368 nm LED irradiation of metal decorated $TiO_2$, such as $Pd@TiO_2$, suspended in the reaction mixture. While our work concentrates on organic solvents, the reaction is also water-tolerant (See SI, Figure 3.3.1). The photolysis generates $H_2$ gas as a by-product, just as many sacrificial electron donors do.[16] This gives the system the ability to remove $H^+$ from solution, making base unnecessary for reactions that can withstand mild acidic conditions. Scheme 3.2.3 shows our proposed mechanism, where we anticipate that the hole will reside in the $TiO_2$ valence band (VB), while the electrons will migrate rapidly to the metal particle, effectively their host. Dihydrofuran and furan were detected by NMR (See SI, Figures 3.3.9 and 3.3.10).

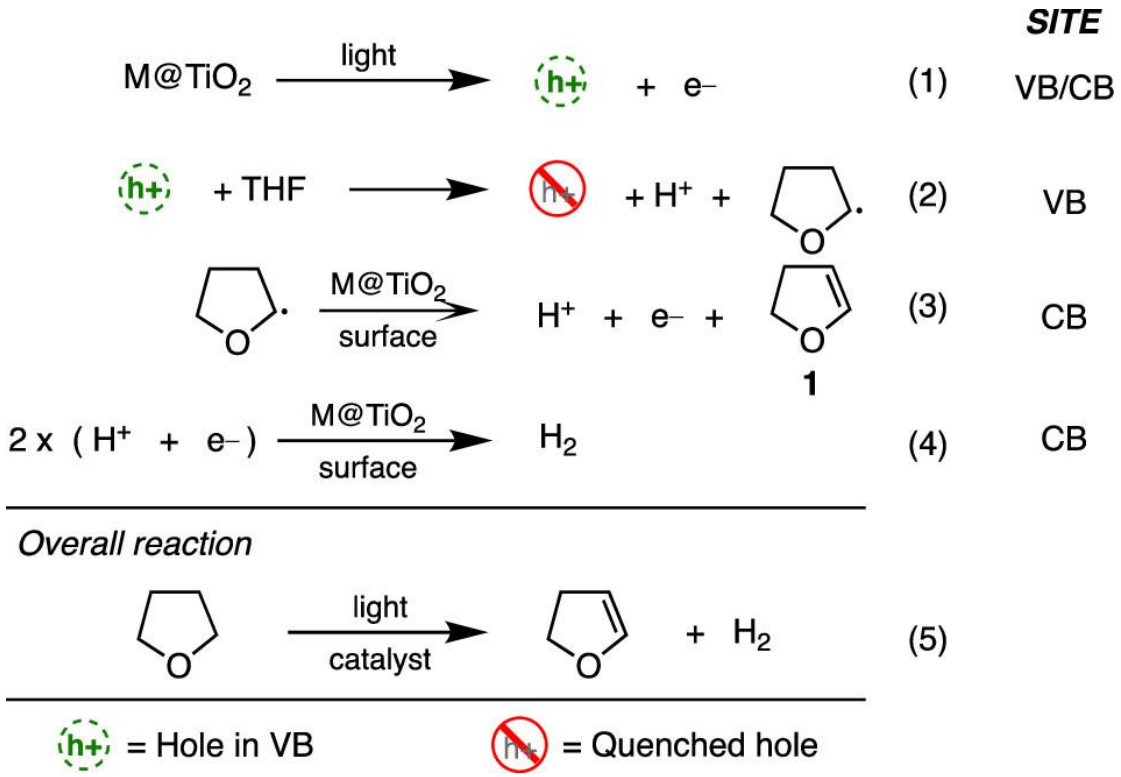


**Scheme 3.2.3.** Mechanism for the formation of $H_2$ and dihydrofuran from THF. THF-derived radicals (eq 2) are mobile and undergo solution reactions.

The generation of radicals does not guarantee they are “free”, in the sense that they are mobile and can participate in solution reactions, as in some cases surface-generated

intermediates can remain and react on the surface. In order to validate the mechanism and evaluate if the THF radical is truly free, we used TEMPO (2) as a free radical scavenger. Equation 6 (Scheme 3.2.4) illustrates the process, where the product can be readily detected by gas chromatography.

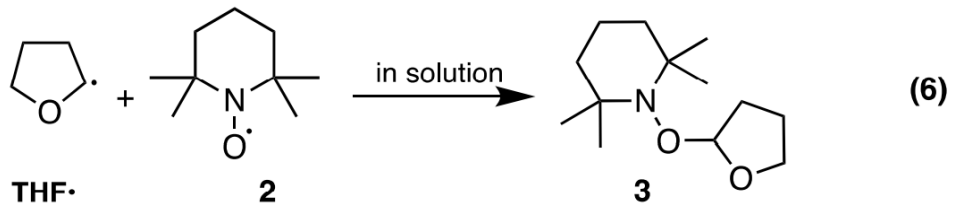


**Scheme 3.2.4.** Radical scavenging of ether-radicals (illustrated with THF) by TEMPO leading to the formation of a stable TEMPO-Ether adduct (Product 3).

Product 3 is formed quantitatively in the presence of TEMPO and different M@$TiO_2$ nanocomposites (Figure 3.2.2). In order to establish how efficient the process was, we examined eight different catalysts, including bare $TiO_2$. These materials were used in earlier reports, such as the research presented in chapter 2. Details and characterization are available in the appendix, with % metal loading summarized in Table A.2.1.

We monitored the time required for 50% of the TEMPO to yield radical trapping products upon UV irradiation, with the full kinetic profiles of each shown below (Figure 3.2.1).

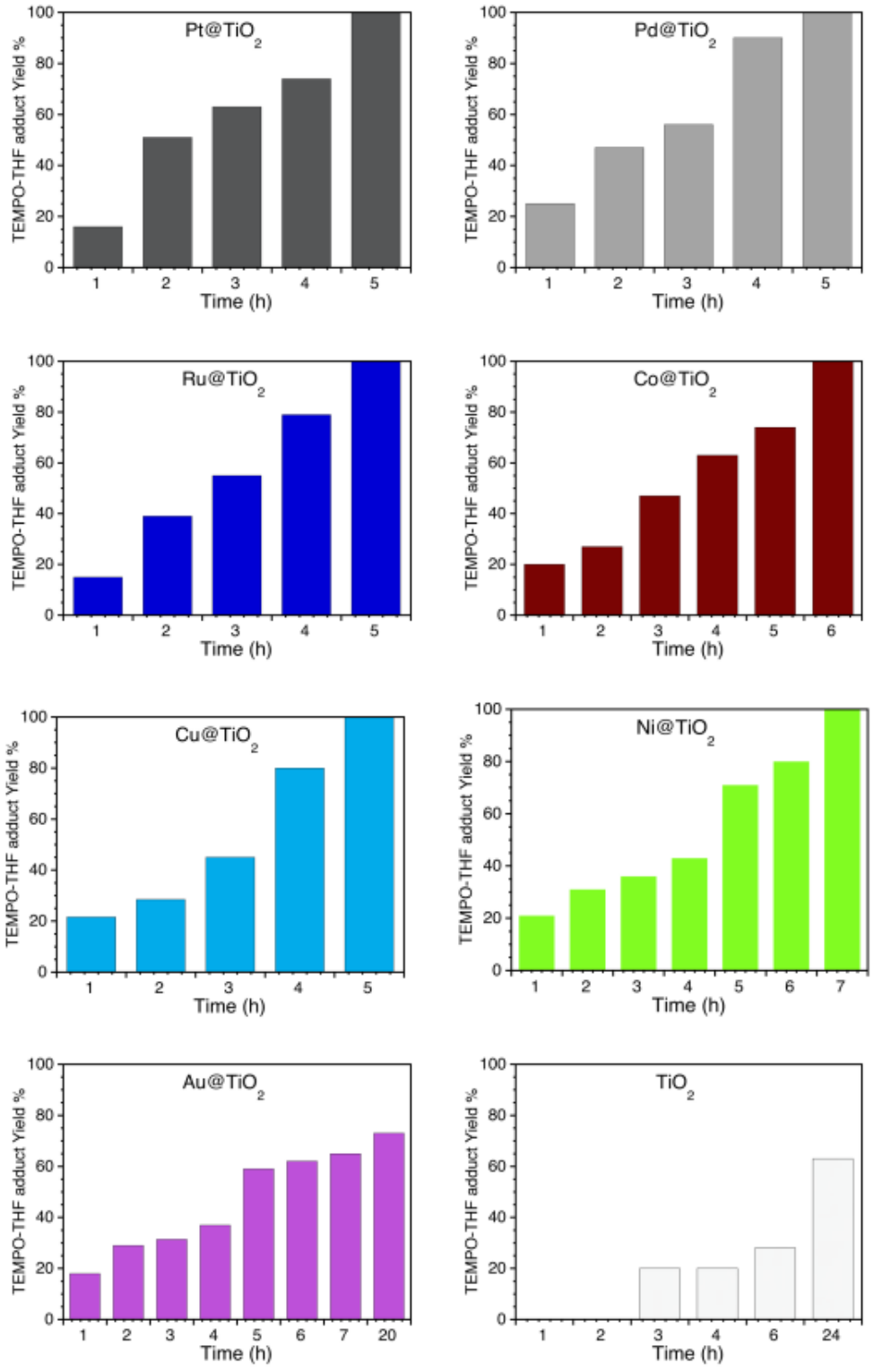


**Figure 3.2.1.** Kinetics of the TEMPO-THF adduct under the reaction conditions: 5 ml of THF, 25 mM of TEMPO, 25 mM $Cs_2CO_3$, and 20 mg of catalyst under Ar atmosphere. Irradiation using a 368 nm LED working at 2500 W $m^{-2}$.

Figure 3.2.2(A) shows a summary of the results, where all decorated materials show similar performance, and are about five times more efficient than bare $TiO_2$. This virtual independence of the electron trapping material supports the $TiO_2$ hole as responsible for the electrophilic properties observed. It is clear that the dominant feature of these materials is that surface metals (or their oxides) can greatly increase the longevity of hole−electron pair, slowing down charge recombination and favoring trapping by molecules in the medium, such as THF in these examples.

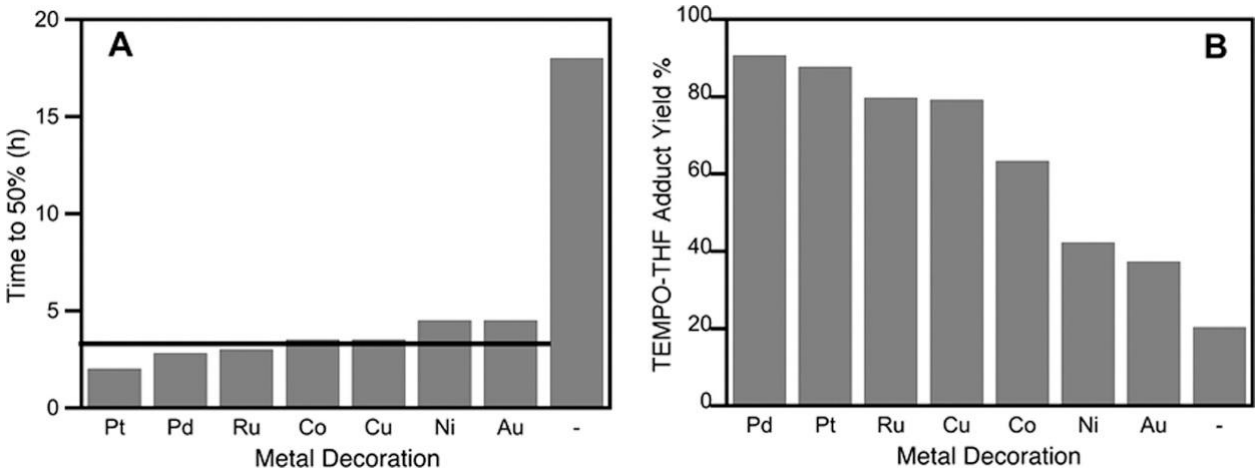


**Figure 3.2.2. (A)** Time for 50% TEMPO to product 3 conversion under 368 nm irradiation. Horizontal line at 3.4 h represents average time for all M@$TiO_2$ samples. Full kinetics details in Figure 3.2.1. **(B)** Yield of product 3 using various M@$TiO_2$. Conditions: 5 mL THF, 25 mM TEMPO, 25 mM $Cs_2CO_3$, 20 mg catalyst, Ar, hv at 2500 W $m^{-2}$, 4 h.

The formation of $H_2$ (eqs 4 and 5) was followed in the absence and in the presence of TEMPO. As illustrated in Figure 3.2.3, $H_2$ production is significantly reduced when TEMPO is present. This is consistent with generation of conduction band (CB) electrons by photoexcitation of the semiconductor, while the secondary source of electrons, eq 3, is inhibited in favor of scavenging by eq 6. TEMPO trapping supports that the THF radical is free, and thus available for organic chemistry transformations in which it may participate; of course, eq 6 provides one such demonstration.

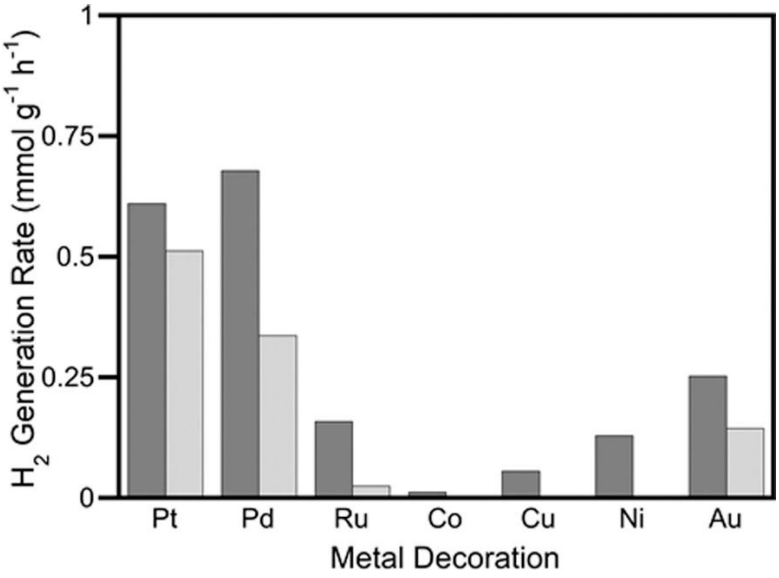


**Figure 3.2.3.** Rates of photocatalytic $H_2$ generation for M@$TiO_2$ in the absence (black) and in the presence of TEMPO (gray). Reaction conditions as in Figure 3.2.2.

For catalysts such as Ru, Ni, Cu, or Co-decorated $TiO_2$, the decorating structures are redox-active oxides that can find alternate pathways for CB electrons,[17] not surprisingly affecting the reducing ability of the material (i.e., $H_2$ formation).[18]

Having established that the THF reactivity of various M@$TiO_2$ is similar among the materials tested, we explored a series of ethers to evaluate the generality of this approach. Note that ethers are known to react rapidly with alkoxyl radicals, another highly electrophilic species.[19] The reaction responds to stereoelectronic effects and THF is one of the fastest reactants toward tert-butoxyl radicals. Our selection of ethers parallels the most interesting examples found for tert-butoxyl.[19] We have also observed that $H_2$ is an excellent way to screen for hole−electron reactivity, even if $H_2$ is derived from CB reactions (eqs 3 and 4).[20] Table 3.2.1 summarizes the TEMPO-ether adduct formation for a series of ethers tested, and the $H_2$ evolution in the absence of TEMPO. Given that many organic reactions are performed in the presence of base, we tested the $TiO_2$ strategy under these conditions and conclude that the system is base-tolerant; indeed, TEMPO-ether adduct yields are slightly higher in basic media (Table 3.2.1), likely due to the decrease of TEMPO-side reactions.[21]

**Table 3.2.1.** Yields of TEMPO-Ether Adducts Using Pd@$TiO_2$ Photocatalyst and $H_2$ Evolution in the Absence of TEMPO. Done in the presence and absence of base. Comparison with the H-abstraction reaction rate constant reported for $tBuO^{\bullet}$.[19]

| **Ether** (label) | **Structure** | **TEMPO-Ether Adduct Yield %[a]** | | **$H_2$ (mmol $g^{-1}h^{-1}$)** | | **$tBuO^{\bullet}$ $10^6$ k ($M^{-1}s^{-1}$)** |
|---|---|---|---|---|---|---|
| | | No Base | Base | No Base | Base | |
| THF | 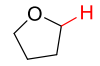 | 63.5 | 77.7 | 0.74 | 0.47 | 8.25 |
| DEE | 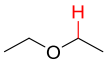 | 62.8 | 67.2 | 0.51 | 0.24 | 3.9 |
| DOX | 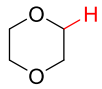 | 39.2 | 48.0 | 0.52 | 0.31 | 1.5 |
| THP | 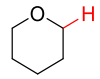 | 28.2 | 35.4 | 0.72 | 0.20 | 2.7 |
| DMM | 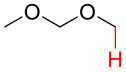 | ND | ND | 1.32 | 1.40 | 0.84 |
| MOP | 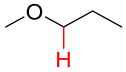 | ND | ND | 1.14 | 0.74 | NA |
| DOL | 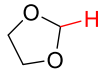 | ND | ND | 1.03 | 0.68 | 7.7 |
| MDOL | 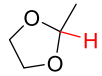 | ND | ND | 0.70 | 0.60 | 11.6 |

*Ethers:* THF (tetrahydrofuran), DEE (diethyl ether), DOX (dioxane), THP (tetrahydropyran), DMM (dimethoxymethane), MOP (1-methoxypropane), DOL (1,3-dioxolane), MDOL (2-methyl-1,3-dioxolane)
*Reaction conditions*: 1 M solution of ether in 5 mL of ACN and 25 mM of base ($Cs_2CO_3$) under Ar atmosphere and irradiation with a 368 nm LED working at 2500 W $m^{-2}$ for 3 hours. [a]25 mM of TEMPO.

While TEMPO trapping works very well with THF and other molecules (e.g., dioxane), the product mixture can be complicated by side reactions in other systems, including some cases where the amine 2,2,6,6-tetramethylpiperidine is produced; TEMPO deoxygenation was reported[21] and has been identified in other systems (see SI, Figures 3.3.1 and 3.3.2).

In many cases, $H_2$ generation can be used to screen which ethers are good candidates as hole scavengers (Table 3.2.1). Interestingly, among the ethers studied the highest production of $H_2$ was detected with some that did not show the formation of a stable TEMPO-ether adduct (i.e., DMM, MOP, DOL, and MDOL). This behavior can be rationalized by understanding the chemistry of the radicals. After radical formation these ethers can break the C–O bond to generate the corresponding aldehyde and the carbon-centered radical, where aldehydes, in particular

formaldehyde, are great SED for the generation of $H_2$. In order to test this hypothesis, we monitored the formation of $CH_2O$ for the systems where this product is anticipated (i.e., DMM and MOP) and using THF as a (negative) control. Equation 7 (Scheme 3.2.5) illustrates the cleavage for the radicals derived from DMM, and the corresponding enthalpy of reaction estimated from known thermodynamic data (See SI, Scheme 3.3.1).[22]

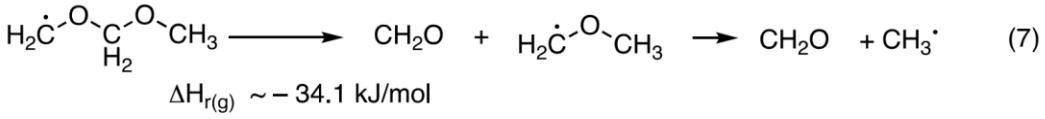


**Scheme 3.2.5.** Fragmentation mechanism of DMM radicals to formaldehyde and further radical products.

In fact, $CH_2O$ can be detected during the early stages of reaction, and quickly reaches a plateau at 8−10 mM, attributed to the fact that $CH_2O$ is an excellent SED, quickly reaching steady state concentration when it is consumed as fast as it is generated. Initial formaldehyde formation can be observed with an increasing rate of $H_2$ generation within the first 15 min of the reaction (Figure 3.2.4). Thus, $H_2$ formation is a good reporter for hole trapping even when TEMPO trapping fails due to product mix complexity.

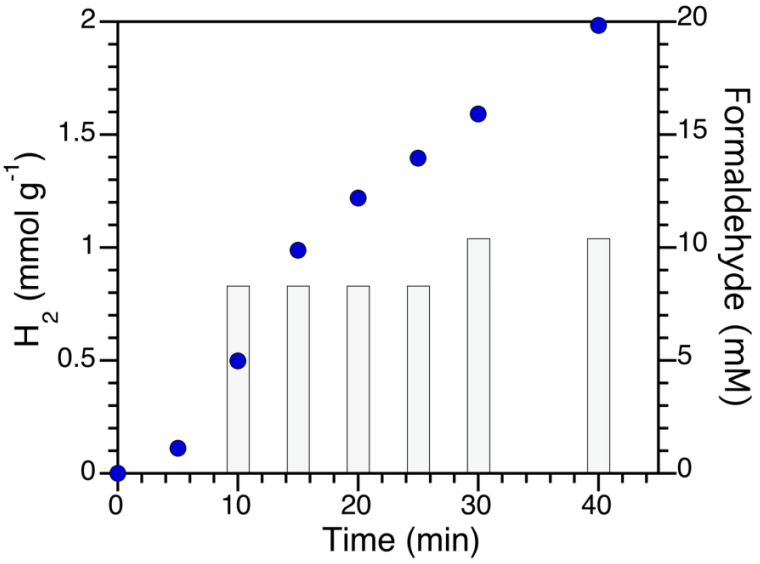


**Figure 3.2.4.** Kinetics of the formaldehyde (grey bars) and the $H_2$ formation (blue dots) in the presence of DMM and 20 mg of Pd@$TiO_2$. Notice that these measurements were performed using a different batch of catalyst from Table 3.2.2.

Further confirmation that the radicals are free and mobile was obtained by EPR spectroscopy (See Figures 3.3.3-5) and in experiments with THF and dioxane, separate or in equimolar mixtures, where radical recombination products are easily observed, including the cross dimer in the case of solvent mixtures (Figures 3.3.6-8). In order to compare ether reactivities, we also performed a few competitive studies between THF and two other ethers that presented uncomplicated chemistry in TEMPO trapping studies (Table 3.2.2). Whereas the tButO• chemistry relies in stereoelectronic control, this is lost in the $TiO_2$-hole chemistry. In the context of Table 3.2.3, tButO• is closer to a HAT mechanism, while PCET probably dominates the $TiO_2$ chemistry. These results combine ether-hole reactivities with surface preference affinities. Computational studies suggest that while dioxane has a modest reactivity, it does have the highest surface affinity. In mix reagents this can lower the relative production of THF radicals in the presence of dioxane due to competition for the reactive surface.

**Table 3.2.2.** Formation of TEMPO-THF adduct in the presence of other ethers by irradiation of Pd@$TiO_2$ over 24h. Relative reactivities of the $TiO_2$ hole and the *tert*-butoxyl radical.

| Ether | TEMPO-THF adduct (%) | TEMPO-ether adduct (%) | Relative reactivity | | [b]IE (eV) |
|---|---|---|---|---|---|
| | | | $TiO_2$ hole | [a]tBuO• | |
| -- | 63[c] | -- | 1.0 | 1.0 | 9.40 |
| DOX | 40 | 10 | 0.28 | 0.18 | 9.19 |
| DEE | 73 | 15 | 0.14 | 0.47 | 9.51 |

DOX (dioxane), DEE (diethyl ether). [a]From reference[19] [b]Ionization Energy from NIST database. [c]3h reaction

To explore further the PCET process, we performed DFT calculations with Quantum Espresso (QE), a package for computing the properties of periodic systems.[23] Association energy ($E_{ads}$) between substrates and solid surfaces is a computational routine in the QE package. Thus, we computed the energy released by the interaction between THF and $TiO_2$ (101) anatase surface, under both conditions neutral or positively charged $TiO_2$ surface. As metals show limited influence on the reactivity of the hole (Figure 3.2.2), only the $TiO_2$ surface was included in this approximation. Figure 3.2.5 shows top and side view for a THF adsorbed on neutral $TiO_2$. A similar

configuration is computed for positively charged $TiO_2$. Importantly, when the surface is positive the stabilization increases by 23.8 kcal/mol. As the positive surface is a reasonable model for the $TiO_2$-hole, this indicates the beginning of the electron transfer process in which THF neutralizes the highly electrophilic hole. In polar media, this becomes the nascent PCET process in which the electron is donated to the hole and the proton stabilized by the solvent, a type of PCET described as dystonic to emphasize the different destination of proton and electron. As expected by their molecular geometry, diethers do not show any preferred adsorption configuration compared to those with one oxygen (See SI, Figure 3.3.11). Further thermodynamic details can be found in Table 3.3.1.

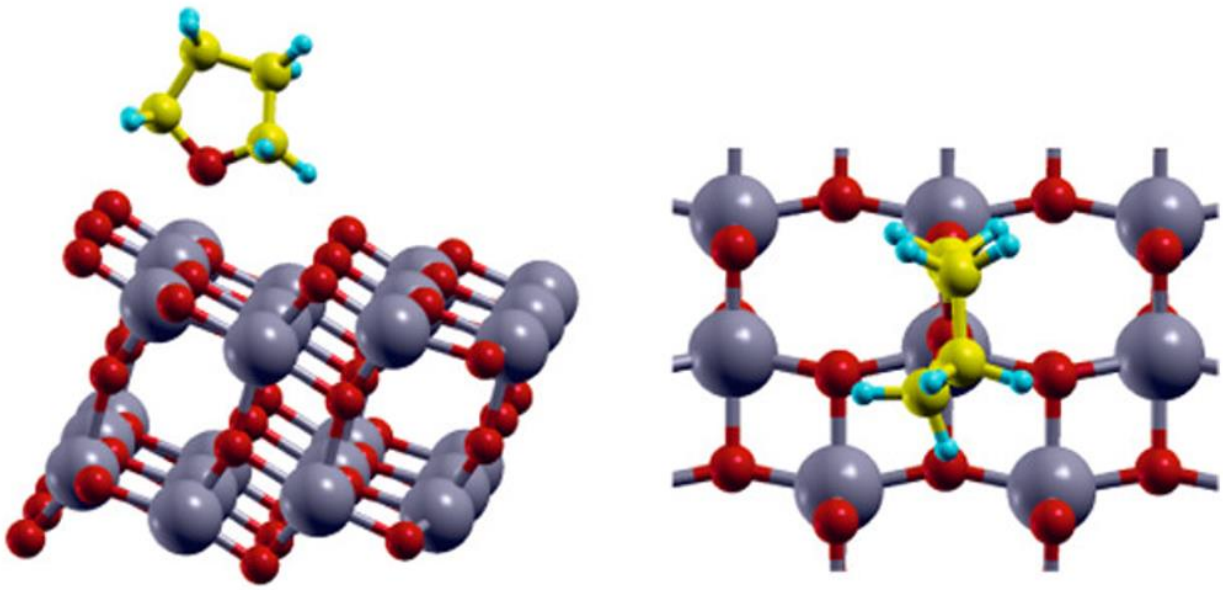


**Figure 3.2.5.** Computed adsorption configuration of THF on anatase $TiO_2$ (101) surface. Side (left) and top view.

Free radical formation for other nonactivated C–H systems was also shown with pure toluene or acetonitrile. For toluene, Figure 3.3.12 shows the formation of bibenzyl and ring coupling products from benzyl radicals. TEMPO also traps $^{\bullet}CH_2CN$ from acetonitrile (See SI, Figure 3.3.13). Although the C–H bond dissociation energy (BDE) in acetonitrile (92 kcal/mol[24]) is within

the same range of BDE in toluene or α-C−H in ethers, this result is appealing as the electron poor nature of $CH_3CN$ makes it rather inert to typical electrophilic radicals,[25] such as $tBuO^{\bullet}$.

In conclusion, hole trapping in $TiO_2$, and probably in other semiconductors of comparable band gap, serves as an excellent free radical source, easy to control, use, and separate once the radical source is no longer required. While pristine $TiO_2$ in its anatase form can perform this function, decorating the material enhances free radical generation by a factor of ca. 5, and is attributed to electron trapping by the metallic center that reduces the rate of electron-hole recombination. While we focused on ethers, the rich SED literature suggests that many molecules can perform similarly, as demonstrated here with toluene and acetonitrile. Numerous molecules should be capable of donating an electron to the VB hole, thus being excellent candidates for a remarkable clean and efficient source of free radicals.

## 3.3 Post-print Version of Supplementary Information

### Materials and instrumentation

All reagents used were purchased from Sigma Aldrich and used as received unless otherwise stated. $TiO_2$ P25 was purchased from Univar Canada and the 1% Au@$TiO_2$ from Strem Chemicals (AUROlite™ Au/$TiO_2$).

Photo-induced radical formation was performed upon irradiation utilizing Light-emitting diodes (LEDs) of 10 W from LedEngin centered at 368 nm. The detection of the TEMPO-ether adduct was performed in a Perkin Elmer, Claurus Gas Chromatograph couple to a Flame Ionization Detector (FID) $H_2$ generated was detected in the same instrument couple to Thermal Conductivity Detector (TCD) using Argon as a carrier gas and a 5A Zeolite molecular sieve column. Characterization of the TEMPO-adducts was performed by mass spectrometry in an Agilent 6890-N Gas Chromatograph with an Agilent 5973 mass selective detector calibrated with acetophenone. Aldehyde formation was detected using colorimetric test strips from Sigma Aldrich. All 1H NMR and 13C NMR spectra were recorded on a Bruker AVANCE 400 spectrometer expressing the chemical shifts in ppm relative to the H(or C)-signal of the solvent (AcN-d3). Electron paramagnetic resonance (EPR) spectra were recorded on a Bruker EMXplus (X-band)

equipped with an ER 4119HS cavity at room temperature with a modulation of 2G and irradiating with a LIGHTNINGCURE Spot light source LC5. Samples were typically 100 µM in pure THF. Spectra simulations were performed using EPRsimulator (http://www.eprsimulator.org/).

**Experimental methodology**

*Synthesis of the catalysts.*

All metal-decorated $TiO_2$ were prepared following a photochemical method, with slight modifications, previously reported.[17, 26] Synthetic procedures are also explained in the appendix, along with characterization of the materials by TEM, XPS, ICP and DR.

*TEMPO-adduct formation.*

Radical trapping experiments were conducted with 5 mL of 1 M ether solution in acetonitrile in the presence of 25 mM TEMPO under Ar and irradiated by 2500 W m-2 368 nm LED for 3 hours. The reaction was followed by monitoring the conversion of TEMPO to the TEMPO-ether adduct by GC-FID. In the cases that it is stated, the reaction was ran in the presence 25 mM $Cs_2CO_3$. Likewise, $H_2$ generation was monitored using GC-TCD, the values were obtained within 15% experimental error.

*Ether competition.*

Equimolar amount of each ether was added into 4.0 mL of MeCN in the presence of 25 mM of TEMPO and 25 mM $Cs_2CO_3$ under Ar and irradiated with a 368 nm LED working at 4000 $Wm^{-2}$ for 24 hours. The reaction was monitored by GC-FID and the $H_2$ formation by GC-TCD.

**Computational methodology**

The spin-polarised DFT calculations (support provided by WestGrid (www.westgrid.ca) and Compute Canada (www.computecanada.ca)) for studying the adsorption interactions amongst ethers were carried out with Quantum ESPRESSO package[23] using ultra-soft pseudopotential with gradient approximation of Perdew, Burke and Ernzerhof (PBE).[27] The electronic wave-functions were expanded using a value of 25 Ry for the kinetic cut-off energy and 200 Ry for charge density, while the Monkhorst-Pack k-point grid selected was set to 4x4x1.

All the atomic positions were allowed to relax during structural optimization until residual forces were smaller than 0.05 eV/Å.

At the level of theory used, the optimized lattice constant of bulk anatase $TiO_2$ structure (c=9.56 Å) is in good agreement with the experimental value.[28] The bulk anatase $TiO_2$ structure was cleaved along (101) direction to create a symmetric periodic slab of 3 $TiO_2$ bilayer with a rectangular surface unit cell of 10.28 x 11.36 Å. A vacuum region of 18 Å between $TiO_2$ (101) slabs was used to minimize interactions between them along the z direction.

To mimic the presence of the photoexcited hole in $TiO_2$, a positively charged anatase $TiO_2$ (101) slab has been considered. The adsorption energies were calculated by the following formula: $E_{ads}$ 125 = $E_{ab} - E_a - E_b$, where $E_{ab}$ is the energy of the optimized complex (substrate + TiO2 slab), $E_a$ is the energy of the optimized substrate and $E_b$ is the energy of optimized $TiO_2$ slab.

DFT calculations for analyzing the electron transfer process amongst THF radical and neutral THF solvent molecule were performed using Gaussian 09.[29] The geometry optimization were performed at B3LYP functional[30-31] with Grimme's dispersion correction[32] using Def2-TZVP basis set.[33] Acetonitrile was used as solvent for the continuum solvation model via keywords SCRF=(IEFPCM, solvent=acetonitrile).

**Thermodynamic Analysis of Aldehyde Formation**

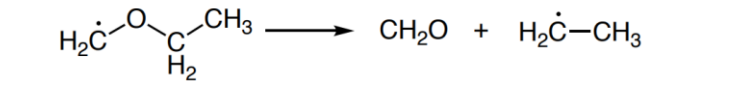


$\Delta H_{f(g)}$ = (-108.6 + 119.2) - (+44.7) = -34.1 kJ/mol

**Scheme 3.3.1.** Representative radical formation of aldehydes from ethers, thermodynamic analysis.

**Gas Chromatography and Mass Spectrometry of TEMPO products**

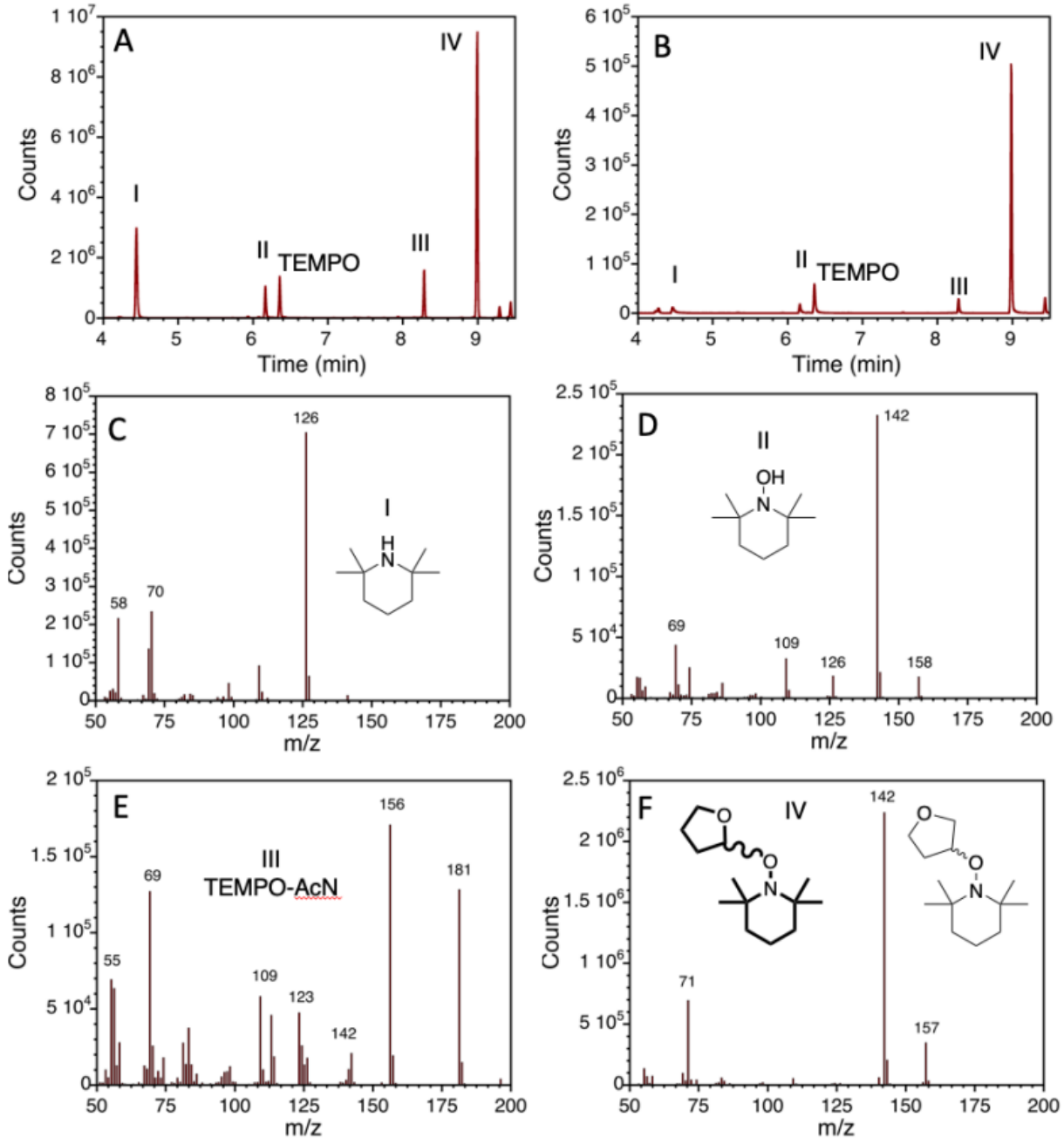


**Figure 3.3.1.** Gas chromatogram of the photochemical reaction of THF in the presence of TEMPO and Pd@$TiO_2$ showing the formation of THF-TEMPO adduct (IV), among other by-products using as solvent **(A)** pure AcN or **(B)** AcN:$H_2O$ 50:50. Corresponding MS spectra of **(C)** 2,2,6,6-tetramethylpiperidine (TEMPH), **(D)** 2,2,6,6-tetramethyl-1-piperidinol (TEMPOH), **(E)** Solvent-TEMPO adduct, and **(F)** THF-TEMPO adduct product – the anticipated isomer is represented by the bold molecular structure, as MS cannot distinguish them.

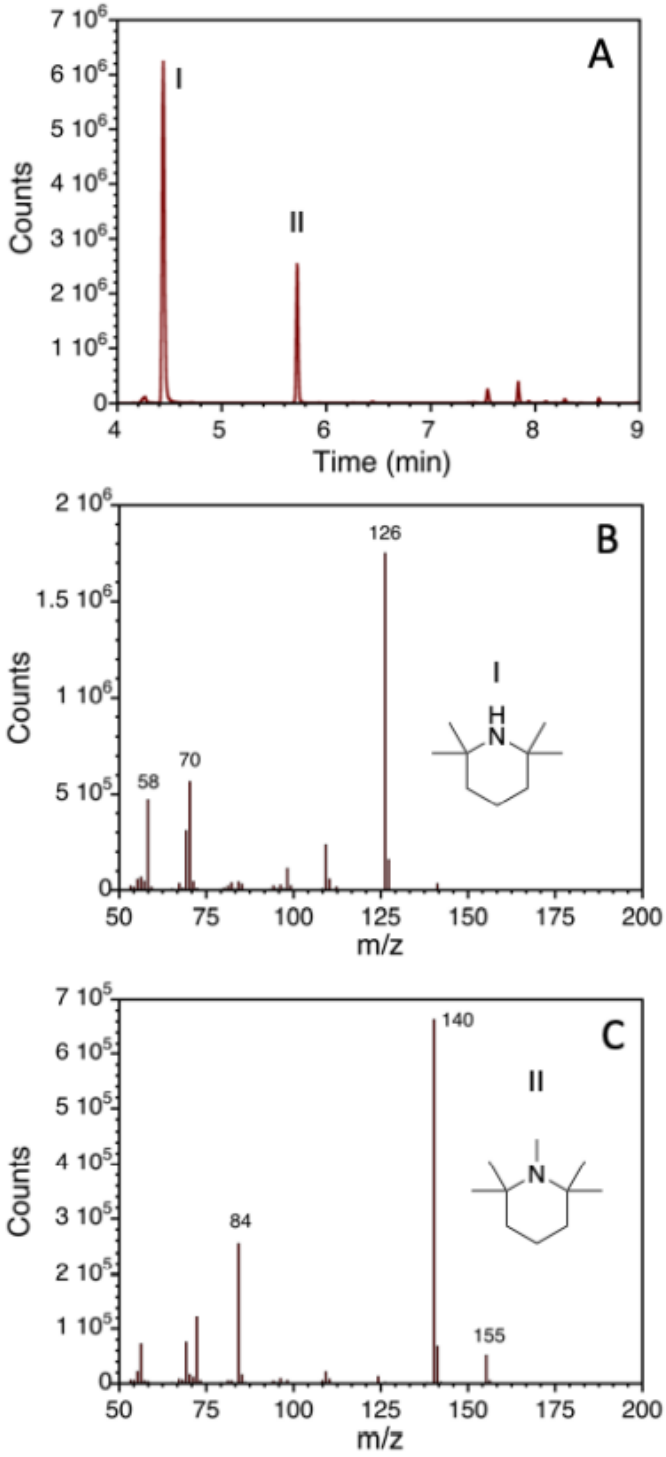


**Figure 3.3.2. (A)** Gas chromatogram of the photochemical reaction of DMM (dimethoxymethane) and TEMPO in the presence of Pd@$TiO_2$ showing the formation of (I) 2,2,6,6-tetramethylpiperidine (TEMPH) and (II) *N*-methyl 2,2,6,6-tetramethylpiperidine (TEMP-Me). **(B-C)** MS spectra of each product.

**Electron Paramagnetic Resonance (EPR) Spectroscopy**

Radical reactions were also tested through direct evaluation of the loss of TEMPO radical EPR signal during direct monitoring of irradiation of a sample of TEMPO in THF with suspended Pd@$TiO_2$ (Figure 3.3.3). Irradiation with a 368 nm LED through the EPR window created a sharp decrease in the strength of the TEMPO signal, as expected due to the loss of nitroxy radical (Scheme 3.3.2). The signal for TEMPO is the expected 3 peaks of equal size expected from splitting by the Nitrogen adjacent to the radical.

DMPO trapping was also conducting in a similar system, as DMPO forms an oxygen centred radical after spin-trapping other radicals (Scheme 3.3.2). The formed radical signal in EPR has splitting by the adjacent nitrogen into 3 peaks ($a_N$), and splitting by the $H_\beta$ by 2 ($a_{H(\beta)}$). There may also be further splitting by coupling with further groups, including with the $H_\gamma$. This is more possible in the final structure due to possible W confirmation due to ring puckering.[34] The chemical structure attached will also alter the observed couplings, and further long range couplings may be possible. Overall, the EPR in argon (Figure 3.3.4) shows relatively expected signals for such a DMPO-trapped product. There however is a background impurity radical that is negatively impacting analysis of the final signals. This complicates accurate analysis of the group attached to DMPO, with the main conclusion being that a radical has indeed been spin-trapped by the DMPO. The addition of air further complicates the signals, most likely due some peroxyl trapping occurring due to initial reaction of THF radicals with oxygen.

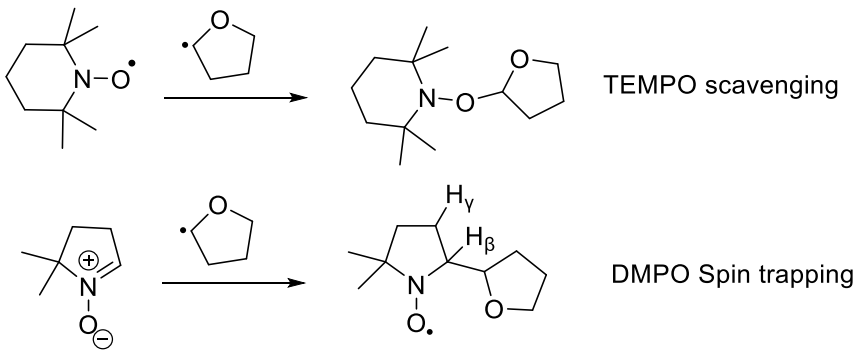


**Scheme 3.3.2.** Expected products for evaluation in EPR experiments with THF radicals.

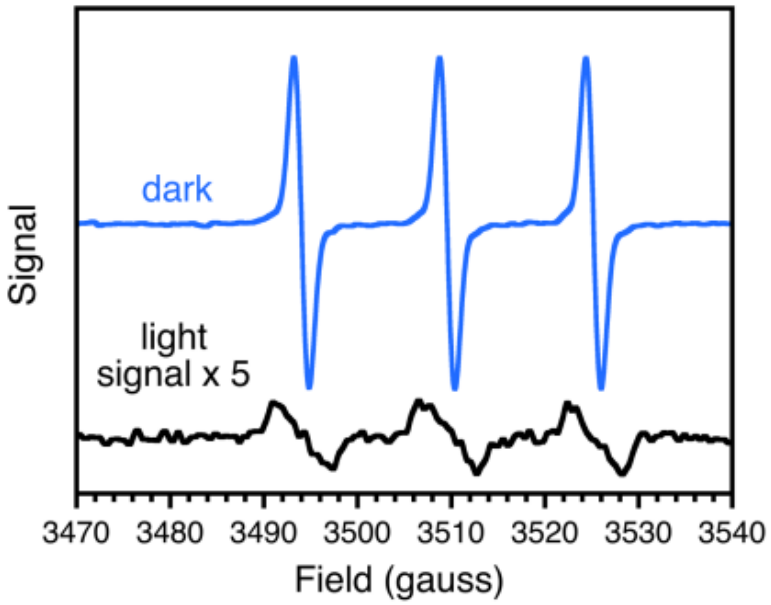


**Figure 3.3.3.** EPR spectra for a sample of Pd@$TiO_2$ containing TEMPO (0.1 mM) in THF under Argon in the dark (blue) and illuminated 30 minutes (black) with a 368 nm LED.

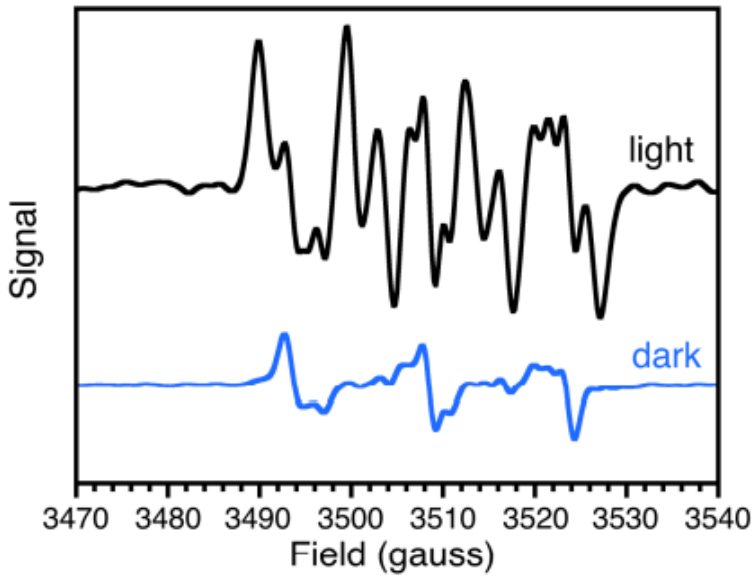


**Figure 3.3.4.** EPR spectra for a sample of Pd@$TiO_2$ containing DMPO in THF under Argon in the dark (blue) and illuminated 30 seconds (black). The illuminated spectrum matches reasonably well $a_N$ = 11.8G, $a_{H(\beta)}$= 15.2G and $a_{H(\gamma)}$≤ 1.5G, with 34% contamination of the impurity spectrum in the dark. Interaction with suspended $TiO_2$ and a different solvent, may influence the coupling relative to literature values.[35] While the impurity radical is persistent, the light-generated component decays in a few minutes.

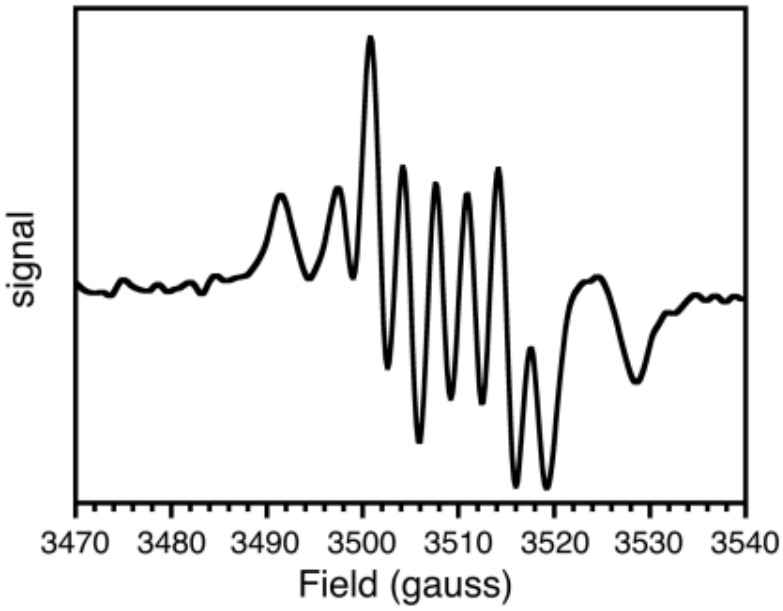


**Figure 3.3.5.** EPR spectra for a sample of Pd@$TiO_2$ containing DMPO in THF under Air illuminated 30 seconds. The spectrum could not be fully characterized but matches reasonably well $a_N$ = 13.8G, with additional proton couplings ~10G. It's shape resembles well those recorded for peroxyl radical trapping.[36] Impurity contamination similar to Figure 3.3.4 hindered a complete characterization.

### Ether Dimer and Heterodimer Formation

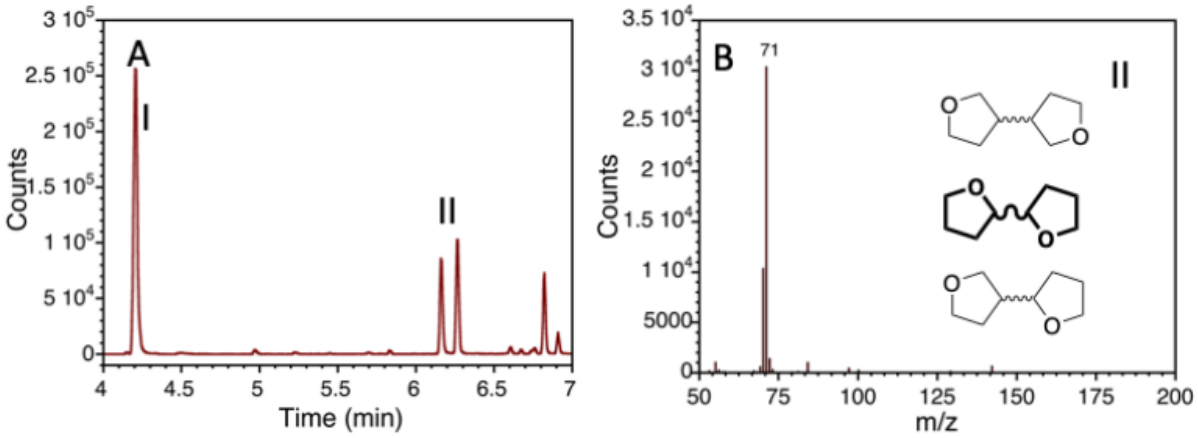


**Figure 3.3.6. (A)** Gas chromatogram of the photochemical reaction of THF in the presence of Pd@$TiO_2$ showing the formation of THF dimer (II), among other by-products (lactone identified as I). The peaks are shown in pairs as the formation of different diastereomers is possible. The anticipated isomers is represented by the bold molecular structure, as MS cannot distinguish them. **(B)** MS spectra of THF dimer product.

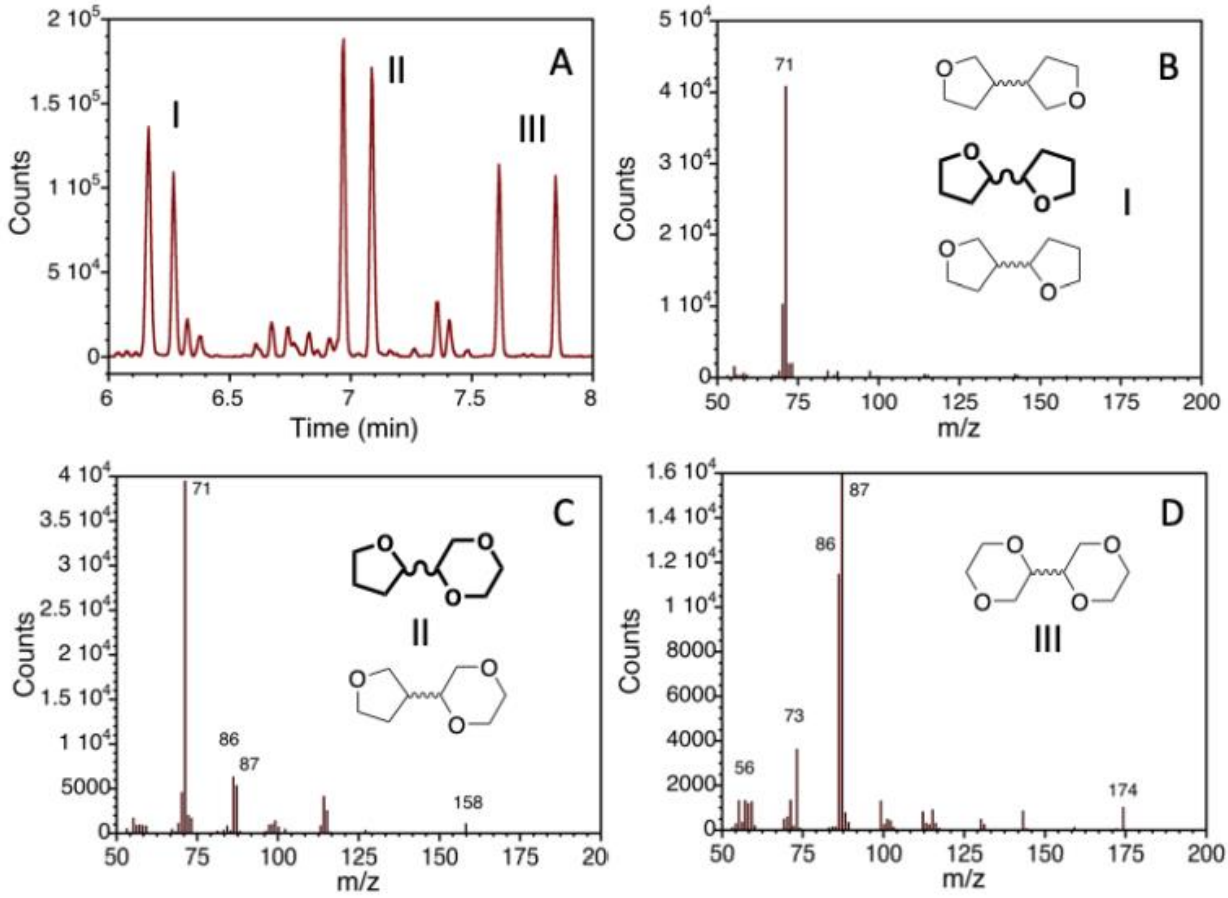


**Figure 3.3.7. (A)** Gas chromatogram of the photochemical reaction of THF and dioxane in the presence of Pd@$TiO_2$ showing the formation of THF dimer (I), THF-dioxane adduct (II), and dioxane dimer (III) among other by-products. The peaks are shown in pairs as the formation of different diastereomers is possible. The anticipated isomer is represented by the bold molecular structure, as MS cannot distinguish them. **(B-D)** MS spectra of each product and their possible isomers.

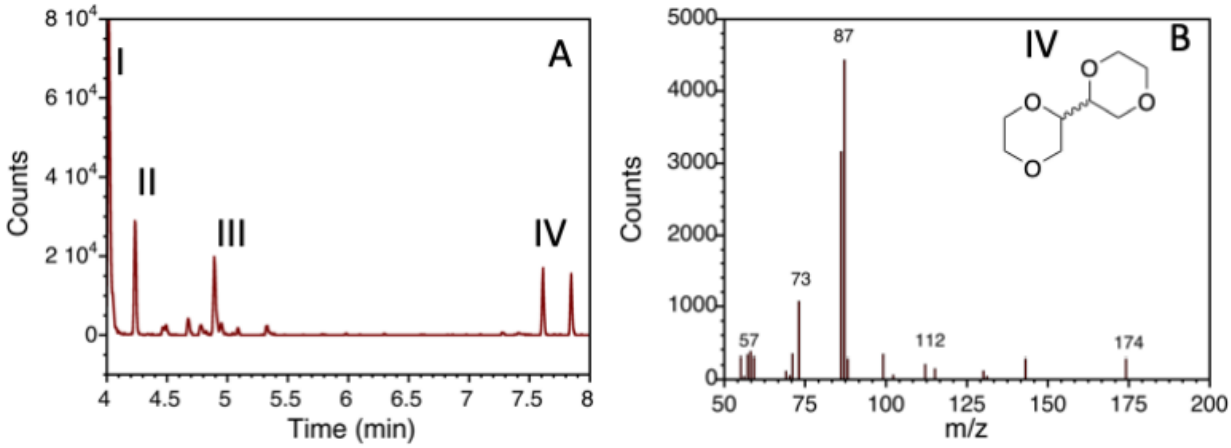


**Figure 3.3.8. (A)** Gas chromatogram of the photochemical reaction of dioxane in the presence of Pd@$TiO_2$ showing the formation of dioxane dimer (IV), among other by-products. The peaks are shown in pairs as the formation of different diastereomers is possible. **(B)** MS spectrum of dioxane dimer product.

**NMR Spectra of tetrahydrofuran oxidation products**

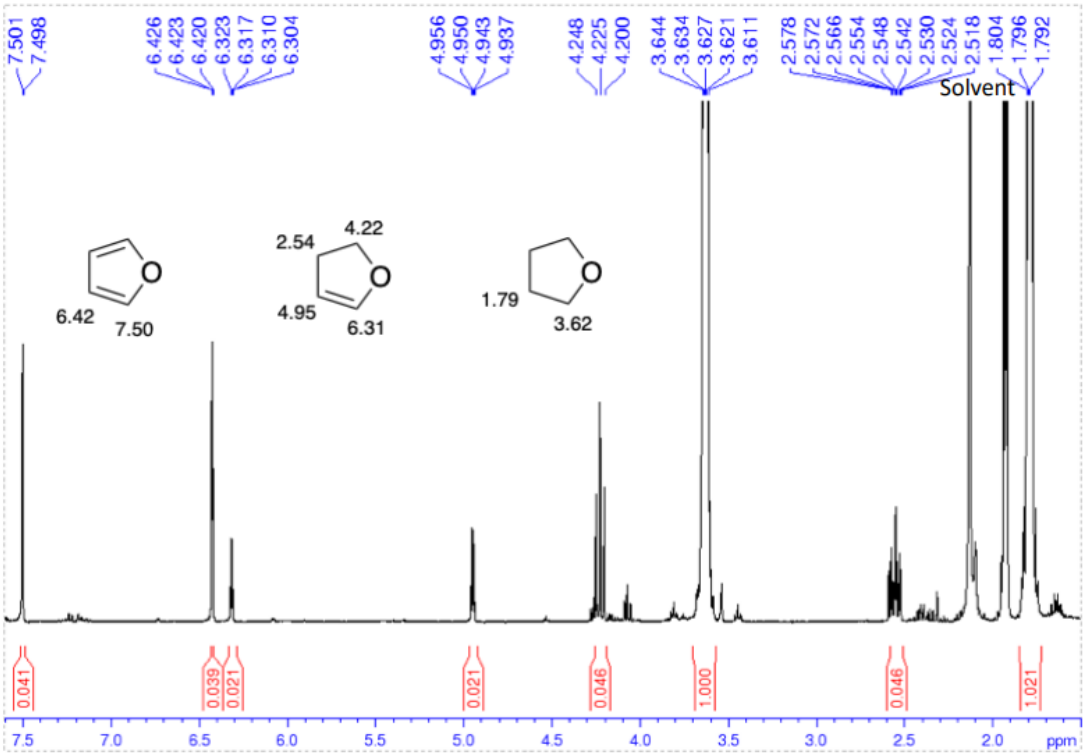


**Figure 3.3.9.** $^1$H NMR spectrum of the reaction of 50 uL of THF in 4 mL of AcN-$d_3$ in the presence of 20 mg of Pd@$TiO_2$ after 48 h of irradiation. The spectrum shows the formation of dihydrofuran (DHF) and furan. Numbers around molecule structures correspond to the $^1$H-chemical shift assignment. Notice that formation of furan at expenses of DHF in the excess of THF is a clear indication of the DHF greater reactivity towards the $TiO_2$-hole.

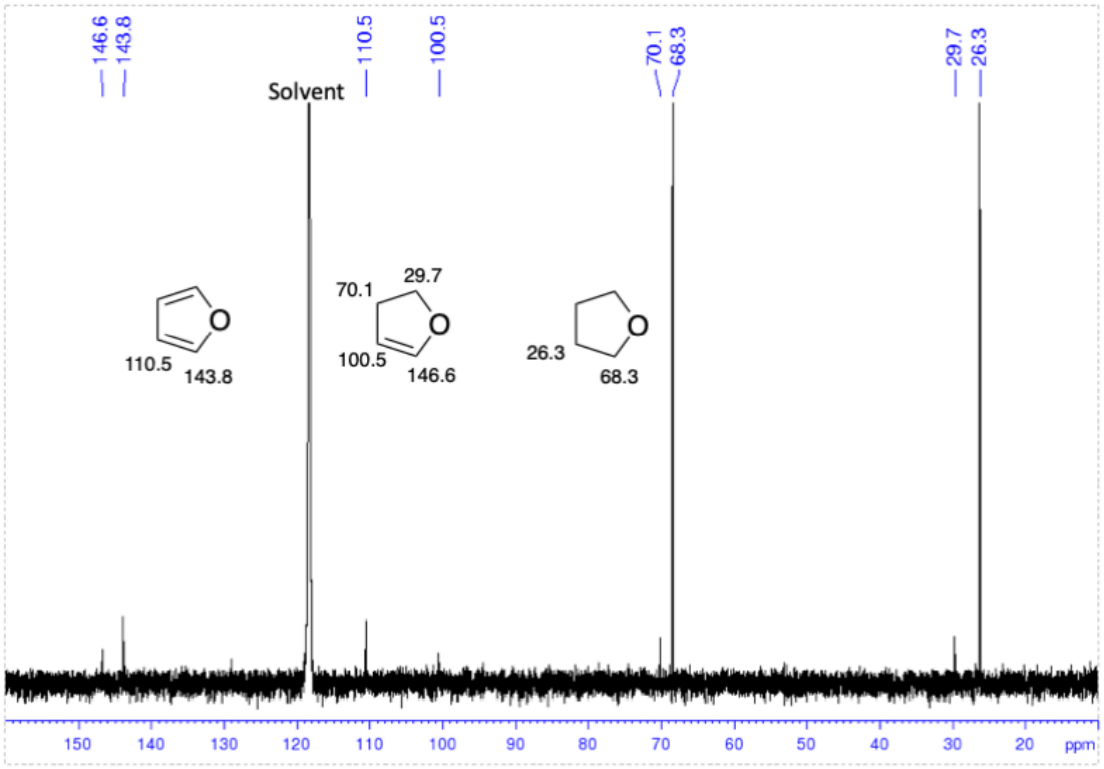


**Figure 3.3.10.** 13C NMR spectrum of the reaction of 50 µL of THF in 4 mL of AcN-$d_3$ in the presence of 20 mg of Pd@TiO2 after 48 h of irradiation. The spectrum shows the formation of dihydrofuran (DHF) and furan. Numbers around molecule structures correspond to the $^{13}$C-chemical shift assignment.

**Thermodynamic analysis of the PCET process**

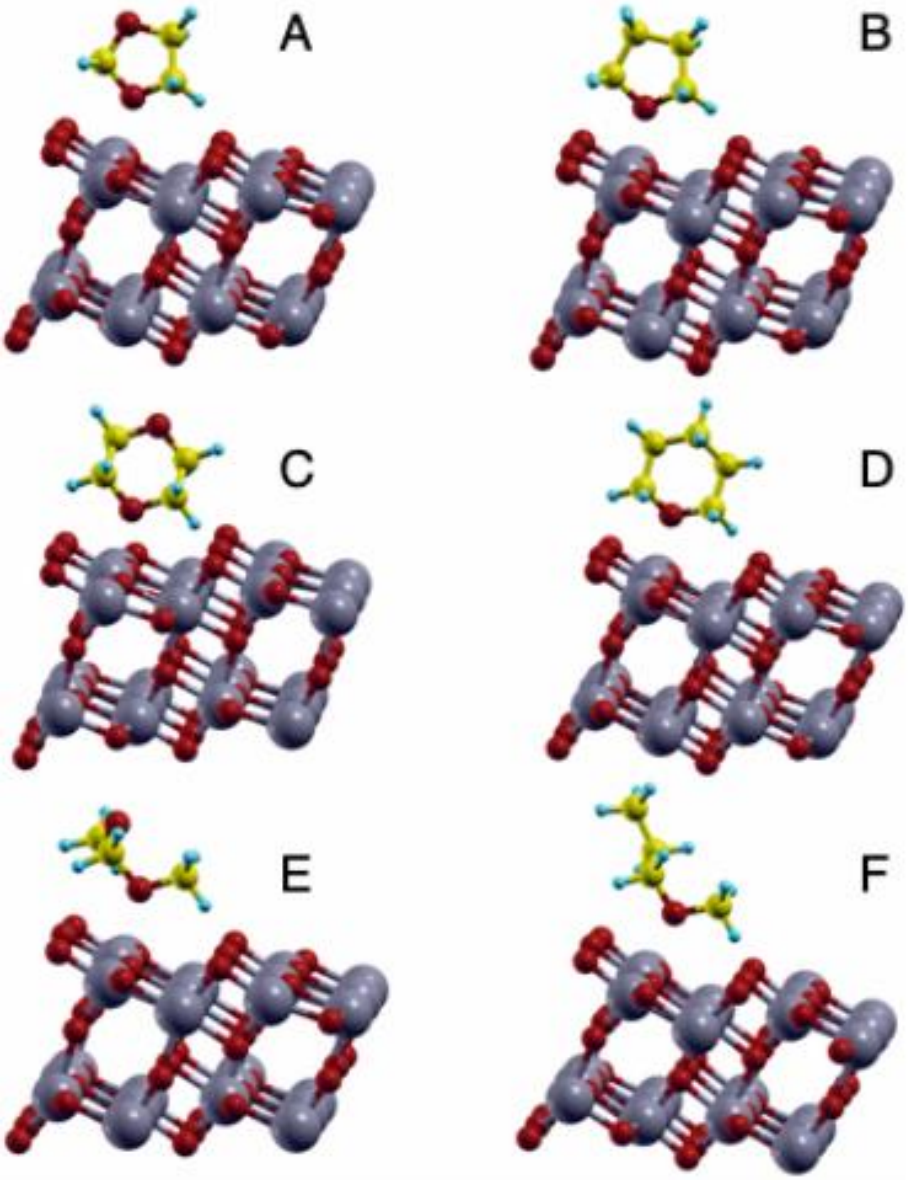


**Figure 3.3.11.** Computed adsorption configuration of the ether molecules on anatase TiO2 (101) surface. **(A)** 1,3- dioxolane (DOL), **(B)** tetrahydrofuran (THF), **(C)** dioxane (DOX), **(D)** tetrahydropyran (THP), **(E)** dimethoxymethane (DMM), and **(F)** 1-methoxypropane (MOP).

**Table 3.3.1.** Computed thermodynamic analysis of ether interaction on the $TiO_2$ surface.

| Ether | $TiO_2$ Surface Binding Energy (kcal/mol) | | | H-Transfer to the Charged Surface (kcal/mol) |
|---|---|---|---|---|
| | Uncharged | (+) charged | Stabilization | |
| **THF** | 15.6 | 39.4 | 23.8 | -11.7 |
| **DOX** | 10.2 | 40.1 | 30.1 | +4.9 |
| **DEE** | 11.4 | 33.1 | 21.7 | -9.2 |

THF (tetrahydrofuran), DOX (dioxane), DEE (diethyl ether)

The binding energy difference between the neutral and positively charged $TiO_2$ surface can be viewed as the stabilization achieved by creating a hole on the semiconductor. While this stabilization is best for dioxane, the transfer of hydrogen (proposed to occur by a PCET mechanism) is least favorable for dioxane. When all energetic parameters are taken into account, THF is most favored as observed experimentally. The transfer of an electron between THF and the $TiO_2$ hole leads to the radical-cation from THF. Gas-phase calculations show that the proton can be readily stabilized on the $TiO_2$ surface, as shown in Scheme 3.3.2(A), thus releasing the THF radical. In a typical solution experiment the stabilization of the proton will be a competitive process between the $TiO_2$ surface and the solvent, which in the case of THF as solvent corresponds to the process in Scheme 3.3.2(B).

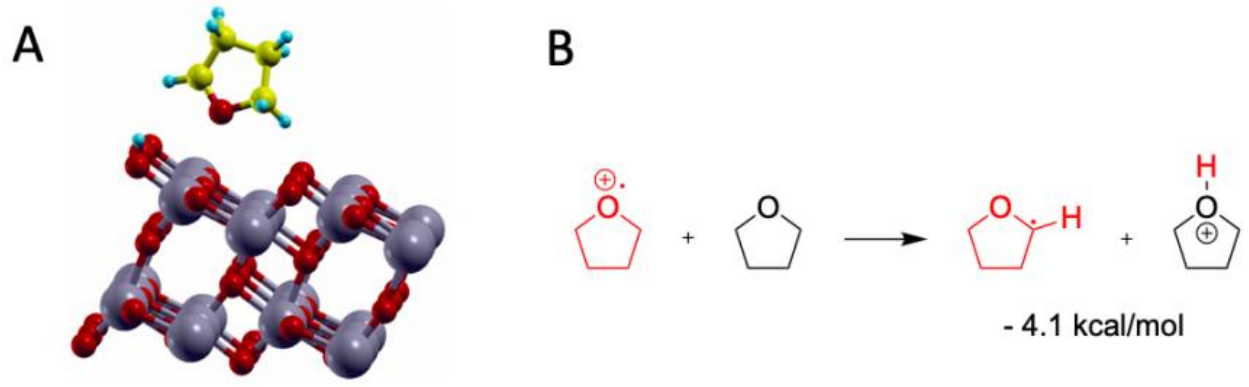


**Scheme 3.3.3.** Proton stabilization on the $TiO_2$ surface **(A)** or by interaction with the solvent **(B)**

Clearly both possibilities, A and B in Scheme 3.3.2 will be favorable and an integral part of the PCET process triggered by electron transfer between THF and the $TiO_2$ hole. While our results cannot distinguish between these two possibilities, option B is somewhat more attractive as it is more likely to enable the proton mobility required for other processes, such as $H_2$ production.

**Radical formation from non-activated C-H bonds: Toluene and Acetonitrile**

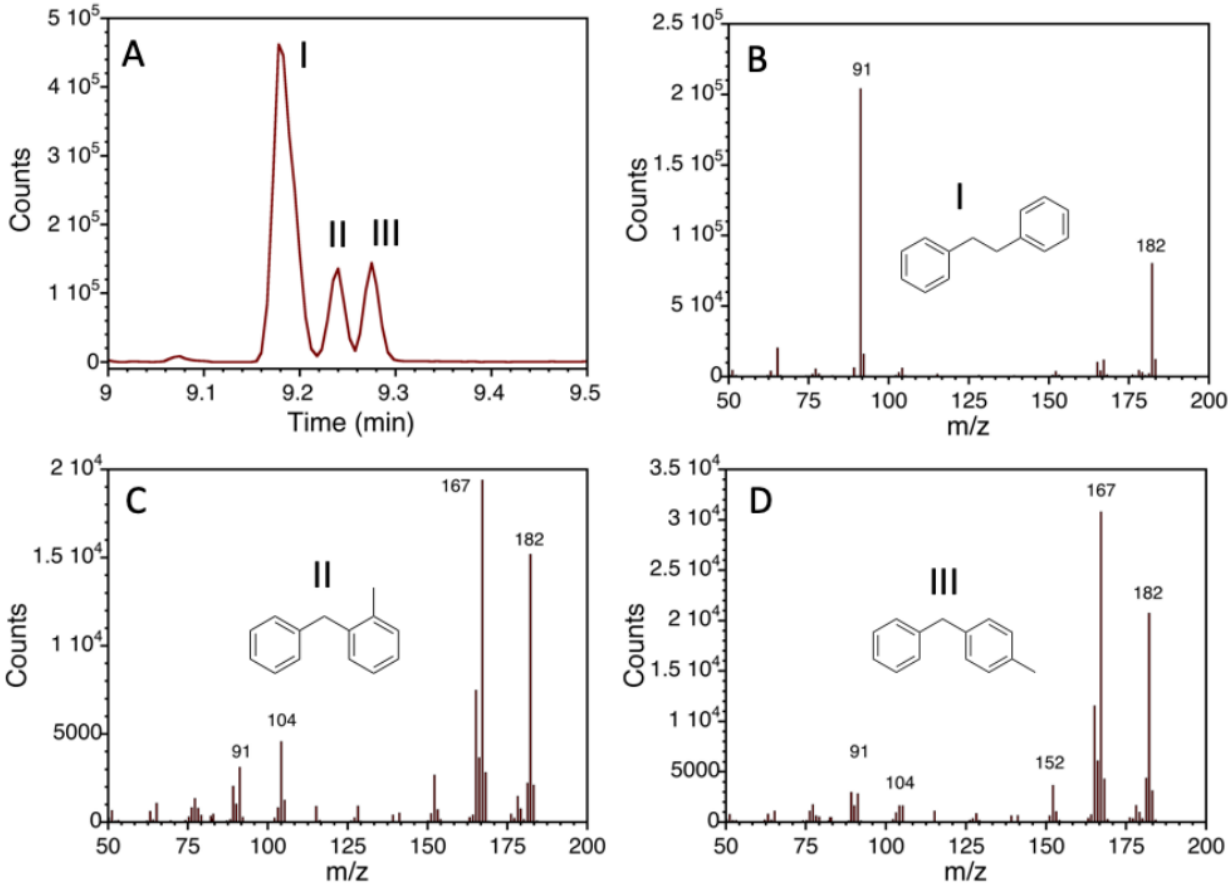


**Figure 3.3.12. (A)** Gas chromatogram of the photochemical reaction of toluene in the presence of Pd@$TiO_2$ showing the formation of bibenzyl (I), *o*-benzyltoluene (II), and *p*-benzyltoluene (III). **(B-D)** MS spectra of each product. Assignment of II and III is tentative and based on the Agilent library of MS spectra.

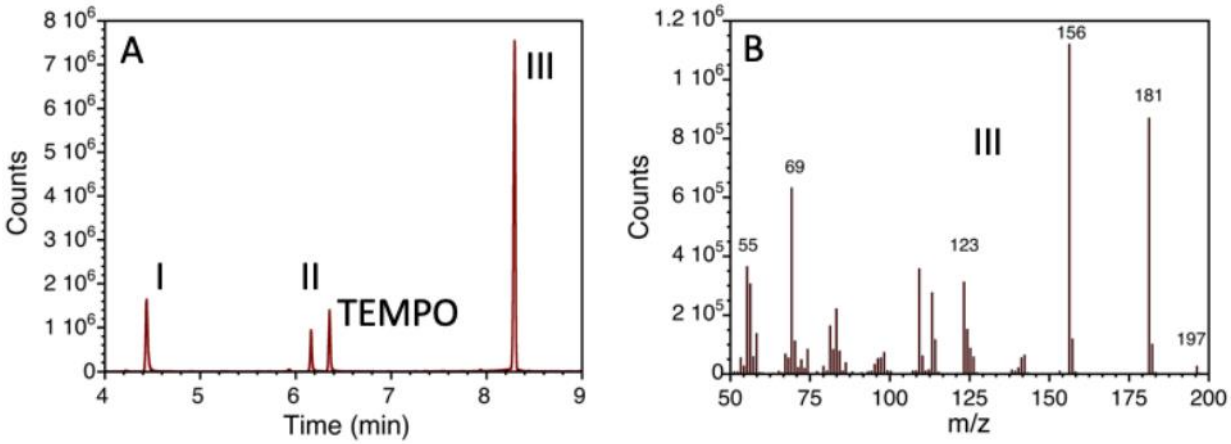


**Figure 3.3.13. (A)** Gas chromatogram of the photochemical reaction of acetonitrile in the presence of Pd@$TiO_2$ showing the formation of (I) 2,2,6,6- tetramethylpiperidine (TEMPH), (II) 2,2,6,6-tetramethyl-1-piperidinol (TEMPOH), and (III) the AcN-TEMPO adduct. **(B)** MS spectrum of AcN-TEMPO adduct product.

## 3.4 Accompaniment to Chapter 3

This manuscript acted as my second peer-reviewed publication, shortly after transferring to the Doctoral program. It also acted as the first step in an overall change in the direction of my research. Originally, it was planned that my focus after my research in chapter 2 would be on the implications given for water purification. However, I found myself to be more focused on the implications for organic radical chemistry, especially after this research in chapter 3. As mentioned previously, I still had some collaboration within the water purification project; however, my main project pivoted in the direction of solvent radical chemistry.

The next chapter will explore a new method of evaluating radical chemistry of heterogeneous systems using laser flash photolysis. Interestingly, this was done using 1,3-dioxolane as a solvent, which was one of the solvents in this chapter that did not give significant yield of a TEMPO-Ether adduct. 1,3-dioxolane was chosen to be explored further since the most commonly generated radical (at the carbon centre adjacent to both oxygens) would be unable to form a double bond, and should be a more long lived radical in comparison to other ethers ('long lived' in a relative sense). I believe that the lack of TEMPO-ether adduct formation with 1,3-dioxolane was not due to no radical formation, but instead other factors of the specific reaction conditions (concentrations, pH, etc…) favoring the formation of other TEMPO side products.

Overall, TEMPO is a useful tool for checking for free radical formation in solution, but still has its limitations. Other methods that can better evaluate the direct reaction occurring, such as the laser-flash photolysis methods in the next chapter, can be better at truly knowing if free radicals are forming in solution.

## 3.5 References


1. Gawargy, T. A.; Costa, P.; Lanterna, A. E.; Scaiano, J. C., Photochemical benzylic radical arylation promoted by supported Pd nanostructures. *Org. Biomol. Chem.* **2020,** *18* (31), 6047-6052.
2. Yi, H.; Zhang, G. T.; Wang, H. M.; Huang, Z. Y.; Wang, J.; Singh, A. K.; Lei, A. W., Recent advances in radical C-H activation/radical cross-coupling. *Chem. Rev.* **2017,** *117* (13), 9016.
3. Zhang, S. Y.; Zhang, F. M.; Tu, Y. Q., Direct $Sp^3$ alpha-C-H activation and functionalization of alcohol and ether. *Chem. Soc. Rev.* **2011,** *40* (4), 1937.
4. Taylor, R. D.; MacCoss, M.; Lawson, A. D. G., Rings in drugs. *J. Med. Chem.* **2014,** *57* (14), 5845.
5. Martins, P.; Jesus, J.; Santos, S.; Raposo, L. R.; Roma-Rodrigues, C.; Baptista, P. V.; Fernandes, A. R., Heterocyclic anticancer compounds: Recent advances and the paradigm shift towards the use of nanomedicine's tool box. *Molecules* **2015,** *20* (9), 16852.
6. Jin, J.; MacMillan, D. W. C., Direct alpha-arylation of ethers through the combination of photoredox-mediated C-H functionalization and the Minisci reaction. *Angew. Chem., Int. Ed.* **2015,** *54* (5), 1565.
7. Shaw, M. H.; Twilton, J.; MacMillan, D. W. C., Photoredox catalysis in organic chemistry. *J. Org. Chem.* **2016,** *81* (16), 6898.
8. Mayer, J. M., Understanding hydrogen atom transfer: From bond strengths to Marcus theory. *Acc. Chem. Res.* **2011,** *44* (1), 36.
9. Gaya, U. I.; Abdullah, A. H., Heterogeneous photocatalytic degradation of organic contaminants over titanium dioxide: A review of fundamentals, progress and problems. *J. Photochem. Photobiol., C* **2008,** *9* (1), 1.
10. Morsella, M.; d'Alessandro, N.; Lanterna, A. E.; Scaiano, J. C., Improving the sunscreen properties of $TiO_2$ through an understanding of its catalytic properties. *ACS Omega* **2016,** *1* (3), 464.
11. Sendra, M.; Sanchez-Quiles, D.; Blasco, J.; Moreno-Garrido, I.; Lubian, L. M.; Perez-Garcia, S.; Tovar-Sanchez, A., Effects of $TiO_2$ nanoparticles and sunscreens on coastal marine microalgae: Ultraviolet radiation is key variable for toxicity assessment. *Environ. Int.* **2017,** *98*, 62.
12. Hanigan, D.; Truong, L.; Schoepf, J.; Nosaka, T.; Mulchandani, A.; Tanguay, R. L.; Westerhoff, P., Trade-offs in ecosystem impacts from nanomaterial versus organic chemical ultraviolet filters in sunscreens. *Water Res.* **2018,** *139*, 281.
13. Tyagi, A.; Yamamoto, A.; Kato, T.; Yoshida, H., Bifunctional property of Pt nanoparticles deposited on $TiO_2$ for the photocatalytic sp(3)C-sp(3)C cross-coupling reactions between THF and alkanes. *Catal. Sci. Technol.* **2017,** *7* (12), 2616.
14. Marina, N.; Lanterna, A. E.; Scaiano, J. C., Expanding the color space in the two-color heterogeneous photocatalysis of Ullmann C-C coupling reactions. *ACS Catal.* **2018,** *8* (8), 7593.
15. Fuchigami, T.; Fuchigami, T. a., *Fundamentals and Applications of Organic Electrochemistry: Synthesis, Materials, Devices*. 2014.
16. Schneider, J.; Bahnemann, D. W., Undesired role of sacrificial reagents in photocatalysis. *J. Phys. Chem. Lett.* **2013,** *4* (20), 3479.

17. Wang, B.; Durantini, J.; Nie, J.; Lanterna, A. E.; Scaiano, J. C., Heterogeneous photocatalytic click chemistry. *J. Am. Chem. Soc.* **2016,** *138* (40), 13127.
18. Hernandez Mejia, C.; van Deelen, T. W.; de Jong, K. P., Activity enhancement of cobalt catalysts by tuning metal-support interactions. *Nat. Commun.* **2018,** *9* (1), 4459.
19. Malatesta, V.; Scaiano, J. C., Absolute rate constants for the reactions of tert-butoxyl with ethers - Importance of the stereoelectronic effect. *J. Org. Chem.* **1982,** *47* (8), 1455.
20. Hainer, A. S.; Hodgins, J. S.; Sandre, V.; Vallieres, M.; Lanterna, A. E.; Scaiano, J. C., Photocatalytic hydrogen generation using metal-decorated $TiO_2$: Sacrificial donors vs true water splitting. *ACS Energy Lett.* **2018,** *3* (3), 542.
21. Ciriano, M. V.; Korth, H. G.; van Scheppingen, W. B.; Mulder, P., Thermal stability of 2,2,6,6-tetramethylpiperidine-1-oxyl (TEMPO) and related N-alkoxyamines. *J. Am. Chem. Soc.* **1999,** *121* (27), 6375.
22. Orlov, Y. D.; Chernova, E. M.; Turovtsev, V. V., Enthalpies of formation of organic free radicals of alcohol and ether derivatives. *Russ. Chem. Bull.* **2010,** *59* (10), 2009.
23. Giannozzi, P.; Baroni, S.; Bonini, N.; Calandra, M.; Car, R.; Cavazzoni, C.; Ceresoli, D.; Chiarotti, G. L.; Cococcioni, M.; Dabo, I.; Dal Corso, A.; de Gironcoli, S.; Fabris, S.; Fratesi, G.; Gebauer, R.; Gerstmann, U.; Gougoussis, C.; Kokalj, A.; Lazzeri, M.; Martin-Samos, L.; Marzari, N.; Mauri, F.; Mazzarello, R.; Paolini, S.; Pasquarello, A.; Paulatto, L.; Sbraccia, C.; Scandolo, S.; Sclauzero, G.; Seitsonen, A. P.; Smogunov, A.; Umari, P.; Wentzcovitch, R. M., QUANTUM ESPRESSO: a modular and open-source software project for quantum simulations of materials. *J. Phys.: Condens. Matter* **2009,** *21* (39), 395502.
24. Holmes, J. L.; Lossing, F. P.; Mayer, P. M., The effects of methyl substitution on the structure and thermochemistry of the cyanomethyl radical and cation. *Chem. Phys. Lett.* **1993,** *212* (1–2), 134.
25. De Vleeschouwer, F.; Van Speybroeck, V.; Waroquier, M.; Geerlings, P.; De Proft, F., Electrophilicity and nucleophilicity index for radicals. *Org. Lett.* **2007,** *9* (14), 2721.
26. Elhage, A.; Lanterna, A. E.; Scaiano, J. C., Tunable photocatalytic activity of palladium-decorated $TiO_2$: Non-hydrogen-mediated hydrogenation or isomerization of benzyl-substituted alkenes. *ACS Catal.* **2017,** *7* (1), 250-255.
27. Perdew, J. P.; Burke, K.; Ernzerhof, M., Generalized gradient approximation made simple. *Phys. Rev. Lett.* **1996,** *77* (18), 3865-3868.
28. Diebold, U., The surface science of titanium dioxide. *Surf. Sci. Rep.* **2003,** *48* (5), 53-229.
29. Frisch, M. J.; Trucks, G. W.; Schlegel, H. B.; Scuseria, G. E.; Robb, M. A.; Cheeseman, J. R.; Scalmani, G.; Barone, V.; Petersson, G. A.; Nakatsuji, H.; Li, X.; Caricato, M.; Marenich, A. V.; Bloino, J.; Janesko, B. G.; Gomperts, R.; Mennucci, B.; Hratchian, H. P.; Ortiz, J. V.; Izmaylov, A. F.; Sonnenberg, J. L.; Williams; Ding, F.; Lipparini, F.; Egidi, F.; Goings, J.; Peng, B.; Petrone, A.; Henderson, T.; Ranasinghe, D.; Zakrzewski, V. G.; Gao, J.; Rega, N.; Zheng, G.; Liang, W.; Hada, M.; Ehara, M.; Toyota, K.; Fukuda, R.; Hasegawa, J.; Ishida, M.; Nakajima, T.; Honda, Y.; Kitao, O.; Nakai, H.; Vreven, T.; Throssell, K.; Montgomery Jr., J. A.; Peralta, J. E.; Ogliaro, F.; Bearpark, M. J.; Heyd, J. J.; Brothers, E. N.; Kudin, K. N.; Staroverov, V. N.; Keith, T. A.; Kobayashi, R.; Normand, J.; Raghavachari, K.; Rendell, A. P.; Burant, J. C.; Iyengar, S. S.; Tomasi, J.; Cossi, M.; Millam, J. M.; Klene, M.; Adamo, C.; Cammi, R.; Ochterski, J. W.; Martin, R. L.; Morokuma, K.; Farkas, O.; Foresman, J. B.; Fox, D. J. *Gaussian 09 Rev. E.01*, Wallingford, CT, 2016.
30. Lee, C.; Yang, W.; Parr, R. G., Development of the Colle-Salvetti correlation-energy formula into a functional of the electron density. *Phys. Rev. B* **1988,** *37* (2), 785-789.
31. Becke, A. D., Density-functional thermochemistry. III. The role of exact exchange. *J. Chem. Phys.* **1993,** *98* (7), 5648-5652.
32. Grimme, S.; Antony, J.; Ehrlich, S.; Krieg, H., A consistent and accurate ab initio parametrization of density functional dispersion correction (DFT-D) for the 94 elements H-Pu. *J. Chem. Phys.* **2010,** *132* (15), 154104.

33. Weigend, F.; Ahlrichs, R., Balanced basis sets of split valence, triple zeta valence and quadruple zeta valence quality for H to Rn: Design and assessment of accuracy. *Phys. Chem. Chem. Phys.* **2005,** *7* (18), 3297-3305.
34. Clément, J.-L.; Ferré, N.; Siri, D.; Karoui, H.; Rockenbauer, A.; Tordo, P., Assignment of the EPR spectrum of 5,5-dimethyl-1-pyrroline N-oxide (DMPO) superoxide spin adduct. *J. Org. Chem.* **2005,** *70* (4), 1198-1203.
35. Janzen, E. G.; Liu, J. I. P., Radical addition reactions of 5,5-Dimethyl-1-pyrroline-1-oxide. ESR spin trapping with a cyclic nitrone. *J. Magn. Reson.* **1973,** *9* (3), 510-512.
36. Jones, C. M.; Burkitt, M. J., EPR detection of the unstable tert-butylperoxyl radical adduct of the spin trap 5,5-dimethyl-1-pyrroline N-oxide: a combined spin-trapping and continuous-flow investigation. *J. Chem. Soc., Perkin trans. II* **2002,** (12), 2044-2051.

# 4. Laser flash photolysis of titanium dioxide suspensions for the evaluation of solvent-mediated radical reactions

This chapter has been adapted from Phys. Chem. Chem. Phys., **2023**, 25, 2747-2751 with permission from the Royal Society of Chemistry. To allow for consistent formatting and clarity, some changes have been made.

## 4.1 Preamble to Chapter 4

The following chapter outlines the development of a new method of evaluating the radical chemistry of $TiO_2$ suspensions using laser flash photolysis (LFP) techniques. As shown in the previous chapter, $TiO_2$ is quite versatile at forming solvent radicals in solution, especially when decorated with metal nanoparticles. With this knowledge, I was interested in further evaluating the chemistry of $TiO_2$ suspensions with time-resolved techniques, such as LFP. Specifically, I was interested in directly monitoring the reaction between solvent radicals and alkenes. By using diphenylethylene as the alkene of interest, the formed benzylic radical intermediate can be directly observed in solution by LFP.

The difficulty of this project came from the characteristics of $TiO_2$ suspensions, as $TiO_2$ absorbs light up to 400 nm, and the heterogeneous nature of the mixture also causes increased light scattering. I was interested if low concentration suspensions could overcome these limitations, while also monitoring transient radicals at 330 nm (within the absorbance spectrum of $TiO_2$). Undecorated $TiO_2$ was utilized to simplify the system being evaluated. Overall, it was found that these suspensions can be adequately evaluated by LFP, with observation of the formation and decay of the benzylic transient radicals from the reaction of solvent radicals and diphenylethylene.

The research outlined in this chapter is quite novel, with very limited work currently published. I believe that evaluation of low concentration heterogeneous suspensions by LFP has the potential of being a very interesting new method of evaluating the chemistry of heterogeneous photocatalysts. I plan on passing my knowledge of this technique to the rest of my research group, and also hope to further explore the scope of this research in the future.

## 4.2 Post-print Version of Manuscript

First published in: Phys. Chem. Chem. Phys., **2023**, 25, 2747-2751

### Abstract

The chemistry originating from the scavenging of the highly electrophillic hole in $TiO_2$ can be readily monitored using laser flash photolysis techniques. Dilute suspensions are sufficiently transparent in the UV region that long lived signals derived from reactions of solvent radicals with 1,1-diphenylethylene can be readily monitored. Transient signals originating from hole, electron and trapped radicals are extremely long lived, showing stretched exponentials (nanoseconds to milliseconds) adequately described by fractal models.

### Manuscript

Titanium dioxide ($TiO_2$) is a versatile catalyst that can be used in a variety of reactions and applications.[1-2] It can readily absorb ultraviolet light, exciting an electron from the valence band to the conduction band. This creates both a reactive electron, as well as a reactive 'hole' in the valence band. Earlier laser flash photolysis (LFP) studies of $TiO_2$ primarily observed the dynamics of the transient signals formed from excited electrons, and corresponding holes, trapped in long lived states in the crystal structure. These studies typically involve diffuse reflectance LFP of $TiO_2$ powders,[3-11] with some studies measuring transient absorbance through thin films,[12] or solution LFP of colloidal $TiO_2$ particles.[6, 13-18] Monitoring transient signals from other reactions initiated by the $TiO_2$ have been limited,[16, 19-20] usually due to the difficulty of working with powder suspensions in LFP; in some cases laser irradiation of dry samples can lead to anatase-to-rutile conversion and generation of Ti(III) centers.[21] Also, as $TiO_2$ absorbs readily below 400 nm, it can limit detection in a region where useful transient signals occur, although in some colloidal examples wavelengths as short as 360 nm were monitored.[6]

In this work, we developed a useful method to evaluate the dynamics of solvent radical reactions initiated by titanium dioxide through laser flash photolysis. In particular,

we had interest in the sensitive detection of transients with overlapping absorbance with $TiO_2$. Our prior research[9, 22] has shown $TiO_2$ to be adept at abstracting hydrogen from organic solvents to form transient solvent radicals. The mechanism of this can be seen in Scheme 4.2.1 (eq. 1&2), and involves the initial formation of a reactive hole in the valence band of $TiO_2$. This reactive hole can then oxidize an organic solvent, such as 1,3-dioxolane, to form the radical cation. This radical cation loses a proton to form a solvent radical. This solvent can then be used in further radical chemistry. We aim to use 1,1-diphenylethylene (DPE) as a probe to react with solvent radicals generated by a $TiO_2$ suspension, as this will form a strongly absorbing DPE-solvent adduct radical. (Scheme 4.2.1, eq. 3) This DPE probe will also help evaluate the activity of these solvent generated radicals for radical-alkene chemistry. The benzylic radical of the DPE-solvent adduct should have a strong characteristic transient signal at ~330 nm in laser flash photolysis.[23] Due to the overlap of our transient signal and the absorbance spectra of $TiO_2$, we considered if low concentration suspensions of $TiO_2$ may still allow for analysis of transients in this spectral region

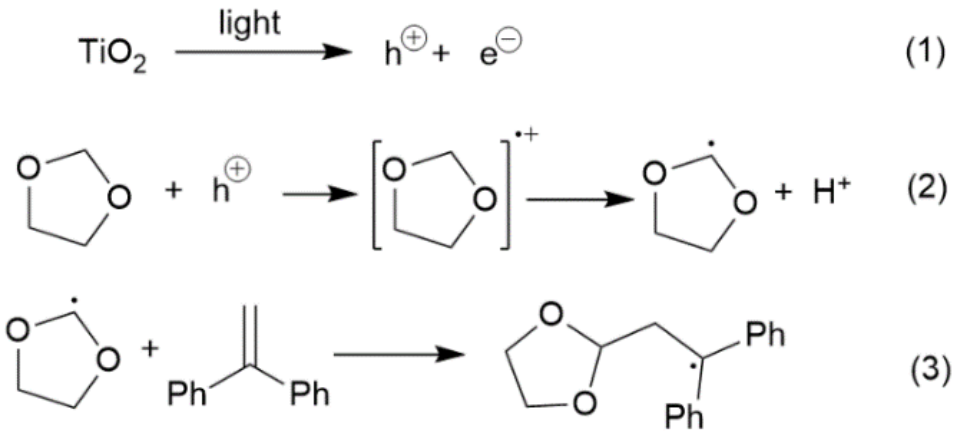


**Scheme 4.2.1.** Mechanism for the formation of 1,3-dioxolane solvent radicals, and the subsequent reaction with DPE. Typical reactions conducted with 5 mg/l $TiO_2$ and 50 mM DPE in dry 1,3-dioxolane under argon at room temperature.

Before examining the system with DPE, the kinetic properties of $TiO_2$ suspensions were evaluated in our solvent of interest, 1,3-dioxolane. 5 mg/l suspensions of $TiO_2$ underwent flash

photolysis ($\lambda_{ex}$ = 355 nm) in a variety of time scales with transient decays observed at 330 nm. This is necessary since $TiO_2$ itself shows transient signals after excitation at 355 nm. We also had interest in the kinetic decay of the $TiO_2$ transients, and how they compare to prior kinetic studies of $TiO_2$. Overall, transient signals below ~500 nm are primarily related to optical changes in the $TiO_2$ due to the presence of trapped photogenerated holes. This can include trapped holes in lattice deformations, or interactions on the surface. The peak of this signal is dependent on the conditions of the environment, as well as the nature of the trapped hole interaction being observed.[12-13] Transient signals in the UV range have been attributed to charge transfer interactions between photogenerated holes and $OH^-$ ions in water based solutions.[12] There is a possibility that similar charge transfer interactions can occur with generated 1,3-dioxolane radicals on the surface of $TiO_2$. The time scales up to 1 ms show decays that can be individually fit with the 2$^{nd}$ order decays expected for the recombination of excited electrons and holes. (Figure 4.2.1) However, the rate constants for these decays decrease with increasing time scale indicating that the overall kinetic behaviour is not simply 2$^{nd}$ order. Also, the excitation intensity dependence expected for a 2$^{nd}$ order relationship is not observed, further showing that it is an unsuitable model to describe $TiO_2$ suspensions. (See SI, Figure 4.3.1)

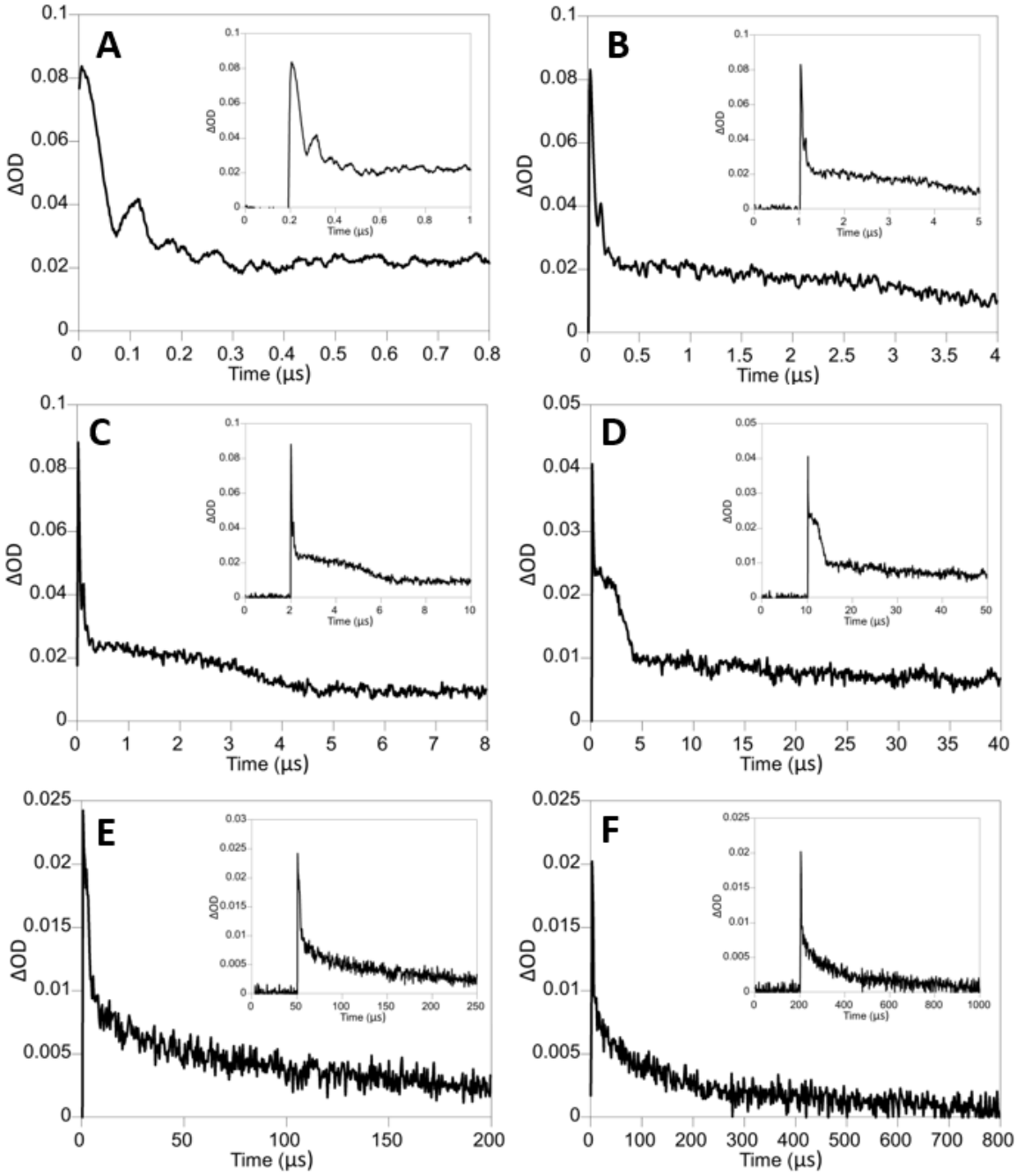


**Figure 4.2.1.** Time shifted (to eliminate pre-trigger data) transient absorbance decays ($\lambda_{ex}$ = 355 nm) at 330 nm for 5 mg/L $TiO_2$ in 1,3-Dioxolane, with corresponding unaltered decays (inset), at a) 1 μs time scale b) 5 μs time scale c) 10 μs time scale d) 50 μs time scale e) 250 μs time scale f) 1 ms time scale.

To further explore the overall kinetics of this transient decay, all time scales monitored were combined into one overall transient absorbance decay. All decays agree well in their

overlapping regions, (Figure 4.2.2) and thus redundant data was removed to allow for connecting them into a combined data set. Since earlier time scales are more accurate for a given time point, time points present in prior time scales were removed and subsequently combined as shown above for a continuous data set. (Figure 4.2.3(A)) Logarithmic scaling was applied to each axis to better represent the scope of the entire data set. Each section of data cleanly connects with the next showing a trend that appears almost linear in the double logarithmic plot. However, it should be noted that data before 0.2 µs contained an oscillating pattern that is most likely attributed to the electronic noise of our laser flash photolysis system. This oscillation is more noticeable due to the relatively low strength of the overall signal. There is also an unusual but reproducible hump in the data around 2 µs that may be related to an effect from the heterogeneous nature of the mixture, perhaps due to a localized heating of the particles. Such observed repetitive oscillating pattern ( at ~ 0.2 us) and hump (at 2 us) is unlikely to be typical noise from the lamp intensity variations or lamp power supply.

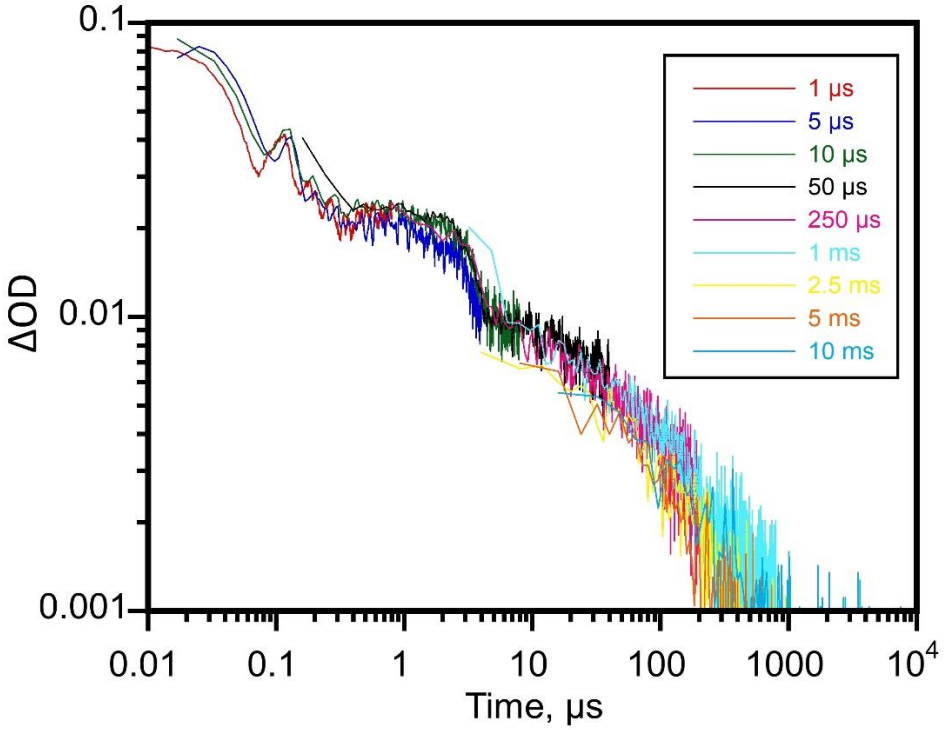


**Figure 4.2.2.** Transient absorbance decays ($\lambda_{ex}$ = 355 nm) at 330 nm for 5 mg/l $TiO_2$ in 1,3-Dioxolane with various time scales overlayed. Logarithmic scaling was done in both axis to better show the full range of the data, and it showed strong overlap in all regions of the decay can be observed. The lower y-axis limit was set to 0.001 due to inconsistent detection for absorbances below this value.

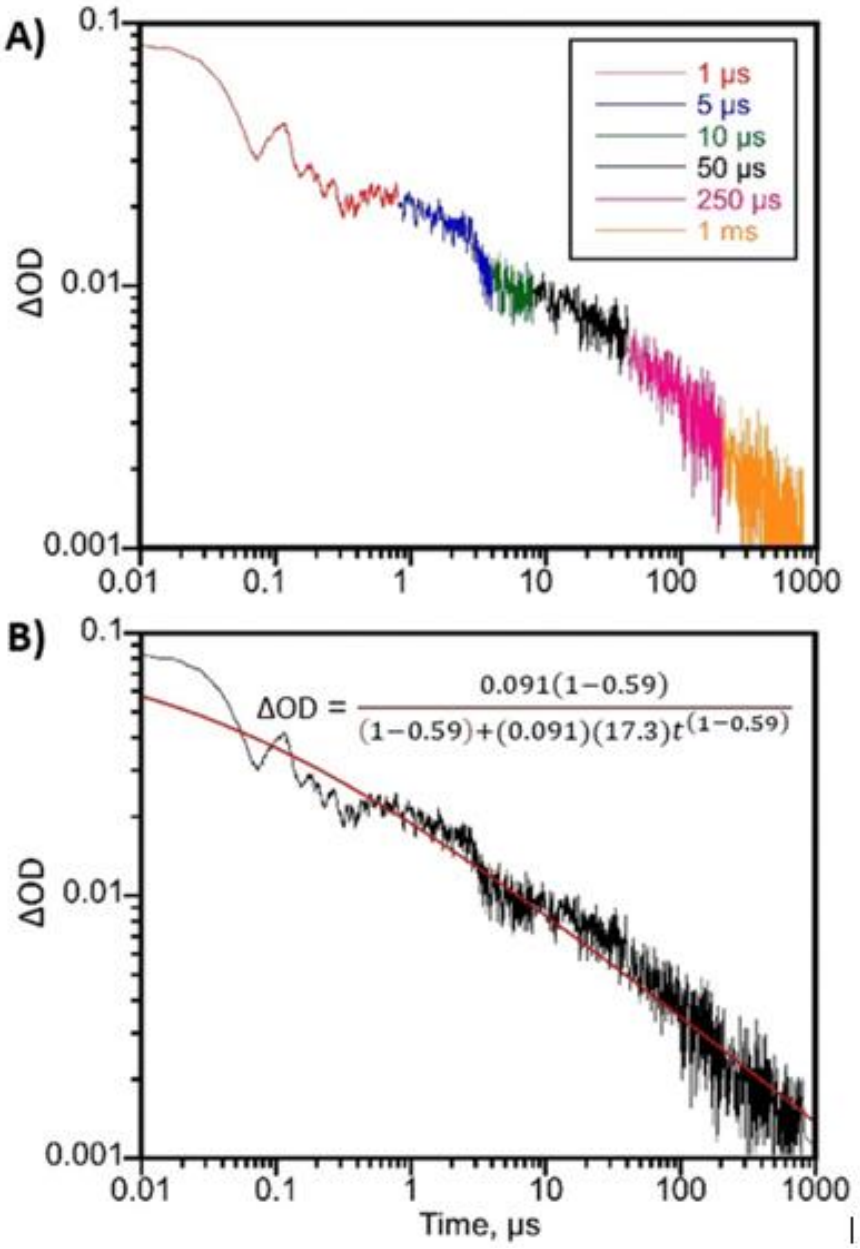


**Figure 4.2.3. (A)** Combined transient absorbance decay monitored at 330 nm for 5 mg/l $TiO_2$ in 1,3-Dioxolane, showing each time scale ($\lambda_{ex}$ = 355 nm). Time scales are constricted to start after the previous time scale. **(B)** Combined transient absorbance decay with a fractal kinetics fitting (see equation 4).

The transient absorbance spectra of the solution from 300-700 nm was also obtained, and showed no clear spectral shape other than a slight upward trend with increasing wavelength (Figure 4.2.4). Signals lower than ~500 nm can be primarily attributed to optical changes in the $TiO_2$ from the presence of trapped (including interactions with

media or solvent) photogenerated holes. The longer wavelengths may be due to signals from trapped excited electrons, which may be slightly longer lived in comparison to the excited holes. This is especially true when considering the reactions between the excited hole of $TiO_2$ with the solvent. Overall, the transient absorbance decay is relatively consistent over the whole spectral range, and can be observed to be similar at 580 nm. (See SI, Figure 4.3.2)

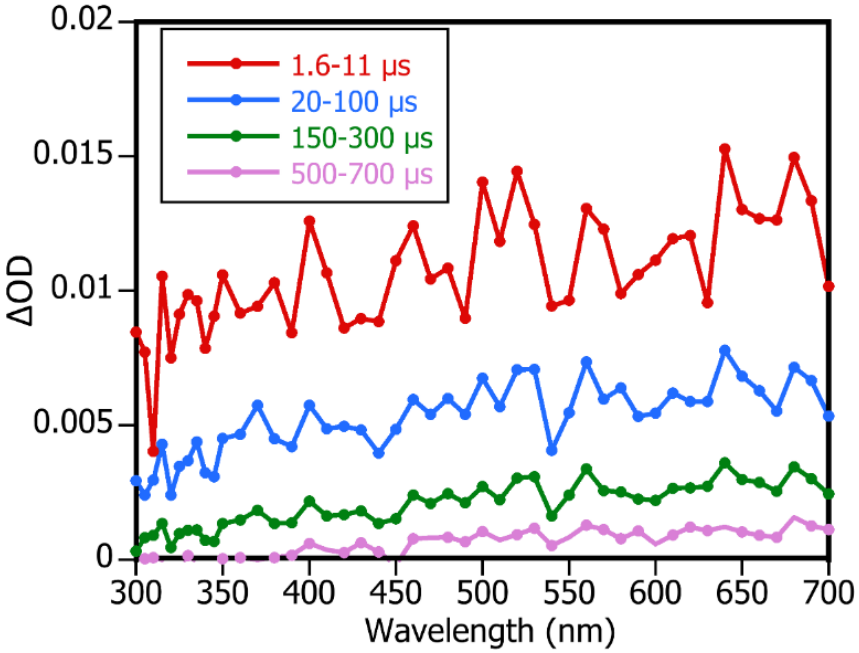


**Figure 4.2.4.** Transient absorbance spectra of 5 mg/l $TiO_2$ in 1,3-Dioxolane ($\lambda_{ex}$ = 355 nm) at various averaged ranges. There is little shape to the spectra, with only a slightly slopping down to the left, and the signal decreases at a similar rate over the whole spectrum down to almost zero by the 500-700 nm range.

The observation of stretched exponentials, sometimes treated as dispersive kinetics is common for bimolecular processes in rigid environments.[24-25] From the perspective of photogenerated radicals on $TiO_2$, a previous report by Sieland *et. al.*[26] has shown the use of fractal kinetics to explain the kinetic behaviour of charge carrier recombination in $TiO_2$.

$$\Delta OD = \frac{A(1-h)}{(1-h)+Akt^{(1-h)}} \qquad (4)$$

**Scheme 4.2.2.** ΔOD represented by fractal kinetics in LFP.

This model accounts for the added complexity introduced by the constrained geometry in the surface of agglomerated particles. The second order rate constant is multiplied by $t^{-h}$, yielding a modified 2nd order rate equation with a new variable *h* ($0 \leq h \leq 1$). "h" describes the fractal scale of the system, with 0 giving normal 2nd order kinetics, and values greater than 0 having more fractal behaviour. While this model was used to describe transient decay from diffuse reflectance laser flash photolysis of $TiO_2$ powder surfaces, it should also be applicable for $TiO_2$ powder suspensions due to agglomeration of particles in solution and variations in particle surface morphology. The use of this fractal model can be observed above. (Figure 4.2.3(B)) The model fits the data set well with an $R^2$ of 0.9113 for decays covering six orders of magnitude in timescale, and has an *h* equal to 0.59, representing a strongly fractal system. While described as a modified second order kinetics, the large fractal value indicates that second order is a very poor model for the observed dynamics. Increasing concentrations of $TiO_2$ were also tested (Fig. 4.2.5), and showed a change in behaviour of the transient decay. Firstly, the transient feature at 2 µs increases in intensity, thus confirming that it is an effect from the heterogenous mixture as it correlates with increasing concentration of $TiO_2$. Additionally, the shape of the decay changes, becoming less representable by a fractal model, especially at 20 mg/L. The dynamics are still changing over the course of the entire time range in a fractal-like way; however, in a more complex fashion as the model fails to fully represent the dataset. Enhanced light scattering, a decrease of monitoring light intensity and some change in the recombination kinetics in $TiO_2$ may account for these changes. It is clear from these results that minimizing the concentration of $TiO_2$ to 5 mg/L allows for decays better represented by the fractal model. The longer lived charge carrier transients caused from the higher $TiO_2$ concentration may also interfere with the observation of transient signals coming from DPE-solvent adducts.

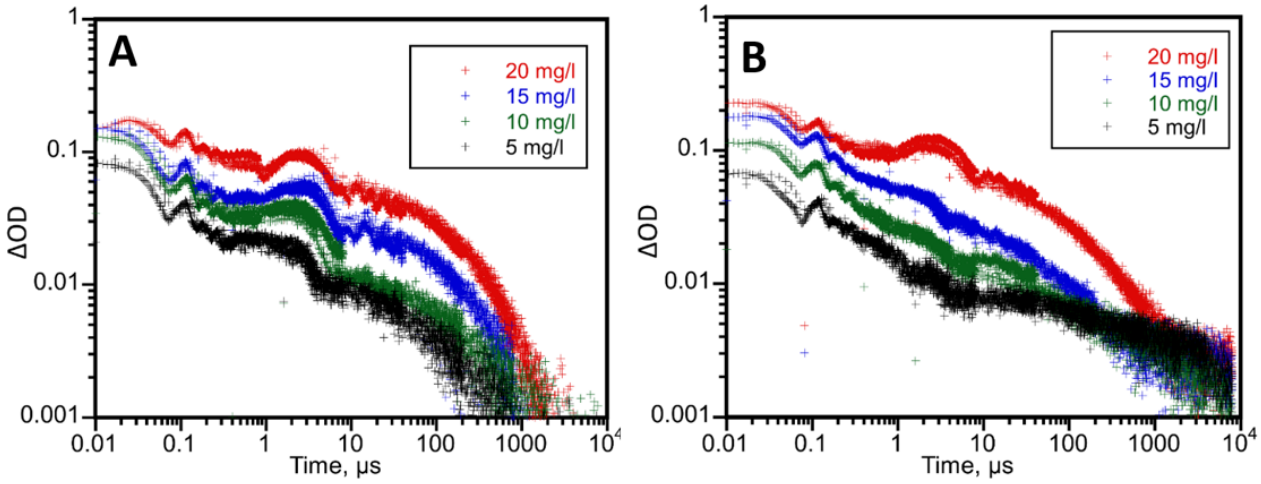


**Figure 4.2.5.** Combined transient absorbance decays ($\lambda_{ex}$ = 355 nm) at 330 nm of 1,3-Dioxolane with various concentrations of $TiO_2$ **(A)** without any DPE, **(B)** and with 50 mM DPE. Changing $TiO_2$ concentration has a strong effect on both the initial strength of the transient signal, as well as the overall shape of the decay. Interestingly, there is little effect on the amount of the DPE-solvent adduct transient signal, and increase $TiO_2$ concentration appears to mask the signal from the adduct radical.

Since the dynamics of the $TiO_2$ suspension alone in 1,3-dioxolane have been evaluated, this system has been then employed to explore and gain insight into the solvent-radical chemistry. A solution of 50 mM DPE with 5 mg/l $TiO_2$ in 1,3-dioxolane was evaluated with the same laser flash photolysis measurements, and compared to the results without DPE. A significant change can be noticed with the addition of DPE as depicted in Figure 4.2.6. The transient decay appears to be similar up to around 10 μs, before diverging with a quite different pattern. The sample containing DPE is much longer lived at longer time scales, and appears to show a residual transient signal with different kinetics from the background $TiO_2$ transient signal. The transient absorbance spectra of the DPE-containing sample, averaged over 500-700 μs, shows a clear peak at 330 nm. (Fig. 4.2.7) This peak is characteristic of a benzylic radical,[23, 27-28] such as the one expected to form from 1,3-dioxolane radicals reacting with DPE (Scheme 4.2.1). There is no significant change in the decay elsewhere in the spectra, including when observing different time scales (See SI, Figure 4.3.3).

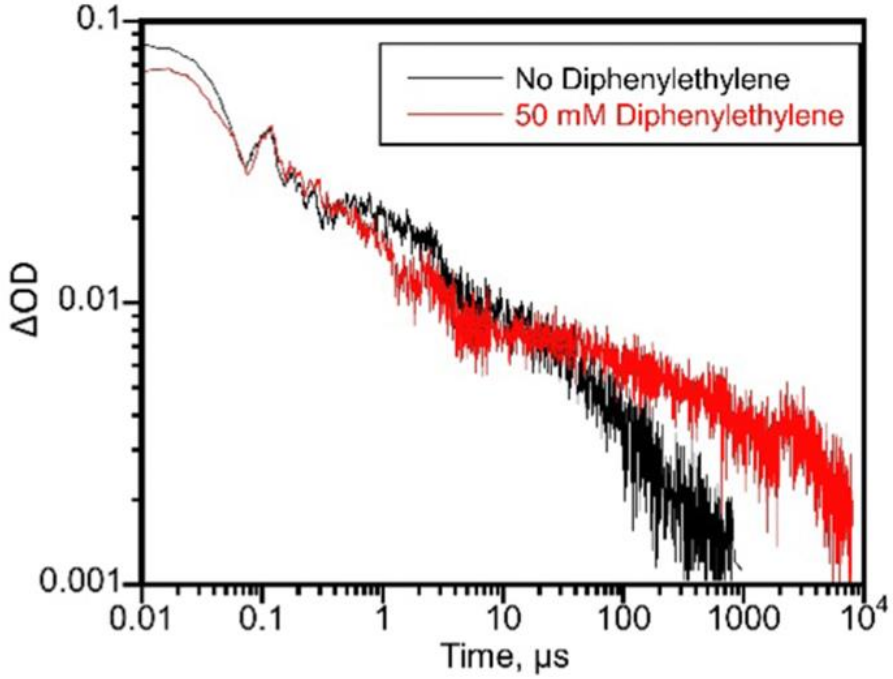


**Figure 4.2.6.** Combined transient absorbance decays at 330 nm with and without DPE in 1,3-Dioxolane with 5 mg/l $TiO_2$ ($\lambda_{ex}$ = 355 nm) over full time range.

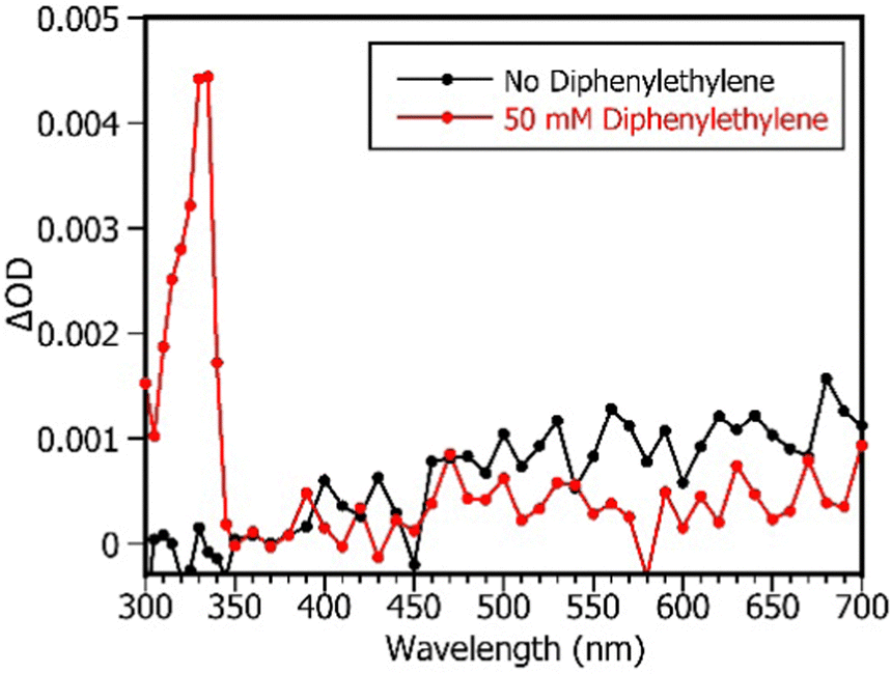


**Figure 4.2.7.** Transient absorption spectra observed at 500-700 μs (averaged) for samples of 5 mg/l $TiO_2$ in 1,3-Dioxolane, with and without DPE, under 355 nm laser excitation.

The increased lifetime of the signal at 330 nm can be entirely attributed to the signal from DPE-solvent adduct. Increasing the amount of $TiO_2$ does not significantly change the residual transient signal from the benzylic radical; however, the increasing background signal of the $TiO_2$ begins to mask the benzylic signal. (Figure 4.2.5) This confirms that maintaining a $TiO_2$ concentration of 5 mg/L is beneficial for observations of other signals in this range. Conversely, altering the concentration of DPE had little effect on the transient absorbance decay. Concentrations between 14 and 140 mM for DPE all gave similar results implying that the formation of this benzylic radical transient is constrained by the amount of solvent radicals formed from the hole of $TiO_2$ after the laser pulse (Scheme 4.2.1 and Figure 4.2.8). This is confirmed through laser intensity experiments where the amplitude of the DPE-solvent adduct signal is proportional to the intensity of the laser pulse. (Figure 4.2.9(A)) However, very low concentrations of DPE can show a reduction of the DPE-solvent adduct formed and thus constrained by the concentration of DPE. (Figure 4.2.9(B)) Here, it is important to highlight that without $TiO_2$, no signal from the benzylic radical was detected. (See SI, Figure 4.3.4) Therefore, it confirms that $TiO_2$ is necessary for the reaction as proposed in Scheme 4.2.1. This also rules out the possibility of the observed signal at 330 nm being from benzophenone, a common impurity in DPE, and known for also giving rise to a strong signal at 330 nm (See SI, Figure 4.3.5). This is to be expected, as the DPE was purified, and further tested with GC-MS, and no trace of benzophenone was detected. Had there been a small amount of benzophenone, a significant 330 nm signal should have been observed in Figure 4.2.9.

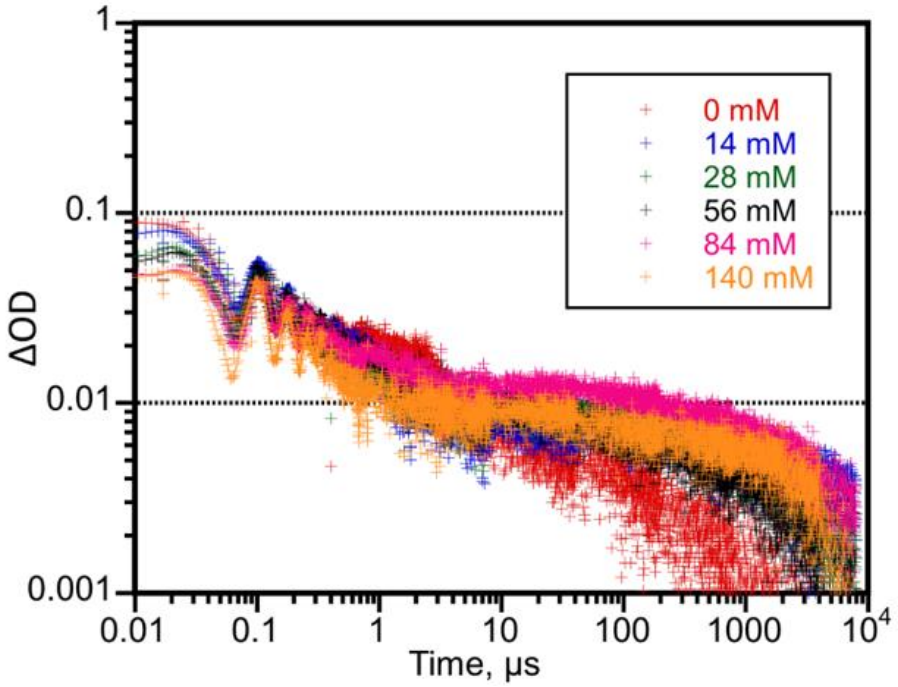


**Figure 4.2.8.** Combined transient absorbance decays ($\lambda_{ex}$ = 355 nm) at 330 nm of 1,3-Dioxolane with 5 mg/l $TiO_2$ and various concentrations of DPE.

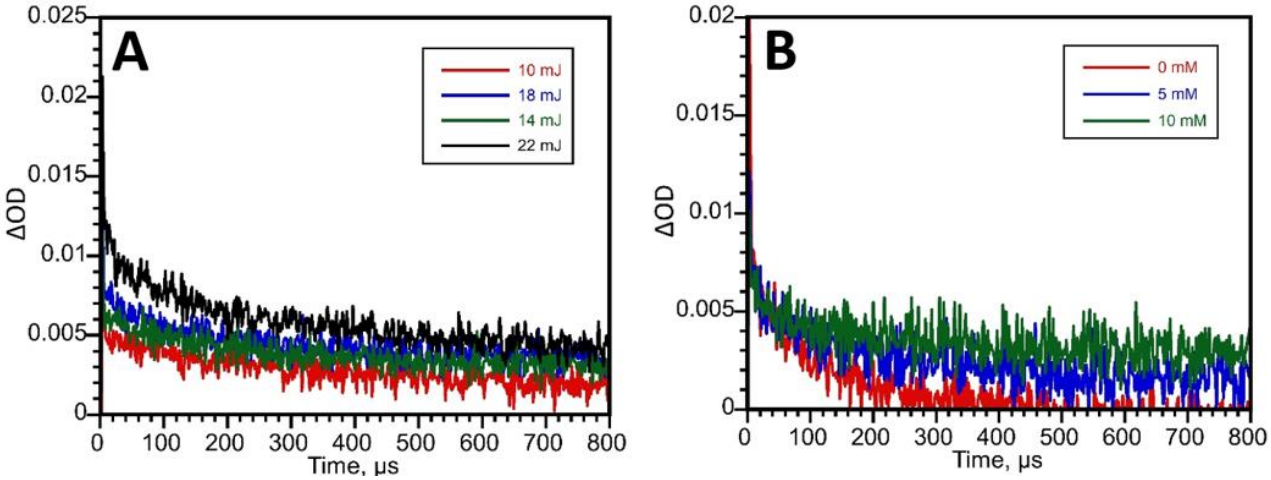


**Figure 4.2.9.** 1 ms time scale transient absorbance decays ($\lambda_{ex}$ = 355 nm) at 330 nm of 1,3-Dioxolane with 5 mg/l $TiO_2$ with **(A)** 50 mM DPE with various laser-excitation powers, and **(B)** various low concentrations of DPE.

The signal contribution from the DPE-Solvent adduct can be extracted from the full data set showing the formation and decay of it (Figure 4.2.10). However, attempts to evaluate

the kinetics of formation and decay of the DPE-Solvent adduct were not possible due to an inadequate signal to noise ratio.

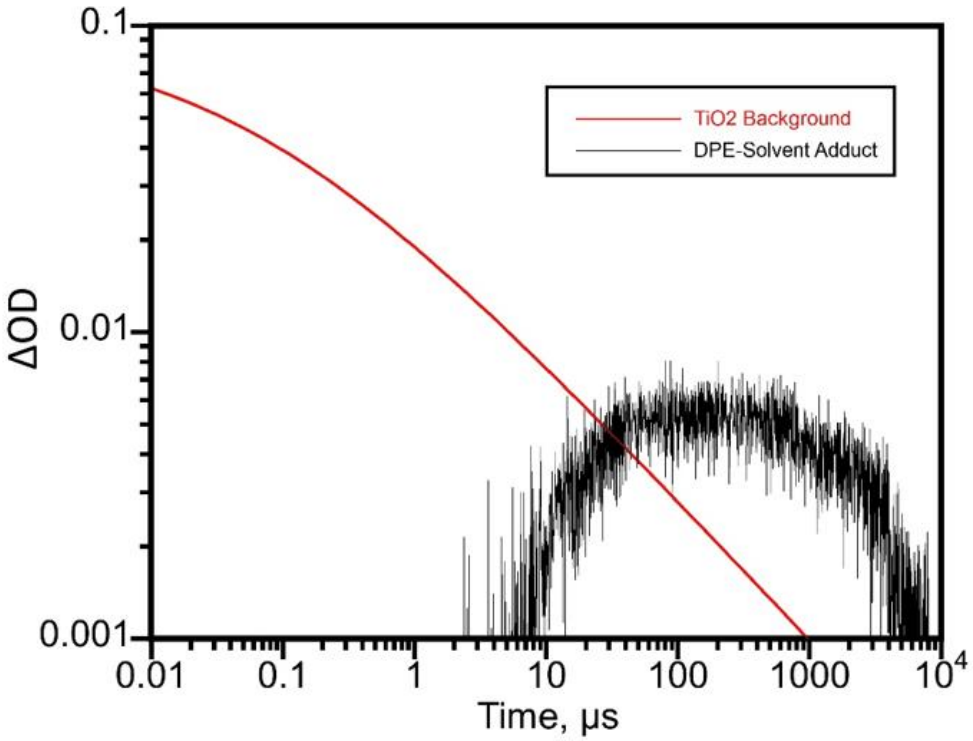


**Figure 4.2.10.** Separated contributions from $TiO_2$ and DPE-Solvent adducted from the Combined transient absorbance decay ($\lambda_{ex}$ = 355 nm) at 330 nm for 1,3-Dioxolane with 5 mg/l $TiO_2$ and 50 mM DPE. The fitting for the $TiO_2$ decay was used as the background to obtain slightly less noise, this approximation should be noted. However, a clear growth and decay of the DPE-Solvent adduct is observed. However, the signal to noise ratio makes evaluation of the rate of formation between different concentrations impossible.

To confirm that the formation of this benzylic radical transient directly involves the solvent, solvents with differing reactivity with the excited hole of $TiO_2$ were tested. Firstly, acetonitrile was used as a relatively inert solvent, as it is expected to have very limited reactivity with the electrophilic hole of $TiO_2$.[22] Acetonitrile is known to rapidly trap photogenerated electrons in solution,[29] which could lead to a longer lived hole in the valence band. However, given the limited reactivity of acetonitrile with this hole, its effect is expected to be minor. As expected, 5 mg/l suspensions of $TiO_2$ in acetonitrile had no significant difference in their combined transient absorbance decays at 330 nm, with and without DPE.

1,4-dioxane was also tested as a solvent with more intermediate expected reactivity with the hole of $TiO_2$. (See SI, Figure 4.3.6) 1,4-Dioxane is expected to have lower activity for hydrogen abstraction for the formation of radicals due to differing stereoelectronics as seen in prior studies involving reactivity with tert-butoxyl radicals, as well as with excited $TiO_2$.[22, 30] The transient absorption spectra averaged from 500-700 µs for all 3 solvents are shown in Figure 4.2.11. This clearly shows no signal peak for the benzylic radical in acetonitrile, a weak peak in 1,4-dioxane, and the strong transient peak when in 1,3-dioxolane. This shows a strong dependence on the solvent for this signal, and indicates that the solvent is directly involved in the reaction. This supports that the likely reaction occurring is a solvent radical formation from a reaction with the hole of $TiO_2$, followed by solvent radicals reacting with the double-bond of DPE to form a DPE-solvent adduct with a benzylic radical. This was also further supported through detection by GC-MS of the two expected final products of the DPE-Solvent adduct after a 1 week upscaled reaction in a photoreactor with 12 UVA bulbs (See SI, Figure 4.3.7). Yields of these products are too low for further evaluation with NMR.

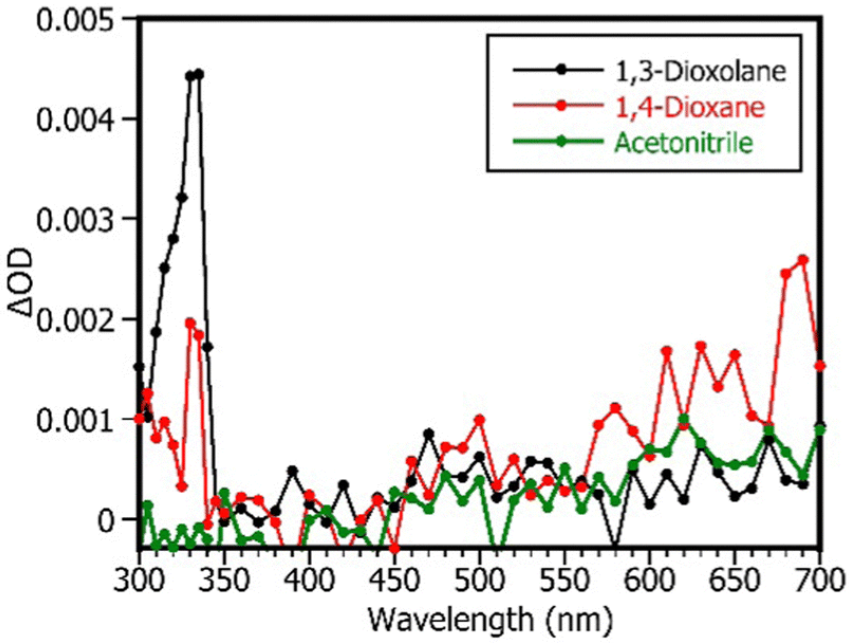


**Figure 4.2.11.** Transient absorption spectra observed at 500-700 µs (averaged) for samples containing 50 mM DPE and 5 mg/l $TiO_2$ in various solvents under 355 nm laser excitation.

The signal from DPE is strong and characteristic, allowing kinetic analysis over an exceptionally wide range of timescales. The remarkably long 'stretched' decays can be rationalized by using a fractal model. For the first time we detect transient signals in the 330 nm region (>300 nm) where normally the interference by the strong absorption of $TiO_2$ prevents accurate measurements. We show that proper experimental design makes this spectral UV region accessible, opening the door to other studies, particularly in the field of catalysis. The use of other favourable reactions for the formation of radicals from $TiO_2$ – rather than solvent generated radicals– should allow for much stronger transient signals to compete with the background transient from $TiO_2$, allowing for proper evaluation of kinetics of the formed radicals. Such studies are planned for the future, using the LFP strategies developed and shared in this contribution.

## 4.3 Post-print Version of Supporting Information

**Materials and Instrumentation**

All reagents used were purchased from Sigma Aldrich and used as received, with the exception of 97% 1,1-diphenylethylene. 1,1-diphenylethylene was purified using a Silica column with pentane as the mobile phase to allow for removal of all traces of benzophenone. $TiO_2$ P25 was purchased from Univar Canada.

All laser flash photolysis experiments were performed using a Surelite Nd-YAG laser with wavelength of 355 nm (18 mJ $pulse^{-1}$) in a customized LFP-111 laser flash photolysis system (Luzchem Inc., Ottawa, Canada) and 0.7 $cm^2$ x 0.7 $cm^2$ cuvettes from Luzchem. Samples had an absorbance of ~ 0.3 at the laser wavelength, with some variation when selecting for $TiO_2$ concentration.

**Experimental methodology**

*Sample Preparation*

Stock solutions of 0.4 g/l $TiO_2$ P25 were made with each of the 3 solvents (1,3-dioxolane, acetonitrile, and 1,4-dioxane), with 20 min sonication so suspend the mixture (repeated before each use). Typical sample preparation involved the addition 25 µL of 0.4 g/L $TiO_2$ suspension diluted to 2 ml with additional solvent, for a final $TiO_2$ concentration of 5 mg/L inside 0.7 cm x 0.7 cm cuvettes with stir rods. Samples were purged with argon for 10 min, and sonicated for 10 min to insure consistent suspension of the $TiO_2$. 1,1-diphenylethylene (DPE) was added via syringe between LFP experiments to allow direct comparison between the same sample with and without DPE.

*Laser flash photolysis*

Sample cuvettes were placed in a temperature controlled holder at 25$^oC$ with stirring. Samples were also lightly shaken beforehand to insure suspension. Transient absorbance decays were collected at 330 nm and 580 nm at various time scales (1 µs – 10 ms), time scale referring to the maximum time measured in the decay. The resolution was 625 evenly separated points per decay, with the first 20% (first 2 divisions) being pre-trigger before the laser pulse. Decays were averaged in the software from 10 shots. Transient absorption spectra were taken using decays in the 1 ms time scale, with absorbances averaged over time-ranges in the decays.

*Data Analysis*

For each transient absorbance decay, the first 20% was removed and the rest shifted to start at zero to align with the laser pulse timing. The unaltered graphs can be observed in the insets (Figure 4.2.1), alongside the shifted decay curves. If each decay was plotted together in a double logarithmic scale, they showed strong overlap. To obtain a continuous set of data over the entire range of analysis, data points present in prior timescales were removed in subsequent timescales. This allowed for each time-scale to give data in the ranges that they are most accurate in measuring, and have a continuous connected data-set that could be easily plotted (See figure 4.2.5(A)).

## 2nd Order Analysis

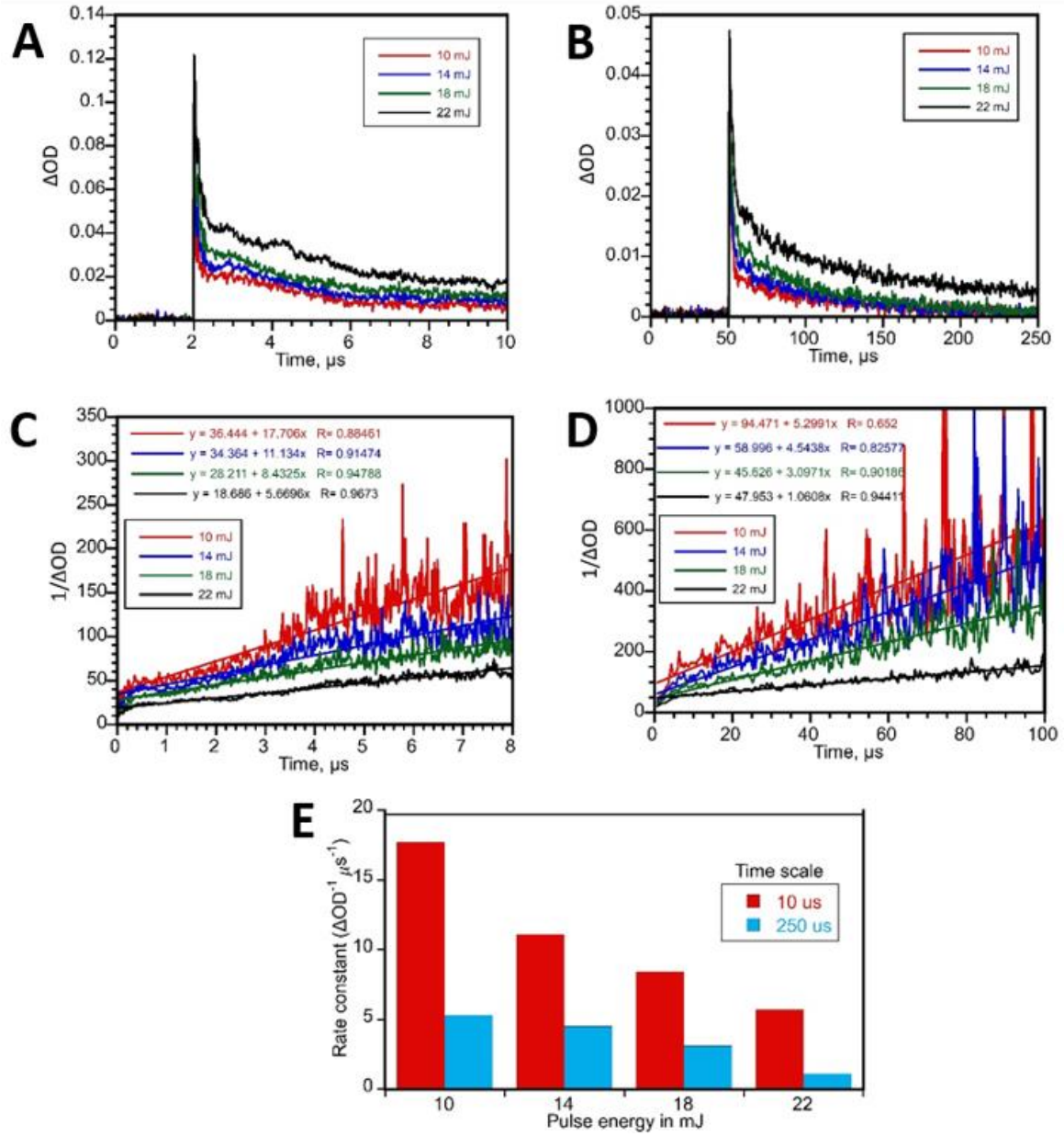


**Figure 4.3.1.** Transient absorbance decays ($\lambda_{ex}$ = 355 nm) at 330 nm for 5 mg/L $TiO_2$ in 1,3-Dioxolane, with various laser excitation intensities for a) 10 μs time scale, b) 250 μs time scale, c,d) the respective reciprocal plots for 2nd order analysis, and e) a comparison of the calculated 2nd order rate constants.

While the kinetics are not strictly 2nd order, within a single time scale you can reasonably fit a 2nd order trend. However, at higher time scales the found 2nd order rate constant becomes

much smaller. Also, changing the pulse energy of the laser leads to a trend that does not fit expectations for a 2nd order relationship. The rate constant should not decrease with increasing pulse energy as observed. Overall this shows that 2nd order is not adequate in describing the transient absorbance decay of $TiO_2$ suspensions.

## Additional LFP Data

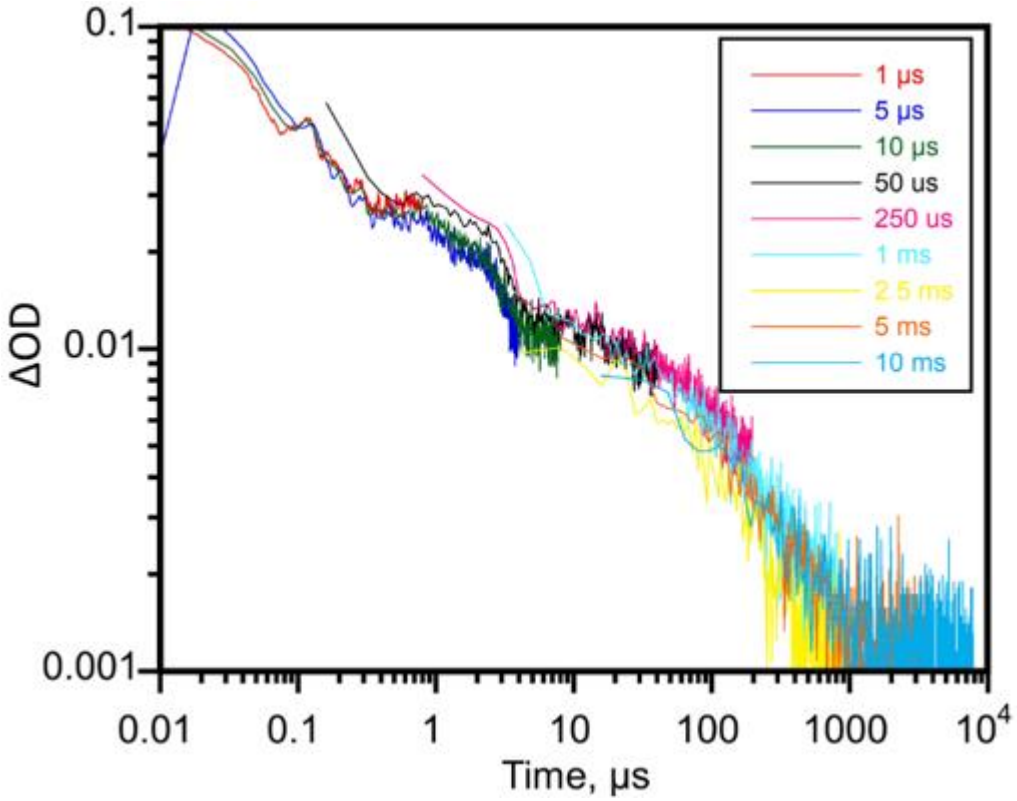


**Figure 4.3.2.** Transient absorbance decays ($\lambda_{ex}$ = 355 nm) at 580 nm for 5 mg/l $TiO_2$ in 1,3-Dioxolane with various time scales overlayed. Similarly to Figure 4.2.2, a logarithmic scaling was used, and strong overlap is present over the entire range. Relatively similar decay in comparison to decay at 330 nm, with a marginal enhancement at very long time-scales.

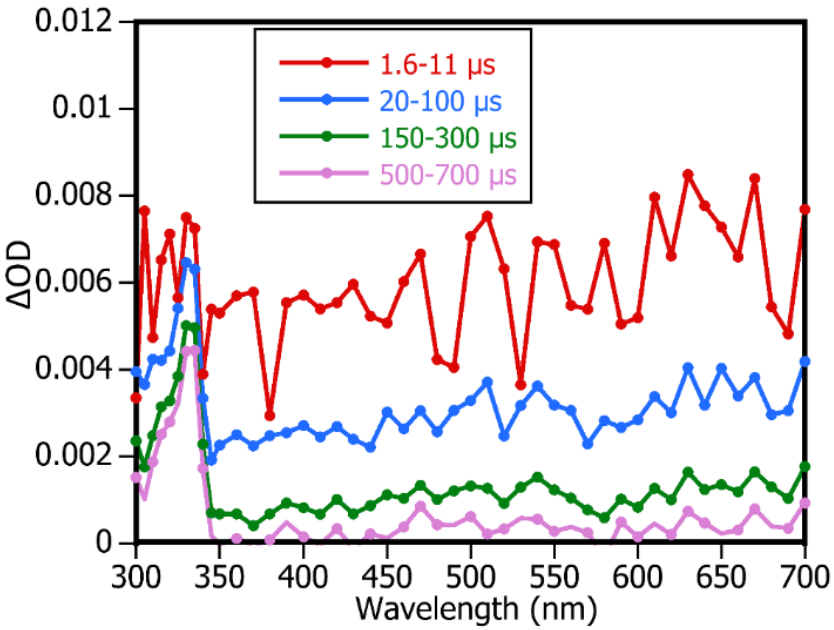


**Figure 4.3.3.** Transient absorbance spectra of 50 mM DPE and 5 mg/l $TiO_2$ in 1,3-Dioxolane ($\lambda_{ex}$ = 355 nm) at various averaged time ranges. The signal from the DPE-solvent adduct transient is mostly covered by the signal from the $TiO_2$ at 1.6-11 µs, before being quite obvious at longer time scales. At 500-700 µs, the peak from the adduct radical is the only significant signal remaining.

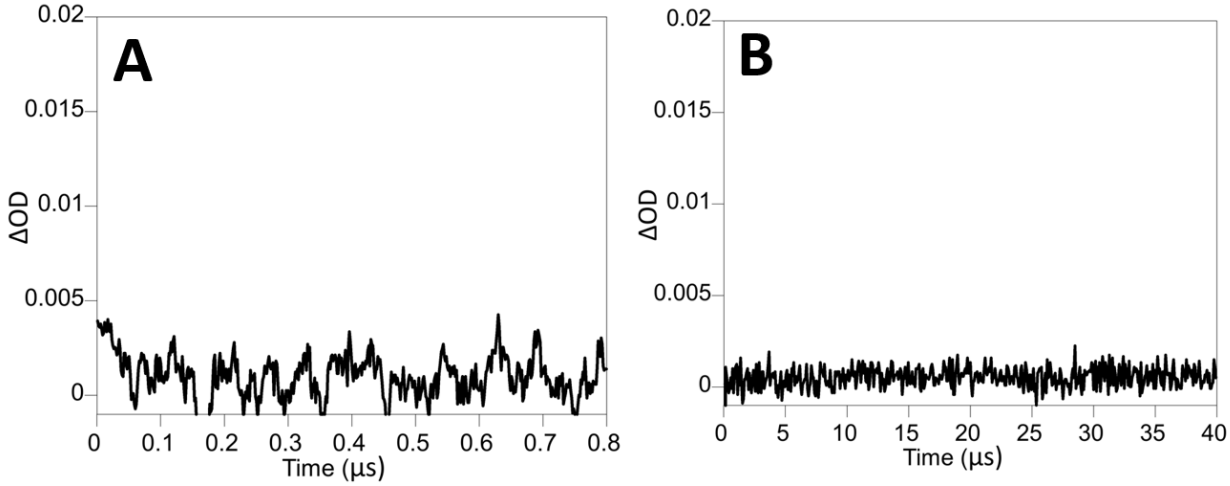


**Figure 4.3.4.** Transient absorbance decays ($\lambda_{ex}$ = 355 nm) at 330 nm of 1,3-Dioxolane with no $TiO_2$ and 50 mM DPE at a) 1 µs time scale and b) 50 µs time scale. There is no significant signal without $TiO_2$, as the signal is oscillating above and below zero. Therefore DPE along will not give detectable transients without $TiO_2$.

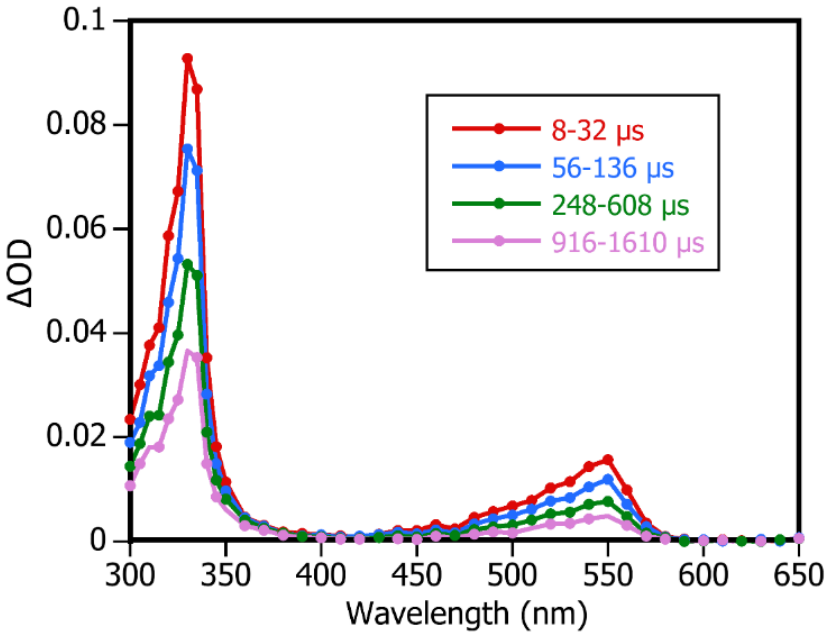


**Figure 4.3.5.** Transient absorbance spectra of 5 mM benzophenone in 1,3-Dioxolane ($\lambda_{ex}$ = 355 nm) at various averaged time ranges. The spectra of the benzophenone radical transient is similar to that of the DPE-solvent adduct; however, with a more noticeable peak at 550 nm.

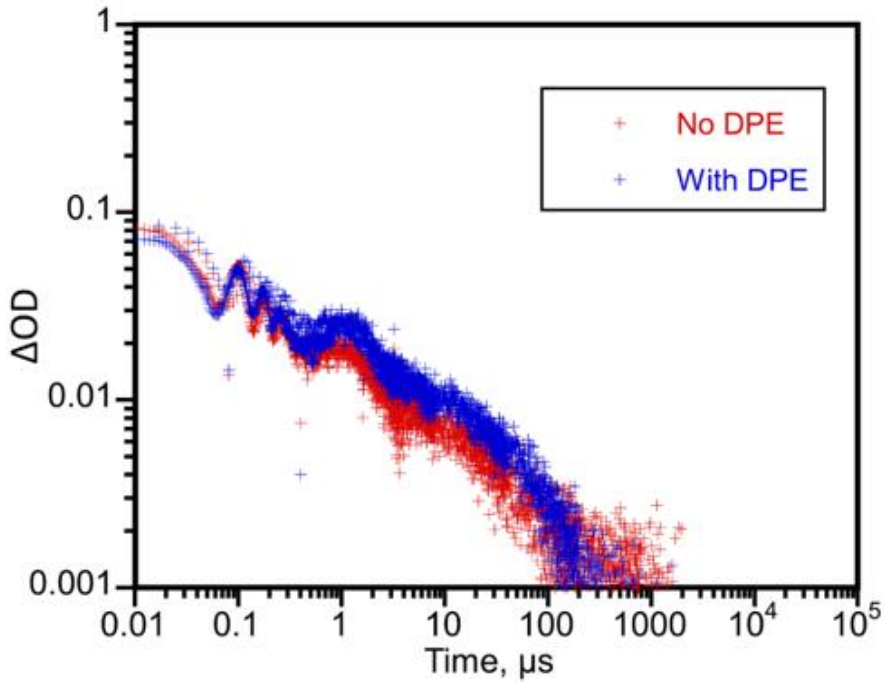


**Figure 4.3.6.** Combined transient absorbance decays ($\lambda_{ex}$ = 355 nm) at 330 nm for acetonitrile with 5 mg/l $TiO_2$, with and without DPE. The decay without DPE is similar to the decay using 1,3-dioxolane as a solvent, but slightly faster in comparison. There is no noticeable difference in decay rate with and without DPE, implying no significant formation of transients from a DPE-solvent adduct transient.

**Detection of Final Product by GC-MS**

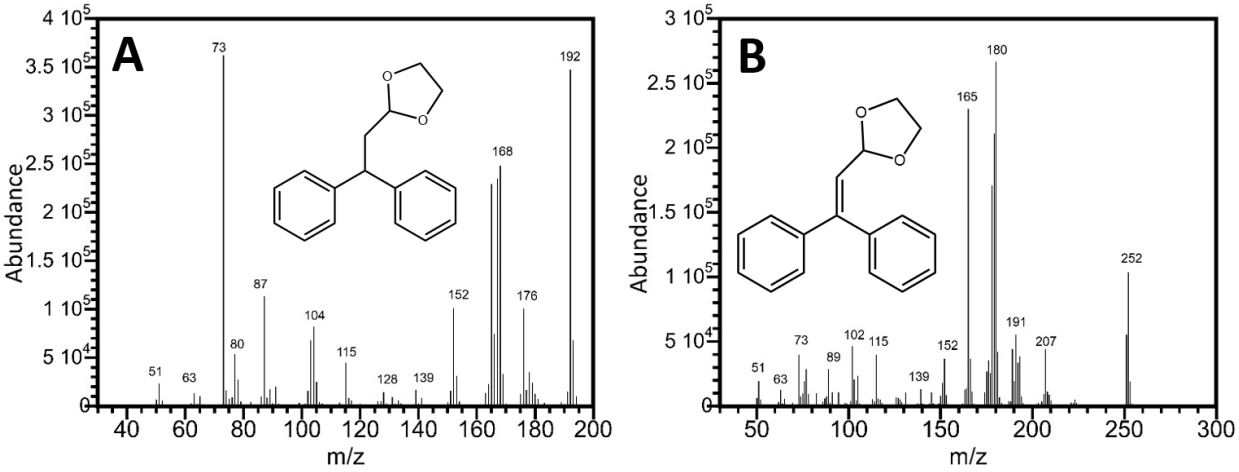


**Figure 4.3.7.** Mass Spectrometry fragmentation patterns (GC-MS) for the two expected final products from the DPE-Solvent Adduct Radical. The two products depend on if the radical **(B)** gains a hydrogen to form a double bond, or **(A)** loses another hydrogen to form a single bond. Due to raising acidity in the system, the single bond is expected to be favored.

## 4.4 Accompaniment to Chapter 4

The work presented in this chapter acted as a good expansion of the research presented in chapter 3. It showed an alternative method to evaluate the chemistry of solvent radicals, and the resulting reactions that they undergo. Interestingly, this research found that 1,3-dioxolane radicals were able to be formed and react with diphenylethylene in solution. This was contrary to what was found when evaluating with TEMPO, implying the limitations of simply using TEMPO to test for radical reactivity. TEMPO is useful to show that radicals are formed, but cannot necessarily prove the opposite (that radicals are not being formed).

I hope that this method can be further improved to allow full kinetic evaluation of radical product formation and decay; however, the research presented here still acts as an impressive first step in the laser flash photolysis of heterogeneous suspensions.

## 4.5 References


1. Fox, M. A.; Dulay, M. T., Heterogeneous photocatalysis. *Chem. Rev.* **1993,** *93* (1), 341-357.
2. Schneider, J.; Matsuoka, M.; Takeuchi, M.; Zhang, J.; Horiuchi, Y.; Anpo, M.; Bahnemann, D. W., Understanding $TiO_2$ photocatalysis: mechanisms and materials. *Chem. Rev.* **2014,** *114* (19), 9919-9986.
3. Schneider, J.; Bahnemann, D., Strong transient absorption of trapped holes in anatase and rutile $TiO_2$ at high laser intensities. *J. Phys.Chem., C* **2018,** *122* (25), 13979-13985.
4. Wilkinson, F.; Willsher, C. J.; Uhl, S.; Honnen, W.; Oelkrug, D., Optical detection of a photoinduced thermal transient in titanium dioxide powder by diffuse reflectance laser flash photolysis. *J. Photochem.* **1986,** *33* (3), 273-8.
5. Kamat, P. V.; Gopidas, K. R.; Weir, D., Photoelectrochemistry in particulate systems. Photosensitized charge injection into opaque titanium dioxide semiconductor powder as probed by time-resolved diffuse reflectance laser flash photolysis. *Chem. Phys. Lett.* **1988,** *149* (5-6), 491-6.
6. Tamaki, Y.; Furube, A.; Murai, M.; Hara, K.; Katoh, R.; Tachiya, M., Direct observation of reactive trapped holes in $TiO_2$ undergoing photocatalytic oxidation of adsorbed alcohols: Evaluation of the reaction rates and yields. *J. Am. Chem. Soc.* **2006,** *128* (2), 416-417.
7. Kim, W.; Tachikawa, T.; Kim, H.; Lakshminarasimhan, N.; Murugan, P.; Park, H.; Majima, T.; Choi, W., Visible light photocatalytic activities of nitrogen and platinum-doped $TiO_2$: Synergistic effects of co-dopants. *Appl. Catal., B* **2014,** *147*, 642-650.
8. Fabian, S.; Jenny, S.; Thorsten, L.; Detlef, W. B. In *Understanding charge transfer processes on metal oxides: a laser-flash-photolysis study*, Proc.SPIE, 2016.
9. Hainer, A. S.; Hodgins, J. S.; Sandre, V.; Vallieres, M.; Lanterna, A. E.; Scaiano, J. C., Photocatalytic hydrogen generation using metal-decorated $TiO_2$: Sacrificial donors vs true water splitting. *ACS Energy Lett.* **2018,** *3*, 542-545.
10. Nie, J.; Patrocinio, A. O. T.; Hamid, S.; Sieland, F.; Sann, J.; Xia, S.; Bahnemann, D. W.; Schneider, J., New insights into the plasmonic enhancement for photocatalytic $H_2$ production by Cu-$TiO_2$ upon visible light illumination. *Phys. Chem. Chem. Phys.* **2018,** *20* (7), 5264-5273.
11. Nie, J.; Schneider, J.; Sieland, F.; Xia, S.; Bahnemann, D. W., The role of Au loading for visible-light photocatalytic activity of Au-$TiO_2$ (anatase). *J. Photochem. Photobiol., A* **2018,** *366*, 111-117.
12. Yoshihara, T.; Tamaki, Y.; Furube, A.; Murai, M.; Hara, K.; Katoh, R., Effect of pH on absorption spectra of photogenerated holes in nanocrystalline $TiO_2$ films. *Chem. Phys. Lett.* **2007,** *438* (4-6), 268-273.
13. Bahnemann, D.; Henglein, A.; Lilie, J.; Spanhel, L., Flash photolysis observation of the absorption spectra of trapped positive holes and electrons in colloidal titanium dioxide. *J. Phys. Chem.* **1984,** *88* (4), 709-711.
14. Zhou, Z.-X.; Qian, S.-P.; Yao, S.-D.; Zhang, Z.-Y., Photosensitization of a colloidal $TiO_2$ semiconductor system with hypocrellin B. *Dyes Pigm.* **2001,** *51* (2-3), 137-144.
15. Friedmann, D.; Hansing, H.; Bahnemann, D., Primary processes during the photodeposition of Ag clusters on $TiO_2$ nanoparticles. *Z. Phys. Chem. (Muenchen, Ger.)* **2007,** *221* (3), 329-348.
16. Qiu, Y.; Zhao, J.; Hou, H.; Li, T.; Chen, L.; Zhu, Z., Transmission flash photolysis of titanium dioxide photooxidation of pyrogallol. *C. R. Chim.* **2008,** *11* (1-2), 120-124.
17. Bettoni, M.; Del Giacco, T.; Elisei, F.; Rol, C.; Sebastiani, G. V., Evidences in favor of a single electron transfer (SET) mechanism in the $TiO_2$ sensitized photo-oxidation of α-hydroxy- and α,β-dihydroxybenzyl derivatives in water. *Phys. Chem. Chem. Phys.* **2010,** *12* (20), 5425-5430.
18. Ramos, D. D.; Bezerra, P. C. S.; Quina, F. H.; Dantas, R. F.; Casagrande, G. A.; Oliveira, S. C.; Oliveira, M. R. S.; Oliveira, L. C. S.; Ferreira, V. S.; Oliveira, S. L.; Machulek, A., Jr., Synthesis and characterization of $TiO_2$ and $TiO_2$/Ag for use in photodegradation of methylviologen, with kinetic study by laser flash photolysis. *Environ. Sci. Pollut. Res.* **2015,** *22* (2), 774-783.

19. Tojo, S.; Tachikawa, T.; Fujitsuka, M.; Majima, T., Direct observation of one-electron oxidation processes of aromatic sulfides in $TiO_2$ colloidal solution by laser flash photolysis. *Phys. Chem. Chem. Phys.* **2004,** *6* (5), 960-964.
20. Conceicao, D. S.; Ferreira, D. P.; Graca, C. A. L.; Julio, M. F.; Ilharco, L. M.; Velosa, A. C.; Santos, P. F.; Vieira Ferreira, L. F., Photochemical and photocatalytic evaluation of 1D titanate/$TiO_2$ based nanomaterials. *Appl. Surf. Sci.* **2017,** *392*, 418-429.
21. Schneider, J.; Nikitin, K.; Dillert, R.; Bahnemann, D. W., Laser-flash-photolysis-spectroscopy: a nondestructive method. *Faraday Discuss.* **2017,** *197* (Catalysis for Fuels), 505-516.
22. Hainer, A.; Marina, N.; Rincon, S.; Costa, P.; Lanterna, A. E.; Scaiano, J. C., Highly electrophilic titania hole as a versatile and efficient photochemical free radical source. *J. Am. Chem. Soc.* **2019,** *141* (11), 4531-4535.
23. Bromberg, A.; Schmidt, K. H.; Meisel, D., Photochemistry and photophysics of phenylmethyl radicals. *J. Am .Chem. Soc.* **1984,** *106* (10), 3056-3057.
24. Doba, T.; Ingold, K. U.; Siebrand, W.; Wildman, T. A., Structural interpretation of non-exponential hydrogen transfer in glassy methanol. *Chem. Phys. Letters* **1985,** *115*, 51-54.
25. Siebrand, W.; Wildman, T. A., Dispersive kinetics: a structural approach to nonexponential processes in disordered media. *Acc. Chem. Res.* **1986,** *19*, 238-243.
26. Sieland, F.; Schneider, J.; Bahnemann, D. W., Fractal charge carrier kinetics in $TiO_2$. *J. Phys. Chem. C* **2017,** *121* (43), 24282-24291.
27. Bromberg, A.; Schmidt, K. H.; Meisel, D., Photophysics and photochemistry of arylmethyl radicals in liquids. *J. Am .Chem. Soc.* **1985,** *107* (1), 83-91.
28. Scaiano, J. C.; Tanner, M.; Weir, D., Exploratory study of the intermolecular reactivity of excited diphenylmethyl radicals. *J. Am. Chem. Soc.* **1985,** *107* (15), 4396-4403.
29. Anbar, M., The reactions of hydrated electrons with organic compounds. *Adv. Phys. Org. Chem.* **1969,** *7*, 115-151.
30. Malatesta, V.; Scaiano, J. C., Absolute rate constants for the reactions of tert-butoxyls with ethers: the importance of stereolectronic effects. *J. Org. Chem.* **1982,** *47*, 1455-1457.

# 5. Beyond acetylene: Solvent stabilisation of calcium carbide-derived acetylide intermediates for small organic molecule synthesis

This chapter is adapted from a final manuscript currently undergoing submission. Final published version may have small differences.

## 5.1 Preamble to Chapter 5

This chapter evaluates the formation and stabilisation of solubilized calcium carbide-derived intermediates in solution for use in organic synthesis such as the Sonogashira-like formation of symmetrical diarylethynes. This acts as a somewhat different chapter from the overall story of my thesis, as it involves a thermal mechanism rather than photochemical; however, it utilizes the same Pd@$TiO_2$ catalyst discussed in previous chapters. Also, the results I found were quite novel, showing an interesting way to approach calcium carbide chemistry. I also believe this research may still be applicable in photochemical systems, not just thermal, especially after the formation of the initial solubilised intermediate.

This project started with evaluating if calcium carbide could be used as a reagent to react with solvent radicals photo-catalytically formed from M@$TiO_2$ suspensions, similarly to the chemistry shown in chapters 3 and 4. However, preliminary experiments proved to be ineffective, and my research began to shift towards using bromobenzene as a reagent. Pd@$TiO_2$ had been shown in our group to be an effective photocatalyst for the reaction between bromobenzene and phenylacetylene[1], and I was curious if similar chemistry could be done with calcium carbide as the source of acetylene in solution. After testing various approaches to experimental conditions, I found that DMSO was useful as a solvent and gave yields of diphenylacetylene even without added water when thermally catalyzed by Pd@$TiO_2$. This was surprising as most mechanisms for similar systems involved adding water to turn calcium carbide into acetylene prior to reacting with bromobenzene. It eventually became clear that a solubilised intermediate of ethynyl calcium hydroxide was being formed in solution with low amounts of water being present, and acted as an effective reagent to react with bromobenzene in the presence of Pd@$TiO_2$.

## 5.2 Pre-submission Version of Manuscript

This manuscript is currently in the process of submission

**Abstract**

Calcium carbide has been used in the synthesis of organic molecules as a benign source of acetylene. The $CaC_2$ salt reacts with water to produce acetylene *in-situ* providing an excellent and less hazardous method for incorporation of alkyne moieties to organic structures. Using the $CaC_2$ reaction under water-starved conditions we show the reaction with bromobenzene involves a calcium acetylide intermediate, reminiscent of Grignard reaction intermediates, which are stabilised by the solvent. Using this reaction pathway may allow for new chemistry, finer reaction control, and safer chemistry by limiting formation of acetylene gas during the reaction.

**Manuscript**

Calcium carbide has long been used as a convenient precursor for acetylene (Scheme 5.2.1) which can be generated locally in small amounts, thus avoiding the explosion-risk associated with storage of large quantities of acetylene.

$$CaC_2 + H_2O \longrightarrow Ca(OH)_2 + C_2H_2 \qquad (1)$$

**Scheme 5.2.1.** Formation of acetylene gas from calcium carbide using water.

In many cases reaction 1 is performed *in situ* as a convenient precursor of $C_2H_2$; in this case the chemistry involved is simply that of acetylene with the added convenience of local generation, and can be used in a variety of different synthetic processes.[2-3] Reactions include copper click chemistry,[4] Sonogashira-like formation of symmetrical diarylethynes,[5-7] and ethynylation of aldehydes and ketones.[8] *In situ* $C_2H_2$ can also be used as a precursor for vinyl derivatives,[9] including with $^{13}C$ substitution.[10] In the last few years calcium carbide has been explored under water-free conditions as a potential precursor for electronic materials such as graphyne[11] or triazine structures.[12] While not the target of these reports, some studies observed the formation of small molecule by-products that preserve the alkyne moiety. There have also been studies into symmetric diarylethyne

synthesis under low water conditions, where undried solvents supplied adequate water to initiate the catalytic cycles.[3, 6] However, these examples typically behave the same, or are improved, with added water.

In this contribution we report that under controlled thermal conditions and low water content in dimethyl sulfoxide (DMSO), it is possible to direct the chemistry of $CaC_2$ towards the formation of acetylide intermediates in solution to facilitate the formation of symmetrical diarylethynes using Pd deposited on $TiO_2$ as a catalyst (reaction 2).

$$CaC_2 + H_2O \xrightarrow[DMSO]{} HC{\equiv}C{-}CaOH \xrightarrow[2R\text{-}X]{Cat} RC{\equiv}CR + CaX_2 \quad (2)$$

**Scheme 5.2.2.** Proposed mechanism for symmetrical diarylethyne synthesis through ethynyl calcium hydroxide intermediate under low water conditions in DMSO.

For example, in a very simple system used here as a tool for mechanistic studies, diphenylacetylene (tolan) can be prepared from $CaC_2$ and bromobenzene, reaction 3, using a catalyst based on Pd deposited on $TiO_2$ ($Pd@TiO_2$).

$$CaC_2 + 2PhBr \xrightarrow[140\ ^\circ C]{Pd@TiO_2} \underset{\mathbf{P1}}{Ph{-}C{\equiv}CH} + \underset{\mathbf{P2}}{Ph{-}C{\equiv}C{-}Ph} + CaBr_2 \quad (3)$$

**Scheme 5.2.3.** General equation for the formation of phenylacetylene (P1) and diphenylacetylene (P2) from $CaC_2$ and Bromobenzene using $Pd@TiO_2$ under thermal conditions.

$Pd@TiO_2$ has proven effective before in the photocatalysis of the Sonogashira reaction[1, 13] that also involves couplings of alkynes; however, reaction 3 is a thermal process. Here the reaction can be catalysed thermally whereas no activity is observed under visible light excitation at room temperature. Kinetic studies suggest the reaction reaches a maximum yield of diphenylacetylene (P2) after 4 hours of heating at 140 ℃. There is also an initial formation of the intermediate phenylacetylene (P1), reaching a maximum after 1 hour, before being converted to the final diphenylacetylene product (Figure 5.2.1). Only small

traces of unreacted bromobenzene were present at the end of the kinetic studies. The unaccounted-for loss of bromobenzene is likely due to dehalogenation to benzene along with some adsorption to the catalyst.

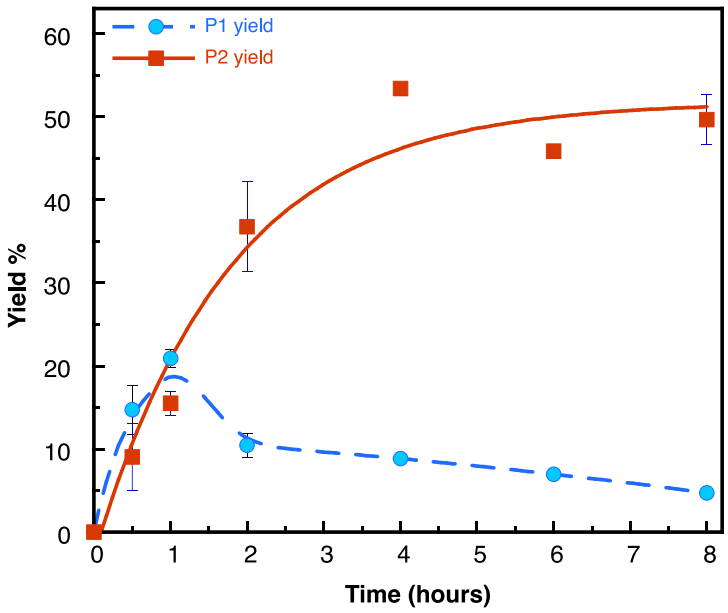


**Figure 5.2.1.** Kinetics of aryl ethyne synthesis at 140℃ under argon. Other conditions: Bromobenzene (0.1 mmol), $CaC_2$ (10 eq), $Cs_2CO_3$ base (2.5 eq), Pd@$TiO_2$ Catalyst (20 mg), DMSO solvent (5 mL).

The reaction conditions ($Cs_2CO_3$ and $CaC_2$) were then optimized to maximize the yield of P2 (Table 5.2.1). It appears that optimal yields of P2 require between 2.5 and 5 equivalents of $Cs_2CO_3$ as a base, and 5 to 10 equivalents of $CaC_2$. Using additional $CaC_2$ can also negatively impact the reaction (See Table 5.2.1, entry 7), perhaps through the formation of larger carbon structures. The best yield of P2 was observed in entry 6, which will be used as the standard conditions moving forward.

**Table 5.2.1.** Optimization of reaction conditions for synthesis of diphenylacetylene (P2), with optimal conditions bolded.

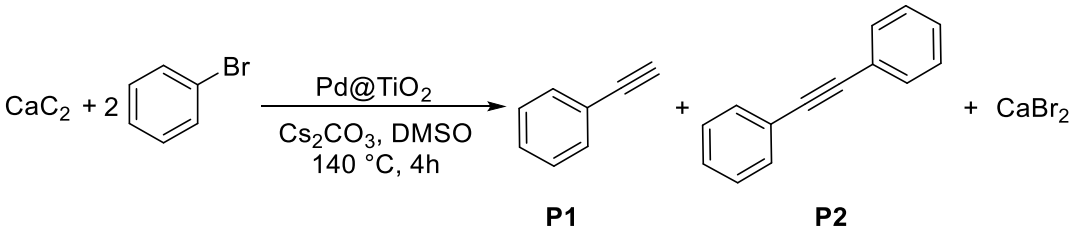


**P1** **P2**

| Entry | $Cs_2CO_3$ (eq) | $CaC_2$ (eq) | Other | % Yield (Error)[b] | |
|---|---|---|---|---|---|
| | | | | P1 | P2 |
| **1** | 2.5 | 5 | - | 10.0 (5.3) | 44.5 (5.7) |
| **2** | 5 | 5 | - | 11.3 (0.5) | 47.0 (0.5) |
| **3** | 1.2 | 5 | - | 8.0 (0.2) | 38.8 (1.5) |
| **4** | 0.6 | 5 | - | 10.2 (0.6) | 18.2 (0.4) |
| **5** | 2.5 | 1.2 | - | 3.9 (1.5) | 9.2 (8.5) |
| **6** | **2.5** | **10** | **-** | **8.4 (0.6)** | **48.3 (2.4)** |
| **7** | 2.5 | 20 | - | 9.4 (4.0) | 21.7 (0.6) |
| **8** | 0 | 10 | - | 0 | 0 |
| **9** | 2.5 | 10 | No catalyst | 0 | 0 |
| **10** | 2.5 | 10 | In DMF | 0 | 0 |

[a] Reaction conditions: bromobenzene (0.1 mmol), $CaC_2$, $Cs_2CO_3$ base, Pd@$TiO_2$ catalyst (20 mg), DMSO solvent (5 mL), argon atmosphere, 140°C, 4 h. [b] Evaluated by GC-FID using trans-Stilbene as external standard.

The initial experiments in Table 5.2.1 were conducted with undried DMSO straight from the bottle. Reported studies of the water content of DMSO, suggest that on average it contains 0.1% water,[14] corresponding to about 5 $\mu$L or 0.25 mmol in the 5 mL of solvent used. Prior studies have shown that small amounts of water can be used catalytically in the use of $CaC_2$ as a precursor, thus evaluating the effects of water content is necessary.[6] Reactions with various amounts of added water were conducted, as well as with DMSO dried with molecular sieves (Table 5.2.2). It can be seen that small amounts of water up to 20 $\mu$L can facilitate the reaction; however, excess water appears to poison the reaction, preventing formation of the product. If the reaction simply involved generation of $C_2H_2$ by reaction with water, we would expect water to directly facilitate the reaction; this is clearly not the case.

**Table 5.2.2.** Effect of water content on the yield of diphenylacetylene (P2)

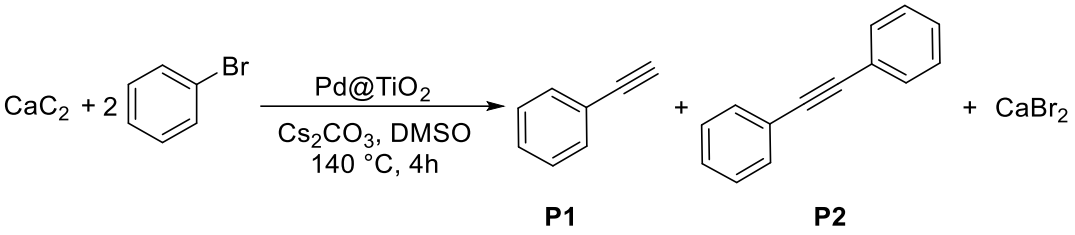


P1 P2

| Entry | Water volume added | % Yield [b] | |
|---|---|---|---|
| | | P1 | P2 |
| **1** | 5 $\mu$L | 16.6 | 43.7 |
| **2** | 10 $\mu$L | 17.0 | 33.1 |
| **3** | 20 $\mu$L | 13.5 | 42.0 |
| **4** | 50 $\mu$L | 11.5 | 21.4 |
| **5** | 200 $\mu$L | 0 | 0 |
| **6** | 0 $\mu$L [c] | 18.1 | 35.4 |

[a] Reaction conditions: bromobenzene (0.1 mmol), $CaC_2$, $Cs_2CO_3$ base, Pd@$TiO_2$ catalyst (20 mg), DMSO solvent (5 mL), argon atmosphere, 140°C, 4 h. [b] Evaluated by GC-FID using trans-Stilbene as external standard. [c]Dry DMSO.

Suspecting that the reaction involved more than the simple reaction of *in situ* generated $C_2H_2$, we decided to explore a two-step methodology that would minimize the reaction of gaseous or dissolved $C_2H_2$. The first step involves heating $CaC_2$ in DMSO to attempt to preload the solvent with a reactive soluble intermediate. After removing any solid material, this mixture was then treated with bromobenzene under standard conditions, without the addition of more $CaC_2$. Significant yield of the expected products would imply a soluble, non-gaseous intermediate derived from $CaC_2$. (Table 5.2.3)

**Table 5.2.3.** Optimization of conditions for two-step reactions

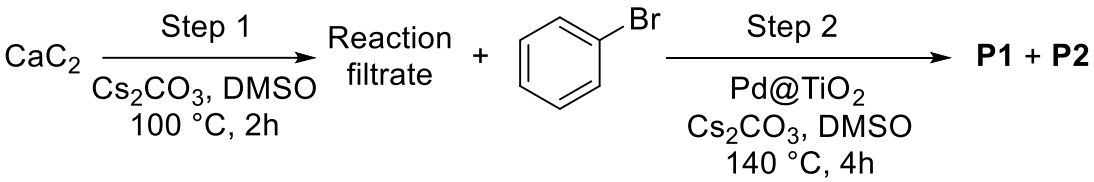


| Entry | Step 1 Changes | Step 2 Changes | % Yield [b] | |
|---|---|---|---|---|
| | | | P1 | P2 |
| **1** | None | None | 15.2 | 29.9 |
| **2** | Pd@$TiO_2$ | None | 13.7 | 55.5 |
| **3** | Pd@$TiO_2$ | No Pd@$TiO_2$ | 10.95 | 47.94 |
| **4** | None | No Pd@$TiO_2$ | 0 | 0 |
| **5** | 5 μL $H_2O$ | None | 10.6 | 35.53 |
| **6** | 10 μL $H_2O$ | None | 10.6 | 52.9 |
| **7** | No $CaC_2$ | None | 0 | 0 |
| **8** | 10 μL $H_2O$; no $Cs_2CO_3$ | None | 11.6 | 49.2 |
| **9** | 10 μL $H_2O$; 60 ℃ | None | 15.2 | 44.5 |

[a] Reaction conditions: ***Step 1.*** $CaC_2$ (10 eq), $Cs_2CO_3$ base (2.5 eq) DMSO solvent (5 mL), argon atmosphere, 100 °C, 2h. ***Step 2.*** $Cs_2CO_3$ base (2.5 eq), step 1 filtrate as solvent (5 mL), Pd@$TiO_2$ Catalyst (20 mg) argon atmosphere, 140 °C, 4h. [b] Evaluated by GC-FID using trans-Stilbene as external standard.

Examination of Table 5.2.3 and comparison of the yields with Table 5.2.1 suggests that a highly reactive species is transferred in the filtrate solution between the two steps. Entry 1 shows a yield of 29.9% for P2, lower than the one observed in the equivalent one-step reaction (entry 6, table 5.2.1), but significant. Not much $C_2H_2$ is likely to remain in solution, particularly given the high working temperatures and the anticipated reduced solubility under these conditions.[15] Therefore, the reactive species transferred between the two steps is unlikely to be simply $C_2H_2$ gas. We propose that the transferable intermediate is a calcium acetylide, most likely species **1**, but possibly **2,** during a one-step reaction, given the presence of bromide in the system.


**1** **2**

**Scheme 5.2.4.** Possible solubilized species of calcium carbide, proposed as ethynyl calcium hydroxide (Species 1), and ethynyl calcium bromide (Species 2).

The structures of species **1** and **2** are clearly reminiscent of Grignard reagents, and their reactivity with bromobenzene seems to follow a typical carbanion-like type of behaviour. Similar species have been suggested and calculated before, with one providing a mass-spectrum of the ethynyl calcium hydroxide intermediate.[6, 16-18] Confirmation of structure **1** was attempted by nuclear magnetic resonance (NMR) and electrospray ionization mass spectrometry (ESI-MS) (See SI, Figures 5.3.1-6). The $^{1}$H NMR spectrum show a very small peak corresponding to a small amount of acetylene in solution; however, the main observed peak is shifted, indicating a similar but significantly different hydrogen atom than those found in acetylene. All product signals also disappear after additional mixing with water, as expected with conversion of product 1. $^{13}$C NMR only shows signals from the carbon of the terminal C-H. In deuterated DMSO, the introduction of a triplet peak indicates some degree of proton exchange with the solvent. The lack of a peak corresponding to the carbon bound to -CaOH is due to the greatly reduced signal intensity of un-protonated carbons, and the overall low concentration of the intermediate. As expected, ESI-MS also showed the introduction of a signal with a molecular weight of 105, corresponding to the $M+Na^{+}$ peak of ethynyl calcium hydroxide observed in the prior literature.

Adding small amounts of water during the first step enhances the reaction to yields comparable with the optimized one-step reaction (Table 3, entries 5-6). The two-step reaction requiring some additional water is expected as it cannot use the water catalytically. The acetylide intermediate transferred between the two steps cannot be remade in step two, which makes it more water dependent. $Pd@TiO_2$ catalyst can also be added in the first step instead of additional water to achieve similar yields. Interestingly, the second step can be run in the absence of the catalyst. This may suggest soluble Pd species can be transferred to the second step, and may not be an entirely heterogeneous process. We note that no Pd was detected in ICP studies, suggesting that if present the amount transferred must be below our detection limit of <0.05 ppm. The first step can also be conducted under milder conditions without the presence of base, or at

temperatures as low as 60°C. No product is detected if the catalyst or $CaC_2$ is missing in both steps of the reaction.

Overall, we have shown the use of DMSO as a solvent to stabilize solubilized intermediates of $CaC_2$ in solution for use in Sonogashira-like reactions such as the synthesis of diphenylacetylene from bromobenzene. Intermediates such as ethynyl calcium hydroxide have been proposed in the past, but not adequately evaluated through mechanistic analysis. The use of a two-step reaction has confirmed the transfer of a soluble reactive species, as well as the stability of this species in solution over short periods of time. Loading the DMSO with these soluble species may also allow for finer control of reactive acetylenic compounds in solution. We propose that the initial 'loading' of DMSO with these reactive species opens up a new controlled approach to calcium carbide based acetylenic chemistry. This method may be applicable in other synthetic systems involving acetylene, as well as with other catalysts (both homogeneous and heterogeneous).

## 5.3 Pre-submission Version of Supplemental Information

### Materials and Instrumentation

All reagents used were purchased from Sigma Aldrich and used as received. $TiO_2$ P25 was purchased from Univar Canada.

Quantification of products was conducted in a Perkin Elmer, Claurus Gas Chromatograph coupled to a Flame Ionization Detector (FID). Confirmation of the products was performed by mass spectrometry in an Agilent 6890-N Gas Chromatograph with an Agilent 5973 mass selective detector calibrated with acetophenone. $^{1}H$ NMR and $^{13}C$ NMR spectra were recorded in a Bruker Avance 300 expressing chemical shifts in ppm relative to the H (or C) of the solvent ($D_6$-DMSO). ESI-MS was conducted with an Agilent InfinityLab Liquid Chromatograph/Mass Selective Detector (single quadrupole detector), with sample injected directly into the MSD (skipping the column).

**Experimental methodology**

*Catalyst synthesis*

The catalyst Pd@$TiO_2$ was prepared photochemically as in earlier reports[19] giving a particle size of ~1.6 nm. In short, this was done photochemically by irradiation of a sonicated mixture (20 min sonication) of P25 $TiO_2$ and $PdCl_2$ salt in MilliQ water with a theoretically mass loading of 2.5%. Irradiation was conducted for 8 hours by 14 UVA bulbs in a photoreactor with constant stirring. The irradiated $TiO_2$ reduces the Palladium to form nanoparticles on the surface.

*One-step reaction system*

For a typical reaction 0.1 mmol of bromobenzene was added to 5 ml of DMSO with 0.25 mmol of $Cs_2CO_3$, 1 mmol of $CaC_2$ and 20 mg Pd@$TiO_2$ catalyst ($Cs_2CO_3$ and $CaC_2$ amounts were varied as noted). To purge with argon, vials were put into a glove bag and put through repeated cycles of removing gas under vacuum and filling with Argon (4 cycles total) and then closed the vials while in the glovebag giving an argon headspace. If water is added to the reaction, it is added in the glovebag before tightly closing the vial. The vial was then heated at 140$^oC$ for 4 hours in an oil bath with constant stirring. Heating at 140$^oC$ was safe in this time frame; however, care should still be taken when heating DMSO at higher temperatures due to the possibility of dangerous decomposition.[20]

*Two-step reaction system*

1 mmol of $CaC_2$ was added to 5 ml of DMSO, with or without $Cs_2CO_3$ and Pd@$TiO_2$ catalyst. Was purged as mentioned in the one-step reaction system then heated at 100$^oC$ (or as otherwise noted) for 2 hours. The reaction mixture was then centrifuged at 10000 rpm for 10 min to remove solid material. The resulting filtrate was then used as a replacement to the DMSO in a normal one-step reaction setup (without additional $CaC_2$ being added).

*Product Analysis by GC-FID*

Reaction mixture was diluted with water and extracted 3 times with hexane. Trans-stilbene was added as an external standard and the concentrations of residual bromobenzene and products P1 and P2 were evaluated by GC-FID. Products identities were also confirmed by GC-MS analysis.

**Preliminary Investigations**

This work focuses on the optimisation and mechanistic analysis of a set of reaction conditions obtained from preliminary investigations. Initial tests involved using tetra-*n*-butyl ammonium fluoride (TBAF) as an additive as it was shown in the past to lead to improved conversion to soluble intermediates through direct complexation with calcium carbide intermediates.[8] However, this approach was found to be incompatible with our catalytic system, and lead to no significant formation of products. Bromobenzene was also chosen after comparing with iodobenzene and chlorobenzene. Bromobenzene was the only effective compound, having a balance of good reactivity without too much of the competing dehalogenation. Using CuI as a cocatalyst also gave no improvement to the catalysis. $Cs_2CO_3$ was chosen as the base after $K_2CO_3$ and KOH proved ineffective at promoting the reaction. Decreasing heating from 140$^o$C greatly decreased speed of the reaction. Some of these conditions are summarized in the table below (Table 5.3.1)

Overall, initial investigations showed that conversion of bromobenzene with Pd@$TiO_2$ on the 0.02 M scale requires a molar excess of $Cs_2CO_3$ and $CaC_2$, and DMSO as a solvent with 140$^o$C heating. Undried DMSO also contained enough water for the reaction to occur.

**Table 5.3.1.** Alterations of conditions from standard conditions established in Table 5.2.1, Entry 6.

| Alterations to Conditions | Results |
|---|---|
| TBAF, no $Cs_2CO_3$, | No detection of desired products |
| TBAF, no $Cs_2CO_3$, 4-iodoanisole (no bromobenzene) | No detection of desired products |
| TBAF, no $Cs_2CO_3$, 4-iodoanisole (no bromobenzene), 2 mg CuI | No detection of desired products |
| Chlorobenzene, 2.5 eq $CaC_2$ | No detection of desired products |
| Iodobenzene, 2.5 eq $CaC_2$ | Trace detection of desired product |
| $K_2CO_3$ as base | Trace detection of desired products |
| KOH as base | No detection of desired products |
| Acetonitrile as solvent | No detection of desired products |
| 40 mg Pd@$TiO_2$ | No improvement |
| 60$^o$C, 24 hours | 20% yield P1, 13% yield P2 |
| 80$^o$C, 24 hours | 24% yield P1, 30% yield P2 |
| 100$^o$C, 4 hours | Trace P1, 9.6% yield P2 |

**Detection of ethynyl calcium hydroxide by ESI-MS and NMR**

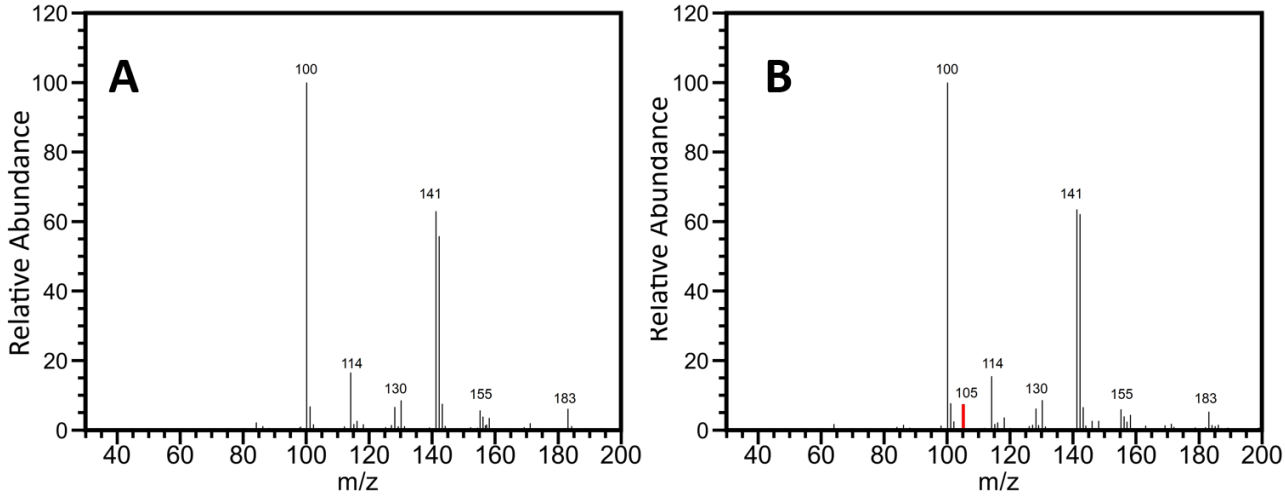


**Figure 5.3.1.** ESI-MS signals for DMSO as a solvent a) before b) and after reaction with $CaC_2$ at 100°C. There are various signals coming from DMSO in both graphs, however, after reaction with $CaC_2$ the addition of a signal at 105 is observed. This correlates well with the expected $M+Na^+$ signal for the proposed intermediate of ethynyl calcium hydroxide (MW of 82 + 23).

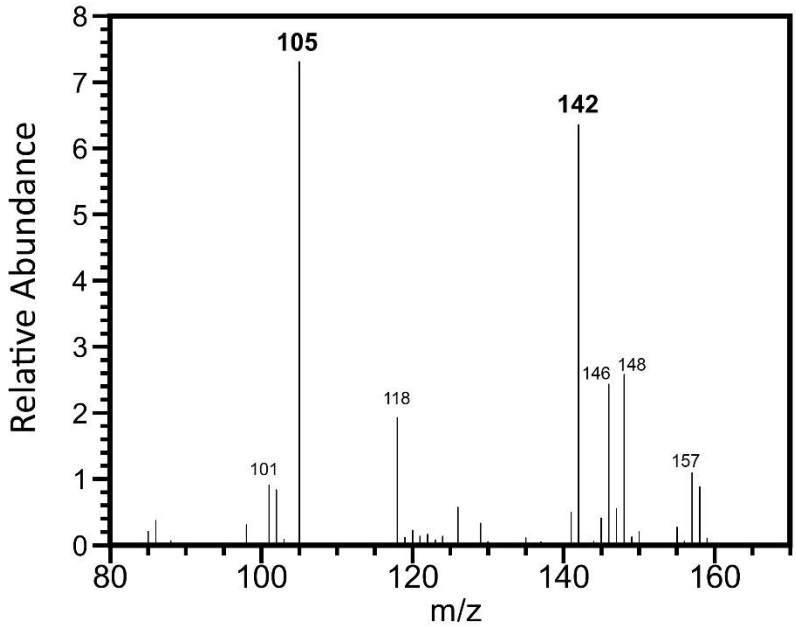

**Figure 5.3.2.** Difference of ESI-MS signals for DMSO as a solvent after reaction with $CaC_2$ at 100°C. The largest change is the signal at 105 corresponding to $M+Na^+$ for the expected ethynyl calcium hydroxide intermediate.

There is also an increase at 142, however this increase is less significant as the initial 142 signal was already significantly present in the initial ESI-MS signals (not a large percent increase). The 142 signal is likely from DMSO-acetonitrile-$Na^+$ (acetonitrile was used as the makeup solvent in the flow).

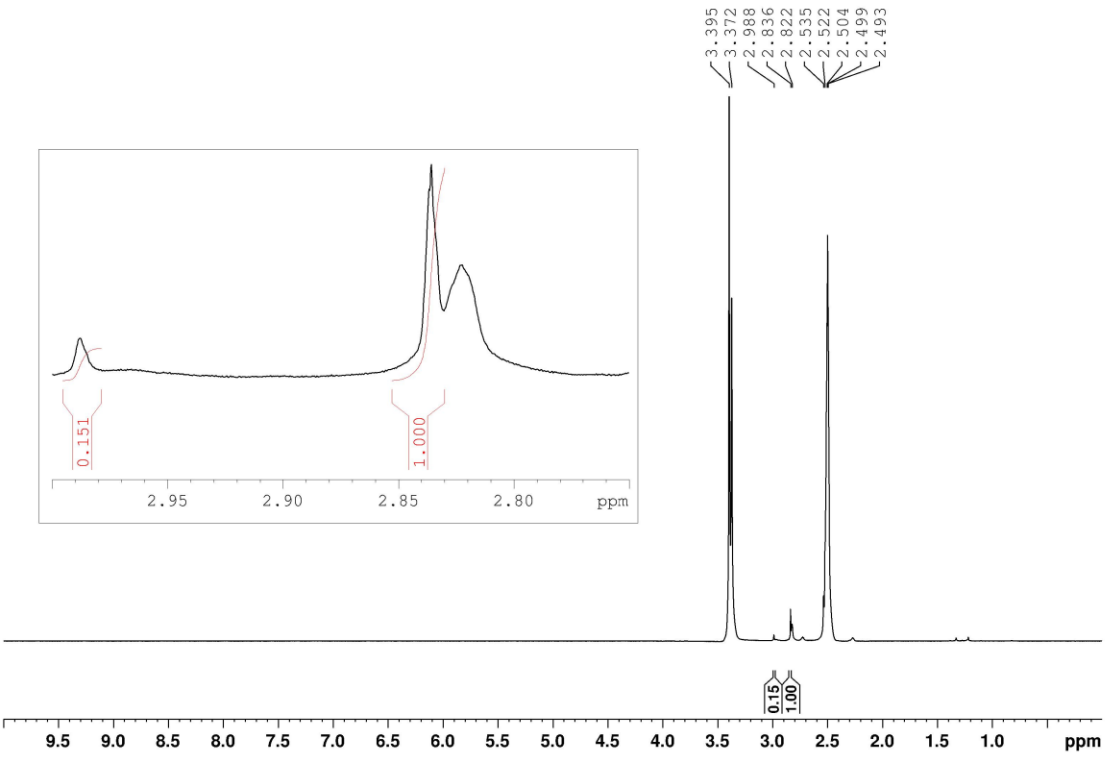


**Figure 5.3.3.** $^1H$ NMR signals of a sample of $CaC_2$ in 2 mL of DMSO-d6 with 20 $\mu$L of added water after heating at 100°C for 2 hours. The spectrum shows expected solvent peaks for DMSO (2.5 ppm) and the water impurity (including $H_2O$ and DHO peaks at 3.395 and 3.372 ppm respectively). The peak at ~3 ppm corresponds to a very small amount of acetylene in solution (Relative integration: 0.151 (2H)). The peaks observed at ca 2.8-2.85 ppm most likely correspond to the terminal hydrogen of the ethynyl calcium hydroxide (Relative integration: 1.000 (1H)) , with the broad peak adjacent being assigned to the OH group. The relative integrations show the amount of acetylene in the media is roughly 13 times lower.

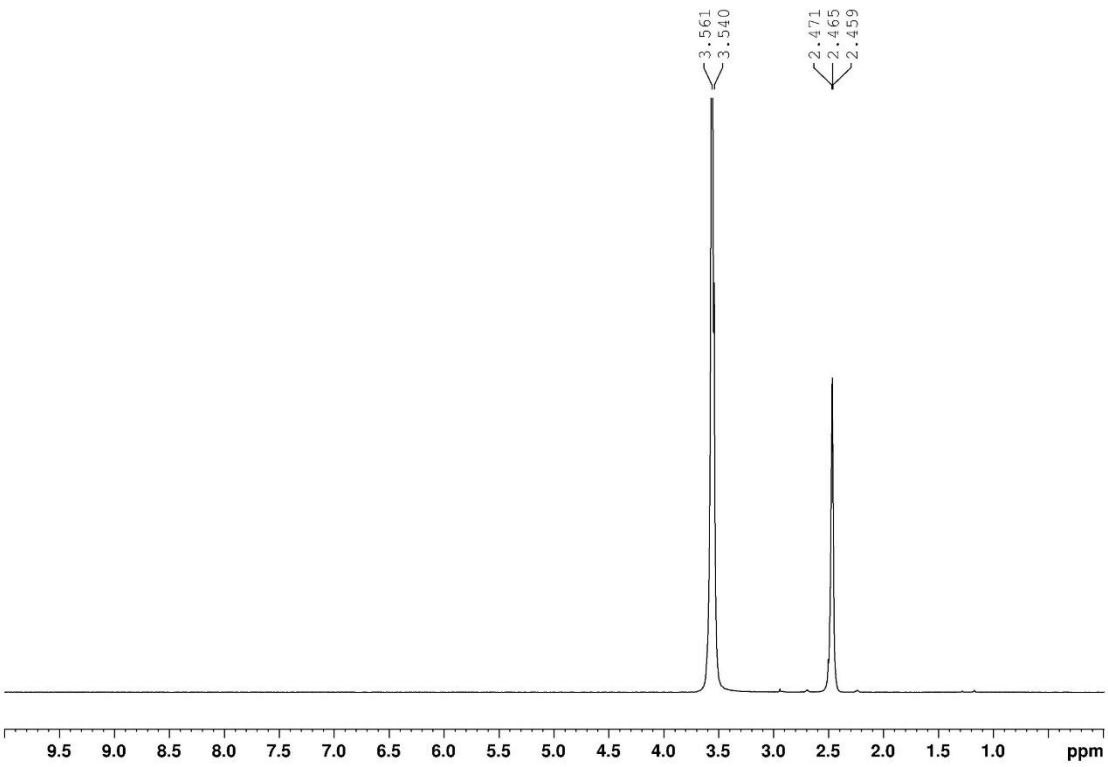


**Figure 5.3.4.** H-NMR signals of sample from figure S3 after addition of additional 100 $\mu$L of water and mixing for 20 min. There is loss of the peaks at 2.8-2.85 ppm, showing formation and loss of this intermediate by gaseous production of acetylene. A small peak around 3 ppm is still present, corresponding to the small amount of acetylene still in solution.

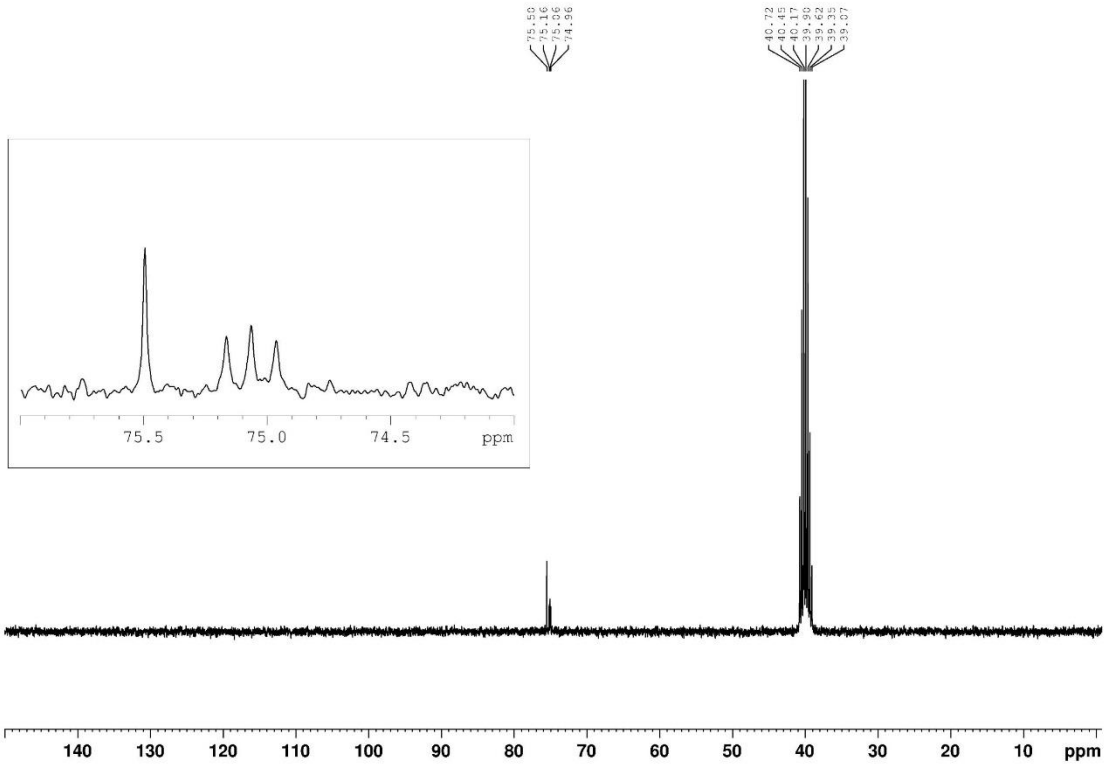


**Figure 5.3.5.** Proton decoupled $^{13}C$ NMR signals of a sample of $CaC_2$ in 2 ml of DMSO-d6 with 20 $\mu$L of added water after heating at 100$^{o}$C for 2 hours. The spectrum shows the expected solvent peaks for DMSO. There appears to be two different carbon peaks at similar shifts around 75 ppm, one singlet and one triplet, which are within the expected region for acetylenic carbons. The triplet splitting of the second carbon indicates it is bound to deuterium. This shows there is likely some degree of proton exchange with the solvent. The 75.5 ppm peak is likely from the carbon of the terminal C-H without deuterium exchange, while the peak at 75 ppm is from the same carbon after exchanging from deuterium from the solvent.

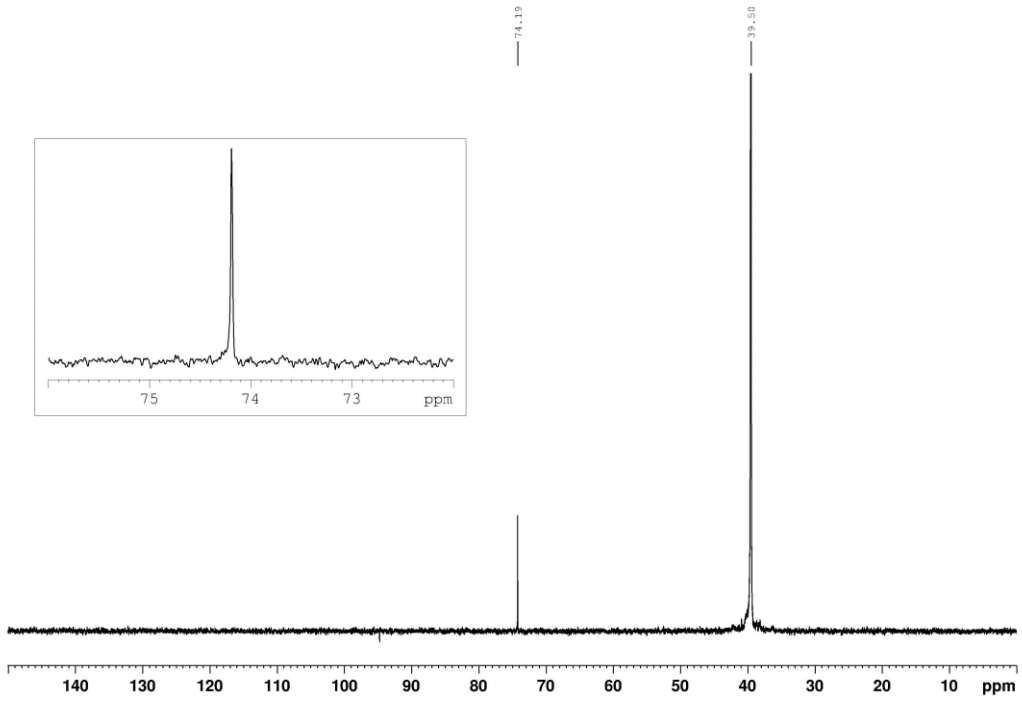


**Figure 5.3.6.** Proton decoupled $^{13}C$ NMR signals of a sample of $CaC_2$ in 2 ml of DMSO (non-deuterated) with 20 $\mu$L of added water after heating at 100°C for 2 hours. The spectrum shows the expected solvent peaks for DMSO and one peak in the acetylenic carbon region. This peak is likely from the terminal C-H carbon, while the carbon attached to -CaOH is not observed. This is likely due to the lower signals observed from unprotonated carbons, making it invisible with the low concentration of intermediate present.

**Confirmation of phenylacetylene and diphenylacetylene products by GC-MS**

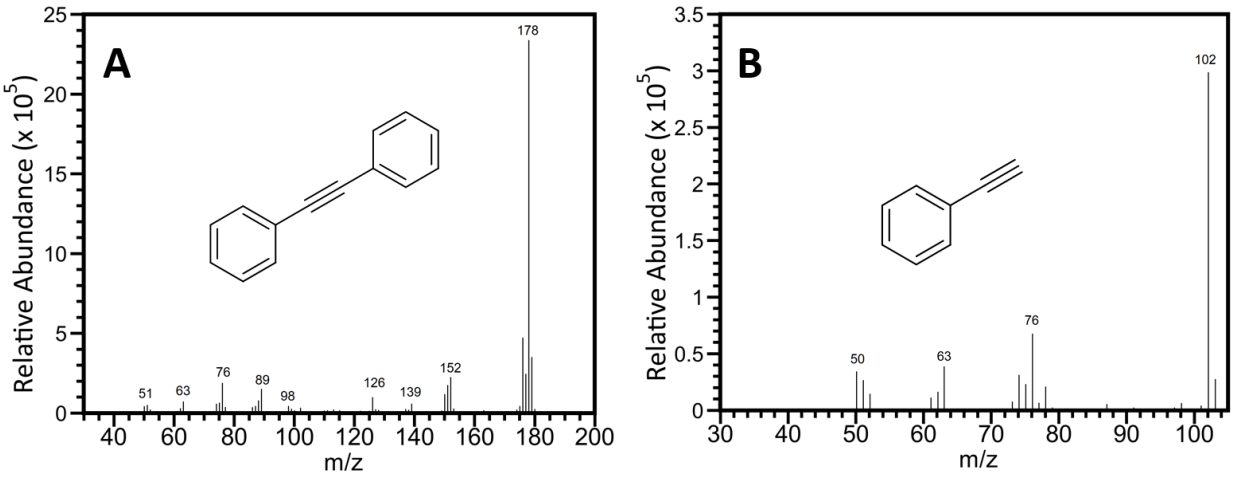


**Figure 5.3.7.** Mass-spectra from GC-MS of the two isolated products of a) diphenylacetylene (P2) and b) phenylacetylene (P1). Identity of products were confirmed through comparison against standards of each.

Phenylacetylene and diphenylacetylene were both confirmed through direct comparison against known standards of each. The fragmentation patterns and retention times obtained from GC-MS were identical between proposed products and standards.

## 5.4 Accompaniment to Chapter 5

This project was an interesting part of my journey as a graduate student, as it evolved greatly from my initial plans for it. I was initially hoping to involve the photocatalytic radical chemistry present in my other publications; however, it pivoted in a different direction entirely. However, I am glad it didn't go as planned as I believe the results I obtained were quite interesting, and also have great potential for future expansion.

The ethynyl calcium hydroxide intermediate that can be stabilized in DMSO is the most interesting aspect of this work, and may be useful in a variety of different reactions as well. Anything that utilizes acetylene chemistry may be able to use this intermediate as a reagent instead. This intermediate has reduced risk of explosion when compared to systems with acetylene gas under pressure, and also may allow for more reagent to be truly in solution when

compared to acetylene gas. I also believe that photochemical systems involving this intermediate may still be possible. Specifically, I wonder if mixed solvent systems of DMSO with solvents that can form radicals photo-catalytically from M@$TiO_2$ catalysts may be possible. This however is dependent on if the ethynyl calcium hydroxide can be adequately stabilized in such mixed solvent systems.

Overall, this project is an interesting compliment to the rest of my research, and highlights the other uses of Pd@$TiO_2$ outside of photochemistry.

## 5.5 References


1. Elhage, A.; Lanterna, A. E.; Scaiano, J. C., Light-induced sonogashira C-C coupling under mild conditions using supported palladium nanoparticles. *ACS Sustainable Chem. Eng.* **2018,** *6* (2), 1717-1722.
2. Rodygin, K. S.; Ledovskaya, M. S.; Voronin, V. V.; Lotsman, K. A.; Ananikov, V. P., Calcium carbide: versatile synthetic applications, green methodology and sustainability. *Eur. J. Org. Chem.* **2021,** *2021* (1), 43-52.
3. Rodygin, K. S.; Werner, G.; Kucherov, F. A.; Ananikov, V. P., Calcium carbide: a unique reagent for organic synthesis and nanotechnology. *Chem Asian J.* **2016,** *11* (7), 965-976.
4. Jiang, Y.; Kuang, C.; Yang, Q., The use of calcium carbide in the synthesis of 1-monosubstituted aryl 1,2,3-triazole via click chemistry. *Synlett* **2009,** *2009* (19), 3163-3166.
5. Zhang, W.; Wu, H.; Liu, Z.; Zhong, P.; Zhang, L.; Huang, X.; Cheng, J., The use of calcium carbide in one-pot synthesis of symmetric diaryl ethynes. *ChemComm* **2006,** (46), 4826-4828.
6. Chuentragool, P.; Vongnam, K.; Rashatasakhon, P.; Sukwattanasinitt, M.; Wacharasindhu, S., Calcium carbide as a cost-effective starting material for symmetrical diarylethynes via Pd-catalyzed coupling reaction. *Tetrahedron* **2011,** *67* (42), 8177-8182.
7. Matake, R.; Niwa, Y.; Matsubara, H., Phase-vanishing method with acetylene evolution and its utilization in several organic syntheses. *Org. Lett.* **2015,** *17* (10), 2354-2357.
8. Hosseini, A.; Seidel, D.; Miska, A.; Schreiner, P. R., Fluoride-assisted activation of calcium carbide: A simple method for the ethynylation of aldehydes and ketones. *Org. Lett.* **2015,** *17* (11), 2808-2811.
9. Rodygin, K. S.; Voronin, V. V.; Ledovskaya, M. S., Synthesis of glucosamine vinyl ether derivative and its deuterated analog. *Russ. Chem. Bull.* **2020,** *69* (7), 1401-1404.
10. Ledovskaya, M. S.; Voronin, V. V.; Rodygin, K. S.; Ananikov, V. P., Efficient labeling of organic molecules using $^{13}C$ elemental carbon: Universal access to $^{13}C_2$-labeled synthetic building blocks, polymers and pharmaceuticals. *Org. Chem. Front.* **2020,** *7* (4), 638-647.
11. Li, Q.; Li, Y.; Chen, Y.; Wu, L.; Yang, C.; Cui, X., Synthesis of γ-graphyne by mechanochemistry and its electronic structure. *Carbon* **2018,** *136*, 248-254.
12. Faghani, A.; Gholami, M. F.; Trunk, M.; Müller, J.; Pachfule, P.; Vogl, S.; Donskyi, I.; Li, M.; Nickl, P.; Shao, J.; Huang, M. R. S.; Unger, W. E. S.; Arenal, R.; Koch, C. T.; Paulus, B.; Rabe, J. P.; Thomas, A.; Haag, R.; Adeli, M., Metal-assisted and solvent-mediated synthesis of two-dimensional triazine structures on gram scale. *J. Am. Chem. Soc.* **2020,** *142* (30), 12976-12986.
13. Elhage, A.; Lanterna, A. E.; Scaiano, J. C., Catalytic farming: reaction rotation extends catalyst performance. *Chem. Sci.* **2019,** *10* (5), 1419-1425.

14. Semin, D. J.; Malone, T. J.; Paley, M. T.; Woods, P. W., A novel approach to determine water content in DMSO for a compound collection repository. *J. Biomol. Screening* **2005,** *10* (6), 568-572.
15. Miyano, Y.; Hayduk, W., Solubility of acetylene in several polar and nonpolar solvents and solvent mixtures. *Can. J. Chem. Eng.* **1981,** *59* (6), 746.
16. Fu, R.; Li, Z., Direct synthesis of symmetric diarylethynes from calcium carbide and arylboronic acids/esters. *Eur. J. Org. Chem.* **2017,** *2017* (45), 6648-6651.
17. Gao, L.; Liu, Z.; Ma, X.; Li, Z., Direct synthesis of propen-2-yl sulfones through cascade reactions using calcium carbide as an alkyne source. *Org. Lett.* **2020,** *22* (13), 5246-5250.
18. Polynski, M. V.; Sapova, M. D.; Ananikov, V. P., Understanding the solubilization of Ca acetylide with a new computational model for ionic pairs. *Chem. Sci.* **2020,** *11* (48), 13102-13112.
19. Elhage, A.; Lanterna, A. E.; Scaiano, J. C., Tunable photocatalytic activity of palladium-decorated $TiO_2$: Non-hydrogen-mediated hydrogenation or isomerization of benzyl-substituted alkenes. *ACS Catalysis* **2017,** *7* (1), 250-255.
20. Yang, Q.; Sheng, M.; Li, X.; Tucker, C.; Vásquez Céspedes, S.; Webb, N. J.; Whiteker, G. T.; Yu, J., Potential explosion hazards associated with the autocatalytic thermal decomposition of dimethyl sulfoxide and its mixtures. *Organic Process Research & Development* **2020,** *24* (6), 916-939.

# 6. Conclusions

## 6.1 Further Analysis and Summary

Overall, this dissertation highlighted the versatility of M@$TiO_2$ catalysts in a variety of different applications. This included hydrogen generation, solvent radical initiation, and organic synthesis utilizing calcium carbide as a precursor. The results of these studies will now be further analyzed, loose-ends tied up, and compared against the current state of research in the field.

### 6.1.1 Photocatalytic Hydrogen Generation

The first application explored was photocatalytic hydrogen generation. In chapter 2, a variety of different M@$TiO_2$ photocatalysts were synthesized and compared against a commercial Au@$TiO_2$ photocatalyst. This comparison was done under various reaction conditions, including pure water splitting, and with SEDs such as methanol or formic acid. Activities for pure water splitting, and with SEDs, were compared to evaluate the assumption that a catalyst with improved activity with SEDs will also show improvement in pure water splitting. With M@$TiO_2$ photocatalysts, the metal-NP is often assumed to simply accept excited electrons from the conduction band and reduce $H^+$ ions into $H_2$ gas. This implies that the electron donor that is oxidized is simply interacting with the photogenerated hole of $TiO_2$ itself. Thus, the only improvement for the oxidation half of the reaction would be in increasing the lifetime of the photogenerated hole by trapping of the excited electron in the metal-NP. However, this assumption does not hold true when comparing the various catalysts with different electron donors (water, methanol, or formic acid). The specific choice of donor directly affects the relative activity of a catalyst, as different trends between M@$TiO_2$ photocatalysts are observed for each (Figure 2.2.4). With no SED present (pure water splitting), the commercial Au@$TiO_2$ performed the best, with Cu, Pt, and Co decorations performing close behind. However, Ru and Pd decorations showed no significant hydrogen generation for pure water splitting. When looking at hydrogen generation with 1% methanol, the trends change quite a bit. With 1% methanol, Pt@$TiO_2$ is the most effective, with Au and Pd decorations also offering high generation. It appears that Pt, Au and Pd decorations have greater enhancement with the addition of SEDs than

with decoration of Cu or Co. A similar trend is seen with 1% formic acid; however, Au and Pt switch places and some generation is seen with Ru@$TiO_2$ (which showed little to no formation with water splitting, and 1% methanol). The differences are very clear when comparing Pd@$TiO_2$ and Cu@$TiO_2$. With pure water splitting, Cu@$TiO_2$ is one of the better catalysts with Pd@$TiO_2$ showing no significant $H_2$ generation. However, when a sacrificial electron donor is added, Cu@$TiO_2$ begins to lag behind in it's relative activity, and Pd@$TiO_2$ becomes one of the better photocatalysts. Some general trends exist, such as Pt and Au decorations being a good choice in all conditions; however, it is clear that the chemistry occurring is different between SEDs and water splitting.

There are a few explanations for the differing trends observed in these various $H_2$ generating systems. Firstly, many of the M@$TiO_2$ photocatalysts are actually $MO_x$@$TiO_2$ catalysts. Most of the NP decorations have some degree of oxidation, as can be seen in the XPS results (Figure 2.3.5). The copper decoration is almost entirely a mixture of $Cu_2O$ and CuO, the main species thus being entirely an oxide, while Pt and Ru decorations show a mix of oxide and metal(0). Although Co did not have strong enough XPS for accurate analysis, it is also assumed to have a higher degree of oxidation similar to copper. Cu, Pt, and Co all perform very well for pure water splitting, with Au being the main outlier as it is primarily unoxidized. It is possible that metal-oxide nanoparticles are able to also take part in the oxidation of $H_2O$, especially near the heterojunction between $TiO_2$ and the metal oxide. For instance, $Cu_2O$ and CuO have a valence band slightly too high in energy to oxidize water efficiently; however, at the interface with $TiO_2$ the band may bend down to lower energies. Due to this, when $TiO_2$ is excited, an electron may be transferred from the VB of the $CuO_x$-NP, moving the photogenerated hole into it. This movement of electrons may even be more favorable than the typical M@$TiO_2$ mechanism, as the conduction bands of CuO and $Cu_2O$ are higher in energy than the conduction band of $TiO_2$ (Figure 6.1.1).[1] This means that the flow of excited electrons would instead be into $TiO_2$. A mechanism involving direct excitation of the $CuO_x$-NP may also be possible, allowing for direct visible light catalysis. However, the actual bandgaps of these semiconductors as NPs may be different, so further evaluation of what is occurring with $CuO_x$-NP in the Cu@$TiO_2$ catalysts would be necessary

for full conclusions on this. Similar chemistry may also be present with the Co@$TiO_2$ materials which also perform reasonably well in pure water splitting.

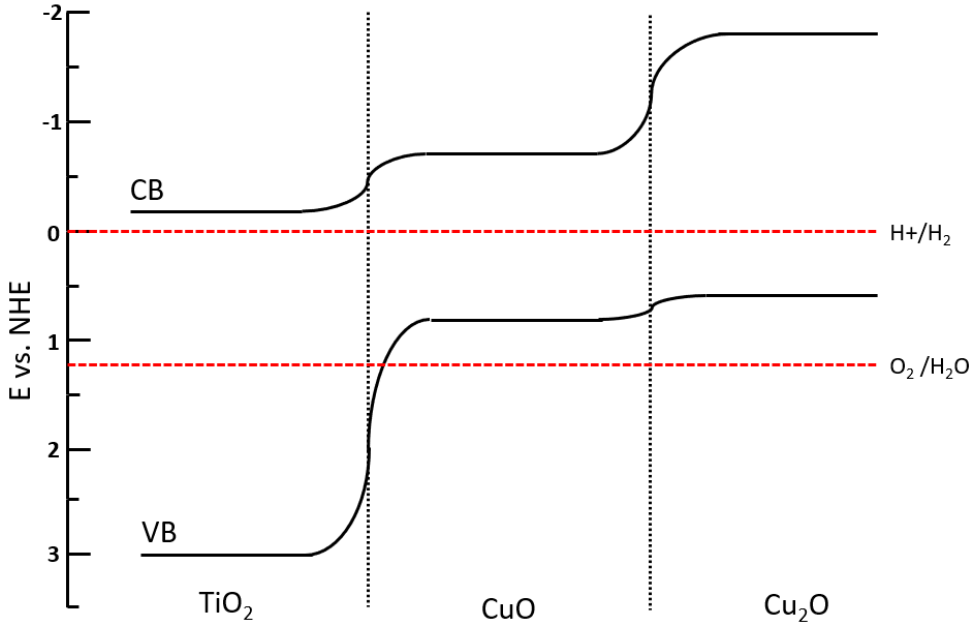


**Figure 6.1.1.** Band-gap energy diagrams of $TiO_2$, CuO, and $Cu_2O$ showing heterojunctions between each semiconductor. $TiO_2$ and $Cu_2O$ could also directly have a heterojunction in a similar fashion. Relevant reduction potentials are also shown.

Au, Pd, and Pt decorations show the greatest improvement in activities when SEDs are present. One reason for this may be due to further chemistry with generated radicals from the SEDs after oxidation. These generated radicals are themselves strong electron donors, and may also directly react with the metal-NP or the CB of $TiO_2$ through another PCET. This is the 'doubling effect' mentioned prior, as you can have the formation of 2 $H^+$ ions in solution and 2 excited electrons in the CB or metal-NP from one absorbed photon. Overall balanced equations of this with methanol as an example are shown below (Scheme 6.1.1). Typically the methanol radical is shown to discretely form an $H^+$ ion after injection of an electron into the CB or metal-NP; however, I propose that the PCET and $H^+$ reduction steps may be closely coupled. It may be possible that it follows a more typical HAT mechanism in which the proton and electron are transferred together, combining with an $H^+$ ion and an excited electron from the CB or metal-NP. This mechanism should be more favorable compared to the typical system that requires two

photoexcited electrons to react with two $H^+$ ions, which is especially difficult when considering all those components would be required to be in relatively close proximity. This same mechanism is expected to occur with the solvent radicals discussed in chapter 3. Enhancement of this 'doubling effect' may be dependent on the metal decoration on the $TiO_2$. Therefore, Au, Pd, and Pt are likely greatly improving this doubling effect, directly interacting with the radicals formed from the SEDs. This is especially true for Pd decoration, since it shows no improvement for water splitting, but is very effective for SED-based $H_2$ generation. With this in mind, the Pd@$TiO_2$ acts as a strong warning for why conclusions from SED experiments cannot be used when developing a photocatalyst for pure water splitting. Even if the decoration being added is meant for improving the reduction reaction, as NP decorations often are, the mechanisms involved with SEDs may interact in other ways not possible under pure water spitting conditions. Further analysis of the mechanisms occurring with SEDs, and their generated radicals, are required to better support these proposed explanations. Perhaps future development of the heterogeneous LFP discussed in chapter 4 would allow for a better understanding of these processes; however, this would be difficult with the current methods.

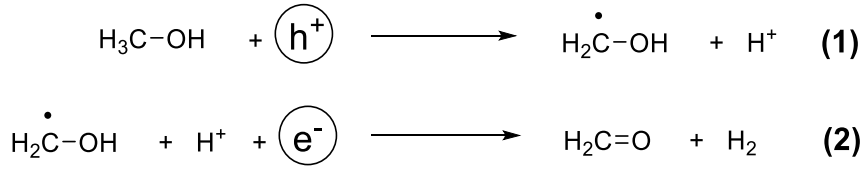


**Scheme 6.1.1** Equations showing proposed mechanism of $H_2$ generation from methanol using photogenerated holes ($h^+$) and electrons ($e^-$) from M@$TiO_2$ photocatalysts

Chapter 2 acts as a strong warning for the dangers of making conclusions from SED experiments, but it also highlights the impressive hydrogen generation from such a simple and cheap heterogeneous photocatalyst. The hydrogen generation rates reported are not record breaking; however, are still comfortably within the ranges of rates found in more complex and expensive photocatalysts. Pt@$TiO_2$ and Pd@$TiO_2$ are impressive with 1% methanol, showing $H_2$ generation rates of 22000 µmol $g^{-1}$ $h^{-1}$ and 12000 µmol $g^{-1}$ $h^{-1}$ respectively. They are similarly impressive with 1% formic acid showing 21000 µmol $g^{-1}$ $h^{-1}$ for Pt@$TiO_2$ and 14500 µmol $g^{-1}$ $h^{-1}$ for Pd@$TiO_2$. However, this is under 368 nm LED irradiation, and showed greatly lowered

activities under solar simulation conditions. One limitation of these catalysts are their mediocre activity under solar light, as this greatly limits use for sustainable fuel production. Generation under solar simulation was likely dependent on the small amount of UVA still present in the spectrum. Cu@$TiO_2$ and Pt@$TiO_2$ were quite impressive under water splitting conditions with ~1500 µmol $g^{-1}$ $h^{-1}$ each. In comparison, most photocatalytic $H_2$ generation yields with true water splitting are less than 1000 µmol $g^{-1}$ $h^{-1}$, making these clear standouts. However, some more recent examples in literature are more effective with a highlight being a rate of 3900 µmol $h^{-1}$ (mass of catalyst not reported; however, likely less than g scale) for an aluminum-doped $SrTiO_3$ with 0.1% Rh, 0.05% $Cr_2O_3$, and 0.05% CoOOH cocatalyst decorations.[2] This example was especially interesting as it was reported to have a quantum efficiency of almost unity. Also 1%Pt/$TiO_2$-NP was shown to have $H_2$ generation rates of 7410 µmol $g^{-1}$ $h^{-1}$.[3] However, this material was irradiated with a 500 W Hg lamp, which may account for much of it's improved activity compared to the Pt@$TiO_2$ in this dissertation. This improvement may also be due to the $TiO_2$-NP used, as it may have improved activity over P25 $TiO_2$, or differences in the Pt-NP decoration. Another standout for pure water-splitting activities are carbon nitride-based materials, as they have strong visible light activity. One strong example being a carbon nitride/carbon-dot hybrid which showed $H_2$ generation rates of 575 µmol $g^{-1}$ $h^{-1}$ from pure water splitting under irradiation with a Xe lamp with a >420 nm cut-off filter.[4] This is lower than our reported rate of ~1500 µmol $g^{-1}$ $h^{-1}$; however, this material is being excited with visible light rather than UVA. Overall, comparison between $H_2$ generating photocatalysts is difficult due to poor standards of reporting, and differing light sources and reactor setups. However, it is still clear that our M@$TiO_2$ photocatalysts are strong contenders from a cost standpoint, especially for Cu@$TiO_2$ as it uses a non-precious metal decoration. The lack of adequate visible light activity remains the main disadvantage to be improved upon.

One other disadvantage of the research conducted in chapter 2, as well as chapter 3, is the inconsistent loading percentages of the metal decorations between types. As was seen in the ICP-OES results in chapter 3, there was great variation in the amount of mass of metal nanoparticle. Pt, Pd, and Ru had good mass percentages of around 1.3%, while the harder to reduce metals such as Co, Cu, and Ni (for chapter 3) had much lower loadings of 0.02-0.11%. The

commercial Au@$TiO_2$ had a standard 1% loading of material. With the current synthetic methods in the group, obtaining higher loading % for Co, Cu, and Ni was difficult. Ultimately, it was decided to directly compare the as synthesized materials, as accurate control of loading was not feasible with the current methods. This is one clear limitation of the photochemical M@$TiO_2$ synthesis approach, as it is very dependent on the reduction potential of the metal. However, this implies that Cu@$TiO_2$ may be limited by it's poor loading compared to Pt@$TiO_2$ or Pd@$TiO_2$. Considering it was not far behind in it's hydrogen generation yields, and was one of the better photocatalysts under water-splitting conditions, it may have greatly surpassed Pt or Pd with similar loadings. It may also be possible that $H_2$ generation under visible irradiation would be improved, due to absorbance by the $CuO_x$ semiconductor nanoparticles. Possible visible-sensitization by the $CuO_x$ was likely limited due to the poor loadings of the decoration. Improving upon the Cu@$TiO_2$ photocatalyst may be a possible direction for visible-light excited photocatalytic water splitting.

### 6.1.2 Solvent Radical Initiation

With chapter 3, research began to focus on the generation of radicals from organic solvents using these M@$TiO_2$ photocatalysts. This was completed with the same photocatalysts discussed in chapter 2, with the addition of Ni@$TiO_2$. In prior research within our group by Nancy Marina, it was proposed that THF radicals being generated in solution from Pd@$TiO_2$ were directly involved in activating an Ullmann cross-coupling reaction.[5] With this in mind, and the knowledge gained about radical generation from SEDs in chapter 2, further evaluation of the effectiveness of M@$TiO_2$ photocatalysts for solvent radical initiation was explored. Organic solvents such as ethers are sufficiently electron rich to be directly oxidized by photogenerated holes in M@$TiO_2$ catalysts undergoing some form of PCET mechanism. As seen in chapter 2, the generated $H^+$ ions may then go on to be reduced to $H_2$ gas. The generated solvent radicals can either react with other compounds in solution, or undergo loss of another electron and proton. As was seen in chapter 2 the additional loss of an electron and proton, often forming a double bond, can involve a form of PCET with the CB if $TiO_2$ or the metal-NP.

To test the usability of generated ether radicals, TEMPO was used as a radical scavenger to follow the formation of a TEMPO-Ether adduct. The generation of $H_2$ gas was also monitored,

as the required protons for this production are a by-product of the ether radical generation. This allowed for monitoring of the chemistry occurring from two different angles. Firstly, THF as a solvent was tested with a variety of different M@$TiO_2$ photocatalysts. All decorated $TiO_2$ photocatalysts, with the exception of Au@$TiO_2$, had full conversion of 25 mM TEMPO into the TEMPO-THF adduct within 7 hours of irradiation. In the case of Au@$TiO_2$, it capped at around 70% yield after 7 hours, with little increase after 20 hours. All metal decorations performed reasonably well, with strong improvement compared to pure P25 $TiO_2$. All metal decorations also allowed for 50% conversion within a time-scale of 2-5 hours of irradiation. Larger differences between decorations were observed for the $H_2$ generation rates. Pt and Pd decorations had $H_2$ generation rates of ~7000 μmol $g^{-1}$ $h^{-1}$, while gold showed generation rates of ~2500 μmol $g^{-1}$ $h^{-1}$. Other metal decorations had lower formation rates of $H_2$ gas, and overall it is not unexpected that $H_2$ generation rates would be affected more by the choice of metal. Since the formation of the THF radical is primarily dependent on the photogenerated hole of $TiO_2$, the metal decoration's primary role is to improve the lifetime of this hole. It is clear that the specific choice of metal decoration has a smaller effect on this part of the mechanism. However, due to the conclusions about SED radicals in chapter 2, the metal-NP decorations may also interact with generated radicals in other ways. One aspect not initially highlighted in the chapter is that the specific choice of metal may alter the subsequent additional oxidation by PCET of the THF radicals to form the alkene product. If this process is significantly improved, this may negatively effect the ability of these ether radicals to be truly 'free' to react in solution with scavengers such as TEMPO. Also, products such as 2,2,6,6-tetramethylpiperidine and 2,2,6,6-tetramethylpiperidinol were observed in some reactions, which may have involved side reactions between TEMPO and $H^+$ ions, coupled with excited electrons in the metal-NP. This may help explain the surprising lower activity of the commercial Au@$TiO_2$ in comparison to what was seen in chapter 2. It is possible that the generated radicals from Au@$TiO_2$ were converted to the alkene more quickly, and also the Au-NP may have increased formation of TEMPO side products. The latter explains the maximum amount of TEMPO-THF adduct capping at <80%. Ultimately from these results, Pd@$TiO_2$ was chosen as a model catalyst for testing with a variety of different ethers. However

in retrospect, Cu@$TiO_2$ may have been an interesting material to explore further as will be discussed later.

Using Pd@$TiO_2$, a variety of different ethers were tested for their TEMPO-ether adduct yield and $H_2$ generation rates under a standard 3 hours of irradiation. In this scope, tetrahydrofuran (THF), diethyl ether (DEE) , dioxane (DOX), and tetrahydropyran (THP) were the only ethers that showed significant formation of TEMPO-ether product. In all cases, the addition of $Cs_2CO_3$ as a base improved the yield of adduct, likely due to 2 reasons. Firstly, the base likely removes the $H^+$ ions from solution faster than the $H_2$ production can alone, thus aiding in further hydrogen abstraction from the ether. Also, more removal of the $H^+$ ions likely reduced the possibility of side products forming with TEMPO by the photoexcited electron and $H^+$ ions. Interestingly, the trends of $H_2$ production do not line up with the trends in TEMPO-ether adduct yields. For the TEMPO-ether adduct, the descending order of reactivity was THF, DEE, DOX, and THP. However, for $H_2$ generation THF and THP had the highest rates of $H_2$ formation with 7400 μmol $g^{-1}$ $h^{-1}$ and 7200 μmol $g^{-1}$ $h^{-1}$ respectively, while DEE and DOX had a rate of ~5200 μmol $g^{-1}$ $h^{-1}$ . Even though THP had less than half the yield of TEMPO-ether adduct compared to THF, it had similar $H_2$ production. A likely explanation is that the generated THP radical more favorably undergoes the secondary PCET for formation of the resulting alkene. Thus, even with a lower amount of radical generation, it has more favorable $H_2$ production. Also, the increased second PCET likely decreases the TEMPO-ether adduct further due to competition from this alternative reaction path. When comparing the trends of TEMPO-ether adduct formation to the rates of H-abstraction by $tBuO^{\bullet}$, a similar order of reactivity is observed. THF, DEE, and DOX are decreasingly active for forming the TEMPO-ether adduct. However, for H-abstraction by $tBuO^{\bullet}$, THP is more reactive than DOX. This can be explained either by differences in $TiO_2$-ether interaction in the PCET process, or by differing fates of the resulting radical. Dioxane has a very high surface affinity with $TiO_2$, which likely increases the rate of radical formation from it compared to other ethers, which may bring it ahead of THP in it's reactivity. Also as mentioned prior, THP likely forms more of the alkene product due to the higher $H_2$ yields observed, meaning that less of the generated radical is able to react with TEMPO in solution. The formation of the TEMPO-ether adduct does not directly show the rate of solvent radical formation, and is dependent on the actual availability

of the radical to react in solution. It is also dependent on the presence of any side reactions with TEMPO.

Dimethoxymethane (DMM), 1-methoxypropane (MOP), 1,3-dioxolane (DOL), and 2-methyl-1,3-dioxolane (MDOL) were also tested for TEMPO-ether adduct formation with Pd@$TiO_2$ and showed no detectable formation of the TEMPO-ether adduct. For DMM and MOP, this is easily explained by the fragmentation to formaldehyde due to the terminal methoxy- group in the linear ether. This explains the very high $H_2$ production observed with no TEMPO-ether adduct, as formaldehyde also acts as a strong SED. However, the inability for DOL and MDOL to form the TEMPO-ether adduct is less clear, and not fully discussed in the chapter. This is further highlighted in chapter 4 where DOL is effective at forming DOL radicals for addition to 1,1,-diphenylethylene. This implies that DOL can form radicals in solution using $TiO_2$ photocatalysts. The reason for this inconsistency may be a mix of the choice of Pd@$TiO_2$ as the catalyst, and TEMPO as the radical scavenger. As mentioned prior, TEMPO side products were observed, and were especially common with ethers that formed no TEMPO-ether adduct. In the case of DOL, the formed DOL radical is less likely to undergo the additional PCET step, as there is no adjacent C-H group to form an alkene. Without this coupled reaction, perhaps side reactions with TEMPO would be more likely due to less favorable removal of $H^+$ ions and photoexcited electrons. This would be due to decreased coupled reactions for $H_2$ generation with the DOL radical, meaning there may be an increase in reactions between TEMPO, $H^+$ ions, and the photoexcited electrons. Also, perhaps some form of fragmentation of the DOL radical is possible with Pd-NPs as the decoration. With MDOL, the lack of reactivity may be due to increased sterics with the $CH_3$ group, which may negatively impact the PCET process, and reactions with TEMPO. Overall, the TEMPO side products bring up the question whether Pd@$TiO_2$ was the best choice of photocatalyst for the generation of these radicals. This is due to Pd@$TiO_2$ being able to form the TEMPO by-products, and being efficient at initiating further PCET with the generated ether radicals. Choosing a photocatalyst that initiates radical formation more effectively, while also being inefficient at the reducing reactions, may be a better choice for ether radical formation. One possibility would be the use of Cu@$TiO_2$ as it is still very efficient at solvent-radical generation, but with reduced $H_2$ production. It overall tends to be less active in reduction reactions, which may lower the other

side reactions occurring. However with lower $H_2$ production, the addition of base will be more necessary due to the reduced removal of $H^+$ ions.

Overall, it is clear that M@$TiO_2$ photocatalysts are very effective at generating radicals from ethers. The main questions that remain are the exact fate of these radicals, and how to better control for making each radical usable for synthesis. Many radicals such as those generated from THF are clearly usable, and can be considered 'free'; however, others from ethers like DOL appear to be greatly dependent on the exact conditions around their formation. It was also found that benzylic radicals from toluene can be generated with these M@$TiO_2$ photocatalysts, which highlights the possibilities of this approach to radical generation outside of just ethers.

Utilizing this knowledge of radical generation, other methods of evaluating the chemistry occurring were explored. This led to the research into heterogeneous LFP in chapter 4. It was considered if adequately dilute heterogeneous suspensions of $TiO_2$ would allow for better evaluation of photocatalytically generated organic solvent radicals through LFP analysis. Typically LFP with $TiO_2$ is done through diffuse reflectance LFP, which has the limitation of only allowing evaluation of transients above 400 nm due to the competing absorbance of $TiO_2$. However, if $TiO_2$ was very dilute in solution, would evaluation of transients in the <400 nm region be possible with a conventional absorbance-based LFP setup? To answer this question, pure P25 $TiO_2$ was chosen for evaluation instead of M@$TiO_2$. This is due to M@$TiO_2$ materials being more complex in the dynamics of its generated transient states, and pure $TiO_2$ may offer a simpler system for understanding the chemistry occurring. 1,3-Dioxolane (DOL) was chosen as a solvent for radical generation from $TiO_2$. DOL was chosen as in chapter 3 it was found that it did not form adducts with TEMPO, even though radicals were likely forming. If radical chemistry is observed in this LFP system, it would highlight the limitations of the TEMPO approach with $TiO_2$ materials. Also, DOL being unable to form an alkene product from its radical through additional PCET means it may be more available for radical reactions in solution. 1,1-diphenylethylene (DPE) was chosen to react with the DOL-based radicals as it will form a strong benzylic radical transient peak at 330 nm after radical attack. By following the formation of this benzylic peak, the reaction of solvent radicals formed by the PCET with the excited $TiO_2$ could be monitored.

Before evaluating the solvent radical chemistry, the baseline transient signal of the $TiO_2$ suspension in DOL after excitation with 355 nm laser was evaluated. Transient signals were observed over the whole spectral range, and all decayed at similar stretched exponential rates. These transient signals occur due to the presence of the photogenerated charge carriers within the $TiO_2$ structure. Within the time-resolution of nanosecond LFP, the transient signals observed are only from the presence of trapped charge carriers. The transient signals are also not of the trapped carriers themselves, but effects of the overall structure of the surrounding $TiO_2$ or solvent at the trapping sites. These signals decayed in a similar fashion as observed in diffuse reflectance LFP studies, following a fractal-like kinetic decay (Figure 4.2.3). The decay stretching over such large time-scales is due to high variation in the fates of the charge carriers. Recombination of the carriers is dependent on the specific trapping states, and the actual geometry of the particles. With P25 $TiO_2$, the particles are not particularly uniform with many agglomerated particles of different size, morphology, and crystal structure (rutile and anatase). This highlights how some photogenerated charge carriers, electrons and holes, can be present even up to 1 ms. Even with most charge recombination occurring within picoseconds, trapped charge carriers can last much longer in P25 $TiO_2$. However, the stretched decay of the $TiO_2$ transients does make evaluation of other generated transients difficult, as they require intensity high enough to overcome the baseline signal from $TiO_2$, or need to be much longer lived. When DPE is added to the $TiO_2$ suspension in DOL, a clear increase in the lifetime of the transient signal at 330 nm is observed. There are now transient signals at 330 nm lasting up to 10 ms with the addition of DPE into the system (Figure 4.2.6). By looking at the transient absorbance spectrum, the longer lived transients appear to be the expected benzylic radicals (peak at 330 nm) for the addition of generated solvent radicals onto the alkene of DPE (Figure 4.2.7). Also, formation of this transient is directly dependent on the solvent, as decreased signal is observed with 1,4-dioxane (DOX), and no benzylic transient is observed with acetonitrile (Figure 4.2.11). Interestingly, this directly shows that formation of solvent radicals is more effective with DOL in comparison to DOX. This is again in direct contrast to chapter 3 where TEMPO-DOX adducts were observed, but no TEMPO adduct was formed with DOL. This further shows that in chapter 3, DOL radicals were likely forming; however, the specific mechanisms involved affected the ability of

TEMPO to scavenge it. This establishes that the TEMPO scavenging experiments in chapter 3 may be effective at initial testing of solvent radical generation; however, false negatives are possible due to conflicts with TEMPO. Performing radical addition reactions with reactive alkenes such as DPE, as done in these LFP experiments, may act as a better standard for testing the chemistry of solvent radicals. Also, it acts as the baseline for a useful chemical reaction with more possible applications in synthetic pathways.

Activating the C-H bonds of solvents for addition to alkenes may prove to be a useful method of partial conversion of solvents into higher value compounds. The reusability of M@$TiO_2$ photocatalysts also make this prospect more attractive in comparison to conventional methods of radical initiation using *tert*-butyl peroxide, or similar radical initiators.

The current limitations of the heterogeneous LFP methods shown is the low signals observed by the benzylic radical transient being followed. The overall intensity can be adequately compared between samples; however, full kinetic evaluation is not possible with the current signal to noise ratio. Since much of the benefit of LFP is in the possibilities of kinetic analysis of transients, the full potential of these techniques has not yet been realized. However, this research acts as the first example of evaluating the chemistry of subsequent $TiO_2$ initiated solvent radical reactions by heterogeneous LFP. Further improvement of the techniques may open the door for better kinetic evaluation of the reactive species formed by $TiO_2$, which will in turn inform further intelligent design of improved $TiO_2$ photocatalysts. $TiO_2$-based heterogeneous photocatalysts can still often be a 'black box', where the only certainties are what goes in and what comes out. This means any further development for techniques of mechanistic analysis are extremely valuable for making better informed design decisions in these systems.

The use of uniform $TiO_2$ nanoparticles may help to improve these heterogeneous LFP techniques. Firstly, smaller uniform particles of $TiO_2$ may suspend better in solution than the larger and somewhat inconsistent particle structure of P25 $TiO_2$. The background transient signals from the $TiO_2$ suspension may also be reduced by decreasing the fractal-like nature of it. With a less inconsistent and agglomerated particle of $TiO_2$, there will be less variation in the charge carrier trapping sites. This means the transient signals may be stretched over a smaller time

range, and off a background of lower intensity. Selecting for one crystal phase, anatase or rutile, will also simplify the chemistry occurring in the photoexcited particle. Suspensions of Metal-NP decorated uniform single-phase $TiO_2$-NPs may act as better systems for heterogeneous LFP.

### 6.1.3 Organic Synthesis using Calcium Carbide

Chapter 5 highlighted an additional project where Pd@$TiO_2$ was used in a Sonogashira-like reaction utilizing calcium carbide as a precursor. At first glance this project seems far removed from the overall theme of this dissertation. However, it utilizes Pd@$TiO_2$ as a catalyst, even if by a thermal mechanism. Also, possible future directions may allow for mixing calcium carbide chemistry with the solvent-radical chemistry discussed in chapters 3 and 4. Nonetheless, it still highlights the versatility of M@$TiO_2$ in many different applications.

Initial experiments tested reactions with Pd@$TiO_2$, bromobenzene, and calcium carbide in DMSO with no additional water added. It was found that with undried DMSO, the low amounts of water still allowed for adequate activation of the calcium carbide for Sonogashira coupling with bromobenzene to form diphenylacetylene. This was not unheard of in Sonogashira reactions involving calcium carbide, as the hydrogen atoms of water can be used catalytically in the activation of calcium carbide into acetylene.[6] However, the addition of too much water appeared to poison the reaction, which is not observed in many other examples of this behaviour. If water was simply turning calcium carbide into acetylene gas, some excess water should not negatively impact this behaviour. After further literature review, it was discovered that a few publications proposed the formation of an ethynyl calcium hydroxide intermediate from calcium carbide when using DMSO as a solvent.[7-9] This is from partial reaction of water with calcium carbide, instead of fully converting it into acetylene gas. This intermediate was proposed, but not well elaborated on in the literature. One publication observed the presence of it by ESI-MS[8]; however, little mechanistic analysis had been conducted to show it was the active species. To further support the activity of this ethynyl calcium hydroxide intermediate, a two-step reaction system was utilized. Initial heating of calcium carbide in DMSO lead to the formation of a solubilized intermediate that, after removal of excess calcium carbide, was able to react with bromobenzene catalyzed by Pd@$TiO_2$. This shows that some form of soluble intermediate is indeed able to act

as a precursor in the reaction, and formation of acetylene gas is not necessary in the reaction. In-fact, formation of the intermediate is likely preferable due to increased solubility compared to a gaseous reactant. The identity of this intermediate was then confirmed to be ethynyl calcium hydroxide through MS and NMR analysis. We also propose that under a one-step reaction, an ethynyl calcium bromide may also be possible due to the presence of bromine in solution.

Overall, chapter 5 was able to better evaluate the chemistry of calcium carbide in DMSO under low water conditions, and highlights the benefits of selecting for a solubilized ethynyl calcium hydroxide intermediate instead of acetylene gas for organic synthesis.

To expand on these findings, it may also be possible to mix the solvent radical initiation with this calcium carbide chemistry. Radicals can react with alkynes similar to how they react with alkenes, meaning that reactions between solvent radicals and ethynyl calcium hydroxide may be possible. If ethynyl calcium hydroxide is pre-formed in DMSO from calcium carbide, then mixed with a miscible solvent such as an ether, initiation of ether radicals by a M@$TiO_2$ photocatalyst may allow for coupling between the calcium carbide intermediate and the initiated radicals. This will be dependent on the effect of the mixed solvent on the ethynyl calcium hydroxide intermediate.

## 6.2 Future Directions

The work presented in this dissertation opens up many directions for further research in this area. Overall, M@$TiO_2$ catalysts have been shown to be extremely versatile, and further modifications may greatly improve them. Firstly, modification and doping of the $TiO_2$ structure itself may offer greatly improved catalysis from typical P25 $TiO_2$. Initial investigations of 'Black $TiO_2$' have been conducted in our group, and may prove to be a useful method of increasing activity into the visible spectrum, while also having an increased amount of surface defect sites. These surface defects often act as traps for photogenerated charge carriers in $TiO_2$. If this modification can be well controlled and characterized, this may allow for a better understanding of the chemistry occurring. This is due to these being induced defect sites, rather than defects randomly dispersed within the material. As mentioned previously, $TiO_2$ materials with better control of their specific structure will be invaluable in further improving their chemistry due to

having increased predictability of the photochemistry occurring from them. $CuO_x$ nanoparticle decorations are another subject that may have room for further exploration. Higher percent loadings of the copper on $TiO_2$ may give a very active photocatalytic material, with very low cost. Also, dual metal decoration by copper oxide with other metallic NP may offer further improvement. The $CuO_x$ nanoparticles likely act as semiconductors, and likely do not easily accept excited electrons from $TiO_2$. It instead may be helping to trap photogenerated holes. Adding a metal decoration such as palladium may allow for better trapping of the photogenerated electrons as well.

Further development of heterogeneous LFP techniques may also be useful in better evaluating $TiO_2$-based materials. Sensitive evaluation of the kinetics of transient species generated from $TiO_2$ suspensions will be useful in understanding the mechanisms occurring in chemical reactions, while also giving hints on how to improve them. Suspensions of uniformly synthesized $TiO_2$ nanoparticles may act as a more consistent analyte for these experiments, with possible reduced issues from scattering. Time-resolved EPR techniques may also be valuable, as it will allow for a better understanding of what radical species are being generated in solution. Overall, time-resolved techniques for heterogeneous reactions is an area of research with great potential impact.

Chemistry of the ethynyl calcium hydroxide intermediate formed from calcium carbide in DMSO may also prove to be useful in a variety of different reactions. The Sonogashira-like reaction with bromobenzene was used as an example; however, many other coupling reactions are possible. Also, due to the asymmetry of the triple bond (H- vs HOCa-), unsymmetrical reactions with the intermediate may be possible. This may allow for control of coupling different species at either location of the triple bond in a one-pot reaction. Also, photocatalysis may be possible using radicals photoinitiated by $M@TiO_2$ catalysts, such as those seen with ethers or toluene. Overall, ethynyl calcium hydroxide is an interesting reagent that can be adequately stabilized in DMSO for short periods of time, and opens up a variety of possibilities for easier acetylene-like chemistry in solution. Any process using acetylene may gain benefits from this approach.

## 6.3 Overall Conclusions

M@$TiO_2$ materials have proven to be extremely versatile in a variety of different applications. These applications include photocatalytic hydrogen generation, and solvent radical initiation. It also includes thermal organic synthesis with calcium carbide as an initiator.

In hydrogen generation, M@$TiO_2$ photocatalysts were shown in chapter 2 as effective with both SEDs and under pure water splitting conditions. Rates of $H_2$ production are impressive when considering the complexity and price of the photocatalyst. In evaluating activities between water splitting, and with SEDs such as methanol and formic acid, the differences between the two mechanisms were highlighted. The differing trends in activity between catalysts highlight that the metal-NPs likely directly interact with radicals generated by oxidation of SEDs. This further interaction makes the mechanisms between water splitting and SED-based $H_2$ generation very different. This means that a photocatalyst with promising activities with SEDs, such as Pd@$TiO_2$, may be completely ineffective with water splitting due to the differences in the mechanisms involved.

Radical initiation by M@$TiO_2$ was also shown to be effective in chapter 3, with a variety of different ethers tested for radical scavenging by TEMPO after the PCET initiation by the photogenerated hole in the VB of M@$TiO_2$ catalysts. These catalysts are very adept at forming radicals from most ethers; however, the usability of these ether radicals by TEMPO is dependent on the exact fate of the generated radical. Some ether radicals, such as the dimethoxymethane radical, may undergo fragmentation preventing their use as a free radical. The strength of M@$TiO_2$ was also shown by its ability to generate benzylic radicals from toluene in solution.

Further evaluation of radical initiation by $TiO_2$ photocatalysts was conducted through novel heterogeneous LFP techniques in chapter 4. Low concentration suspensions of $TiO_2$ in 1,3-dioxolane showed the expected benzylic radical transients from the reaction between the initiated 1,3-dioxolane radicals, and 1,1-diphenylethylene. The formation and decay of this transient could be followed; however, at a somewhat low signal-to-noise ratio due to the interfering transient background of the $TiO_2$ suspension. This reaction also showed dependence

on the solvent, directly showing the relative activities of the solvents for PCET-based radical initiation by the photoexcited $TiO_2$ particles. Further development of these heterogeneous LFP techniques may prove extremely useful in further evaluating radical chemistry from photoexcited $TiO_2$.

M@$TiO_2$, specifically Pd@$TiO_2$, was also shown to be useful in thermally catalyzing a reaction between ethynyl calcium hydroxide and bromobenzene to form diphenylacetylene in chapter 5. Calcium carbide was shown to form a semi-stable ethynyl calcium hydroxide intermediate when heated in DMSO under low water conditions. Small amounts of water allowed for selecting for the partial hydrolysis of calcium carbide into ethynyl calcium hydroxide, rather than full hydrolysis into acetylene gas. This intermediate was shown to be stable enough for initial formation in DMSO, before adding bromobenzene and Pd@$TiO_2$ for catalytic conversion into diphenylacetylene. This ethynyl calcium hydroxide intermediate may prove useful in other M@$TiO_2$ catalysis, including photochemical radical chemistry.

Overall, M@$TiO_2$ materials are popular heterogeneous catalysts for a reason. Their exceptional versatility has not been matched by many other heterogeneous systems. The maximum potential of these materials has likely still not been met, and intelligent evaluation of the catalytic mechanisms of these materials will be valuable in their further development. Developing new techniques, such as heterogeneous LFP, may offer alternative ways of learning about the reaction dynamics of these catalysts.

## 6.4 References

1. Janczarek, M.; Kowalska, E., On the origin of enhanced photocatalytic activity of copper-modified titania in the oxidative reaction systems. *Catalysts* **2017,** *7* (11), 317/1.
2. Schneider, J. T.; Firak, D. S.; Ribeiro, R. R.; Peralta-Zamora, P., Use of scavenger agents in heterogeneous photocatalysis: truths, half-truths, and misinterpretations. *Phys. Chem. Chem. Phys.* **2020,** *22* (27), 15723-15733.
3. Wang, L.; Cao, S.; Guo, K.; Wu, Z.; Ma, Z.; Piao, L., Simultaneous hydrogen and peroxide production by photocatalytic water splitting. *Chin. J. Catal.* **2019,** *40* (3), 470-475.
4. Liu, J.; Liu, Y.; Liu, N.; Han, Y.; Zhang, X.; Huang, H.; Lifshitz, Y.; Lee, S.-T.; Zhong, J.; Kang, Z., Metal-free efficient photocatalyst for stable visible water splitting via a two-electron pathway. *Science* **2015,** *347* (6225), 970-974.
5. Marina, N.; Lanterna, A. E.; Scaiano, J. C., Expanding the color space in the two-color heterogeneous photocatalysis of Ullmann C-C coupling reactions. *ACS Catal.* **2018,** *8* (8), 7593.
6. Chuentragool, P.; Vongnam, K.; Rashatasakhon, P.; Sukwattanasinitt, M.; Wacharasindhu, S., Calcium carbide as a cost-effective starting material for symmetrical diarylethynes via Pd-catalyzed coupling reaction. *Tetrahedron* **2011,** *67* (42), 8177-8182.
7. Fu, R.; Li, Z., Direct synthesis of symmetric diarylethynes from calcium carbide and arylboronic acids/esters. *Eur. J. Org. Chem.* **2017,** *2017* (45), 6648-6651.
8. Gao, L.; Liu, Z.; Ma, X.; Li, Z., Direct synthesis of propen-2-yl sulfones through cascade reactions using calcium carbide as an alkyne source. *Org. Lett.* **2020,** *22* (13), 5246-5250.
9. Polynski, M. V.; Sapova, M. D.; Ananikov, V. P., Understanding the solubilization of Ca acetylide with a new computational model for ionic pairs. *Chem. Sci.* **2020,** *11* (48), 13102-13112.

# A: Appendix

## A.1 M@$TiO_2$ Catalyst Synthesis

All metal-decorated $TiO_2$ were prepared following a photochemical method, with slight modifications, previously reported.[1-2]

Pt@$TiO_2$, Pd@$TiO_2$, Ru@$TiO_2$: approximately 2 wt% of metal precursor salt ($PtCl_4$, $PdCl_2$, or $RuCl_3 \bullet H_2O$, respectively) were mixed together to $TiO_2$ (~500 mg) in 200 mL of Milli-Q water and sonicated for 20 minutes. Only in the case of Ru, 2 eq. of I-2959 were added to facilitate the photoreduction of the metal precursors. After purging with Argon, the slurry was irradiated in a Luzchem photoreactor equipped with 14 UVA bulbs for 8 h with vigorous stirring. The slurry was centrifuged and washed with Milli-Q water at least five times to remove unreacted metal precursor salt and dried overnight in a desiccator under vacuum.

Co@$TiO_2$, Ni@$TiO_2$, Cu@$TiO_2$: approximately 5 wt% of metal precursor salt ($CoCl_2$, $CuCl_2 \cdot 2H_2O$, or $NiCl_2 \bullet 6H_2O$) were mixed together to $TiO_2$ (~200 mg) in 100 mL of Milli-Q water and sonicated for 20 minutes. Then, 2 eq. of I-2959 were added to facilitate the photoreduction of the metal precursors. The mixture was purged with Argon for 20 min, sonicated and then irradiated in a Luzchem photoreactor equipped with 14 UVA bulbs for 5 h under vigorous stirring. The slurry was centrifuged and washed with Milli-Q water at least five times and then dried in a desiccator overnight under vacuum.

## A.2 Characterization of M@$TiO_2$ Catalysts

Cu@$TiO_2$, Pt@$TiO_2$, Pd@$TiO_2$ and commercial Au@$TiO_2$ have previously been characterized by our group[1-4]. Shown below are all the characterizations of the M@$TiO_2$ materials utilized in this work, either completed by myself or by past researchers. Please note that characterization of Ni@$TiO_2$ beyond ICP analysis is not available due to the catalyst being borrowed from another member in the group, and is now unavailable for further characterization.

**ICP-OES for calculation of % metal loading**

Metal loading on the different catalysts was determined by Inductively Coupled Plasma Optical Emission Spectrometry (ICP-OES), using an Agilent Vista Pro ICP Emission Spectrometer. Approximately 10 mg portions were accurately weighed in triplicate and digested with aqua regia. Solutions were further diluted and measured by ICP-OES. The resulting calculated metal loading percentages (by mass) are shown below (See Table A.2.1).

**Table A.2.1.** M@$TiO_2$ catalytic materials utilized in this work. Metal loading quantified with ICP-OES.

| Entry | Metal (M) | % metal loading |
|---|---|---|
| i | Pt | 1.36 |
| ii | Pd | 1.23 |
| iii | Ru | 1.45 |
| iv | Co | 0.06 |
| v | Ni | 0.02 |
| vi | Au | 1.00 |
| vii | Cu | 0.11 |

**Electron Microscopy of M@$TiO_2$ catalysts**

Electron microscopy of the various materials was conducted. The resulting images can be seen below (See figures A.2.(1-6)). In many materials, such as those more oxidized metal decorations, the contrast against the $TiO_2$ background is poor. This makes direct observation of the nanoparticle decorations difficult. Scanning transmission electron microscopy (STEM) was utilized with Cu@$TiO_2$ (Figure A.2.4) to attempt to better see the small nanoparticles. Ru, Pd, and Au are the only samples in TEM that have clear nanoparticles visible on the surface of the titanium dioxide support. Further use of STEM for characterization of these materials may prove more useful in characterization of these materials in the future.

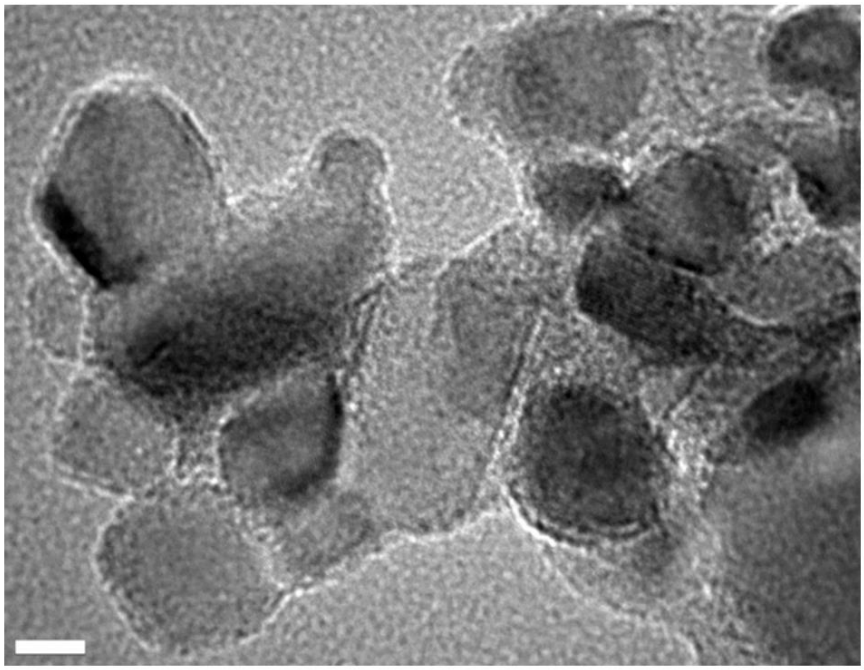

**Figure A.2.1.** HR-TEM image of Co@$TiO_2$. Scale bar: 10 nm

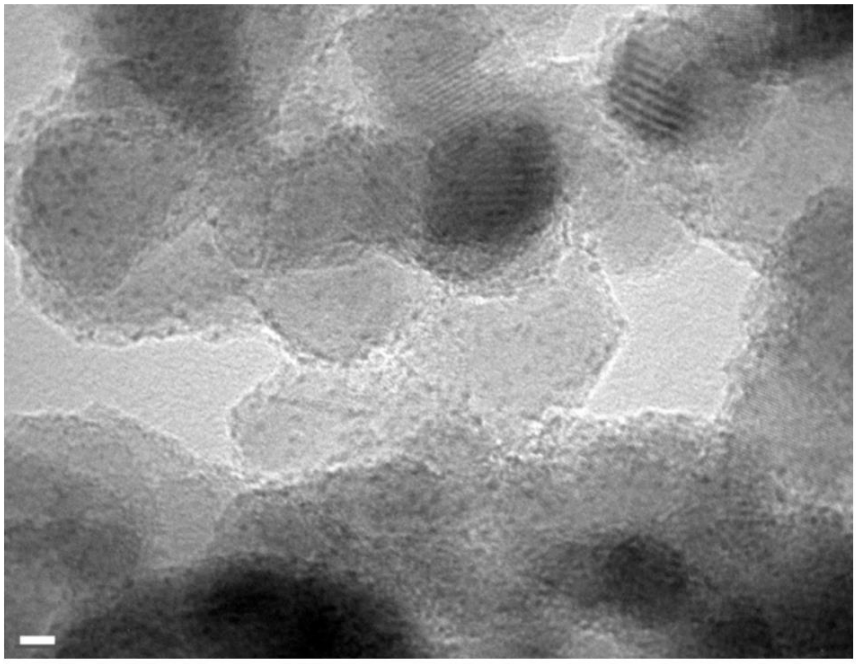

**Figure A.2.2.** HR-TEM image of Ru@$TiO_2$. Scale bar: 5 nm

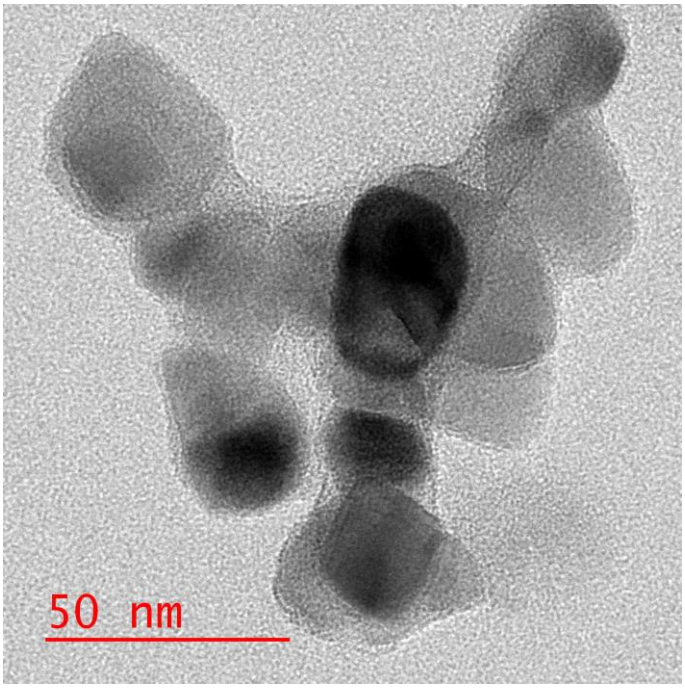


**Figure A.2.3.** HR-TEM image of Pt@$TiO_2$. Scale bar: 50 nm

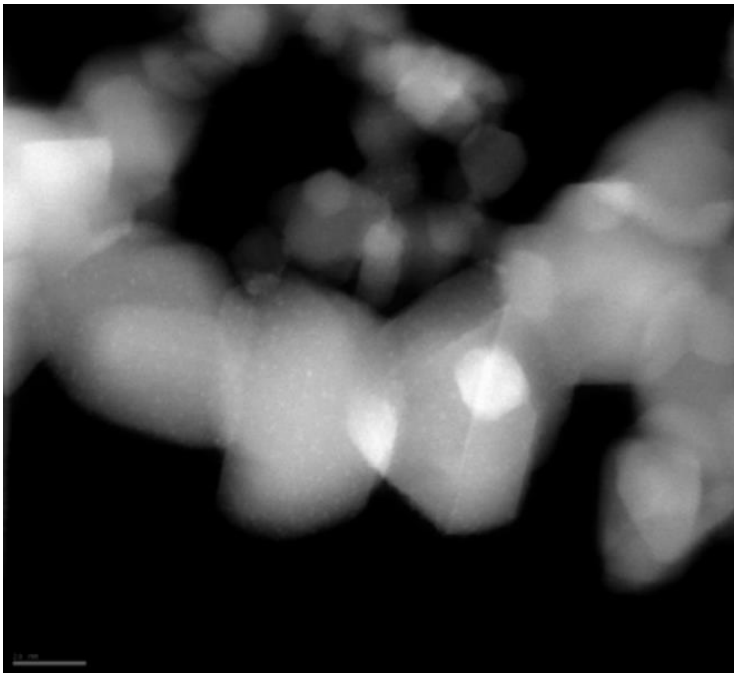

**Figure A.2.4.** STEM image of Cu@$TiO_2$. Scale bar: 10 nm. Obtained with permission from previous publication in our group.[1]

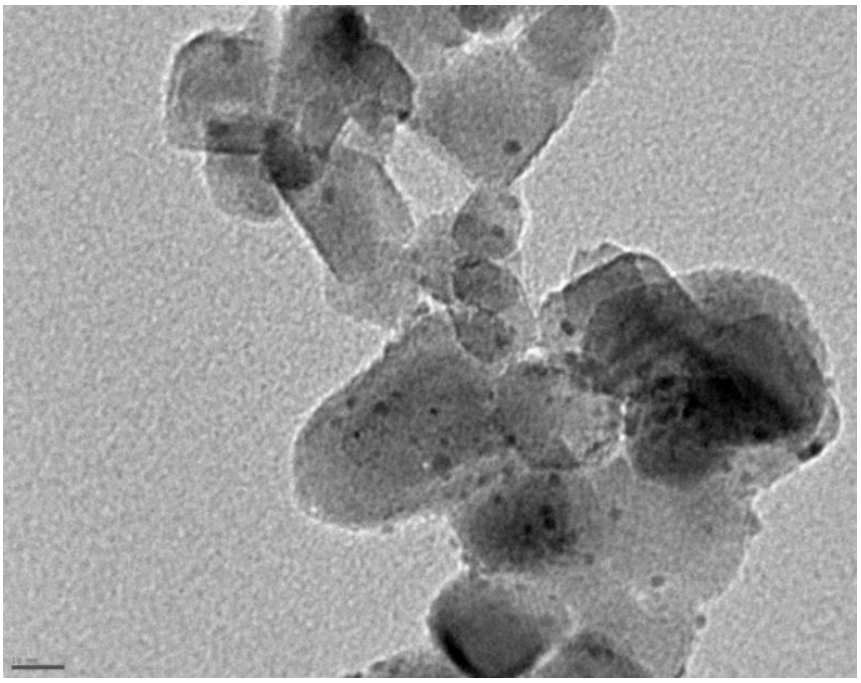

**Figure A.2.5.** HR-TEM image of Pd@$TiO_2$. Scale bar: 10 nm. Obtained with permission from previous publication in our group.[2]

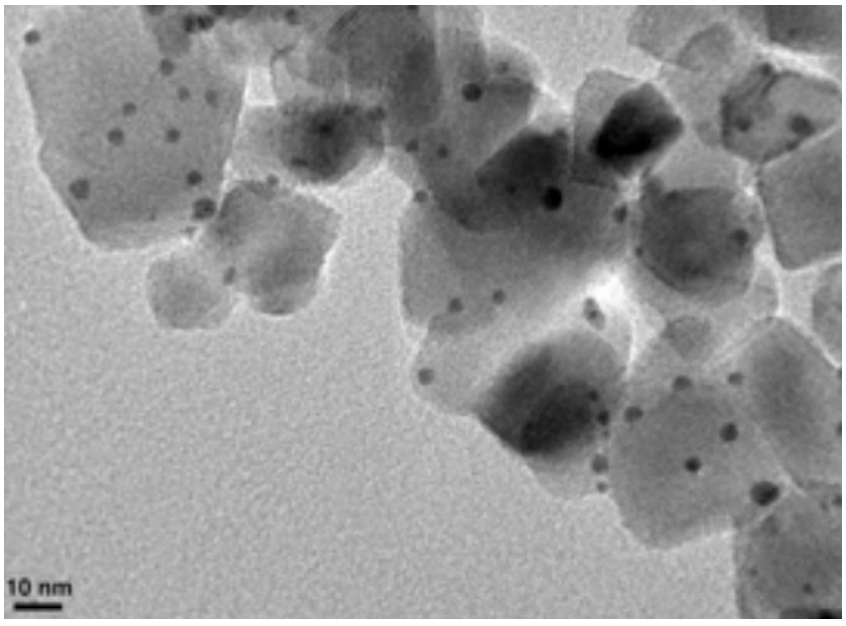


**Figure A.2.6.** HR-TEM image of commercial Au@$TiO_2$. Scale bar: 10 nm. Obtained with permission from previous publication in our group.[4]

**Diffuse Reflectance**

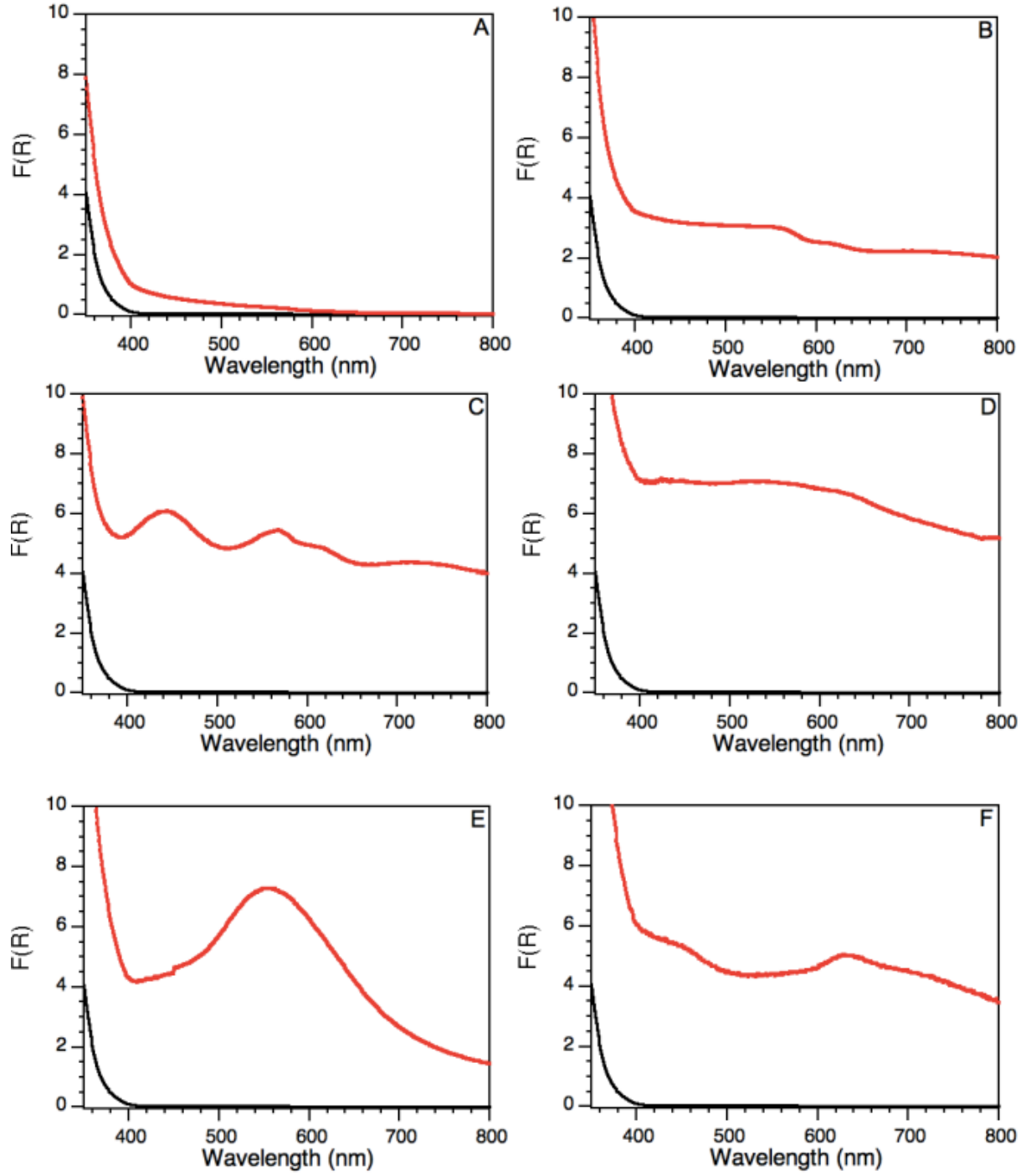


**Figure A.2.7.** Diffuse reflectance spectra of bare $TiO_2$ in black and in red **(A)** Co@$TiO_2$, **(B)** Pt@$TiO_2$, **(C)** Ru@$TiO_2$, **(D)** Pd@$TiO_2$, **(E)** Au@$TiO_2$ and **(F)** Cu@$TiO_2$.

**XPS spectroscopy**

All XPS spectra were calibrated at C 1s 284.8 eV. The HR-XPS spectra show barely detectable amounts of Co (not shown) and Ru (Figure A.2.8(B)) on the respective metal-decorated $TiO_2$ catalysts. Additionally, the Ru 3p signals in the HR-XPS spectrum overlaps with those from Ti 2p, making the analysis even harder. The deconvolution of the HR-XPS peaks reveals two bands that can be attributed to 464.2 (Ru 3p3/2) and 485.9 (Ru 3p1/2) eV corresponding to the presence of RuOx/Ru. The peaks at 458.1 (Ti 2p3/2) and 466.4 (Ti 2p1/2) eV show together with the associated satellites at 460.5 and 475.8 eV, respectively. In contrast, Pt, Pd, Au and Cu signals can be well identified on the corresponding HR-XPS spectra (Figure A.2.8(A,C-E)). Pt 4f HR-XPS spectrum (Figure A.2.8(A)) shows a mix between Pt (0) and PtOx species. The Pt 4f core-level spectrum was performed by using two spin-orbit split Pt 4f5/2 and Pt 4f7/2 components, separated by ~3.3 eV. Figure A.2.8(C) shows that the Pd@$TiO_2$ composite is mainly constituted by Pd(0) species and a reduced amount of PdOx. The Pd 3d corelevel spectrum is performed by using two spin-orbit split Pd 3d5/2 and Pd 3d3/2 components, separated by ~5.2 eV. In the case of Au@$TiO_2$, the sample is constituted by Au(0). The Au 4f core-level spectrum is performed by using two spin-orbit split Au 4f5/2 and Au 4f7/2 components, separated by ~3.5 eV. Finally, for Cu@$TiO_2$ there is a mixture of $Cu_2O$ and CuO, as previously discussed. 1 Briefly, Cu(II) can be confirmed by the satellite peaks detected at 940.8 and 943.1 eV.

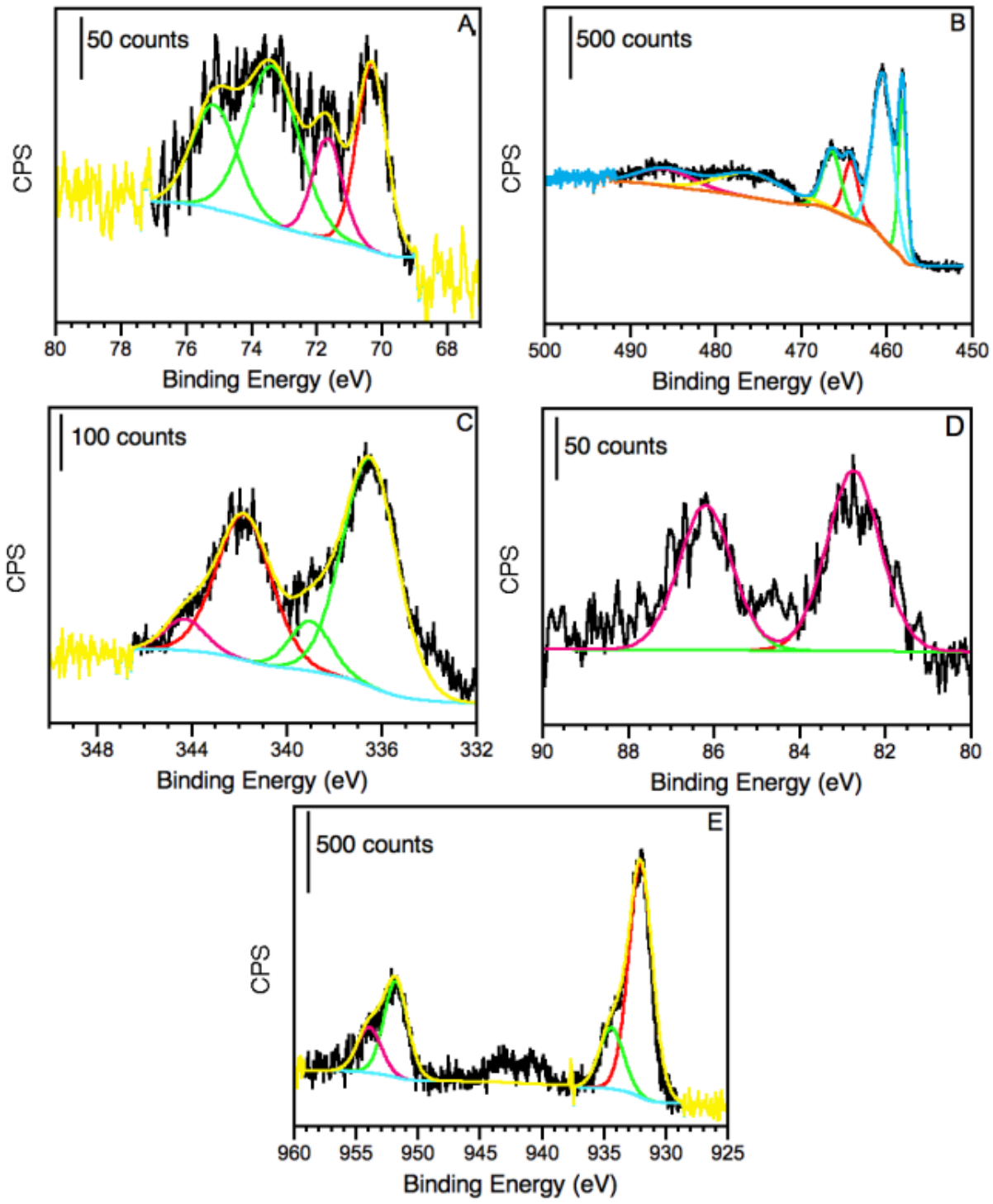


**Figure A.2.8.** Deconvoluted HR-XPS spectra for **(A)** Pt@$TiO_2$, **(B)** Ru@$TiO_2$, **(C)** Pd@$TiO_2$, **(D)** Au@$TiO_2$ and **(E)** Cu@$TiO_2$

## A.3 References

1. Wang, B.; Durantini, J.; Nie, J.; Lanterna, A. E.; Scaiano, J. C., Heterogeneous photocatalytic click chemistry. *J. Am. Chem. Soc.* **2016,** *138* (40), 13127-13130.
2. Elhage, A.; Lanterna, A. E.; Scaiano, J. C., Tunable photocatalytic activity of palladium-decorated $TiO_2$: Non-hydrogen-mediated hydrogenation or isomerization of benzyl-substituted alkenes. *ACS Catal.* **2017,** *7* (1), 250-255.
3. McTiernan, C. D.; Pitre, S. P.; Ismaili, H.; Scaiano, J. C., Heterogeneous light-mediated reductive dehalogenations and cyclizations utilizing platinum nanoparticles on titania (PtNP@$TiO_2$). *Adv. Synth. Catal.* **2014,** *356* (13), 2819-2824.
4. Lanterna, A. E.; Elhage, A.; Scaiano, J. C., Heterogeneous photocatalytic C–C coupling: mechanism of plasmon-mediated reductive dimerization of benzyl bromides by supported gold nanoparticles. *Catal. Sci. Technol.* **2015,** *5* (9), 4336-4340.

## A.4 Journal Permissions

This dissertation contains altered manuscripts and images that are republished under the permissions granted by the publishing journals.